HEAN INVESTIGATION INTO THE SUSPENSION, ATTRITION AND BREAKAGE OF NICKEL CRYSTALS DURING THE NICKEL REDUCTION PROCESS

By Nobert Paradza

Dissertation submitted in fulfilment of the requirements for the degree of Master of Science in Engineering

Department of Chemical Engineering

Faculty of Engineering and the Built Environment

University of Cape Town

April 2011

Declaration: *I know the meaning of plagiarism and declare that all the work in the document, save for that which is properly acknowledged, is my own.*

……

Acknowledgements

I would like to acknowledge my supervisor, Prof. Alison Emslie Lewis for her insightful ideas and guidance in carrying out this research project, and in the preparation of this thesis. The dedication in which she read the thesis draft and the feedback period was always exceptional.

Many thanks also go to the National Research Foundation (NRF) and Murrin Murrin mining company for funding this project through Minerals to Metals and Crystallisation and Precipitation research groups respectively. Without their generous and strong support, this project would not have been possible.

Appreciation is also expressed to the former and current Crystallisation and Precipitation Unit colleagues for their support and encouragement throughout the course of this work: Thanks to Mr. Jeeten Nathoo, Mrs Christine Olsen, Ms Ndishavhelafhi Mbedzi, Mr. Murehwa Mangere, Dr. Freeman Ntuli, Sinethemba Nkukwana (aka Fresh) and other members of the group.

Special thanks also go to other staff members in the Chemical Engineering Department for their assistance, especially Dr. Aubrey Mainza, Mr. Lawrence Bbosa, Prof. David Deglon, Prof. J.P Franzidis, Ms Mymoena van der Fort, Granville de la Cruz and Joachim Macke.

To my family, my fiancé (Chiedza Kurebwa) and my friends (Day Marume, Deside Chibwe, Takura Nyashanu, Lesley Sibanda and Bulelwa Ndlovu): thank you for your encouragement, emotional and moral support.

Last but not least, I thank the MOST HIGH for His guidance throughout this work.

Abstract

During nickel reduction, the rapid growth of nickel crystals sometimes causes the termination of the cycle before the design specification is reached. One of the possible causes of rapid crystal size enlargement could be due to agglomeration of the nickel particles. It is understood that particle agglomeration can be influenced by a number of factors including the chemical environment (additives and supersaturation), the number density of particles and the turbulent energy (agitation) in the autoclave. If there is insufficient agitation in the autoclave, then it is possible that there is not sufficient shear to cause attrition of the crystals and breakage of the newly formed agglomerates. The critical impeller speed (N_{js}) is commonly used to indicate the effectiveness of solids suspension in stirred tanks. Previous investigations have highlighted that the critical impeller speed is a very useful benchmark for evaluating the effectiveness of solids suspension in reactors.

The aim of this study was to characterize the different impeller speeds required for suspension, attrition and breakage of nickel crystals in an autoclave. To ensure optimum operation of the autoclave, the nickel particles must be kept in complete suspension. Suspension tests were carried out in a 75l elliptically bottomed Perspex reactor by using pure nickel powder and glass beads as the solids media and tap water as the liquid medium. The effect of aeration on the critical impeller speed, N_{js} for both the Rushton and the pitched blade impeller system was investigated. It was observed that a pitched blade impeller compared to a Rushton impeller, is very sensitive to gassing rates and tends to flood under high aeration rates. It was also identified that for high density materials like nickel, flooding may occur at Na_{js} values of less than 0.015 for a pitched blade impeller system. From theory, it was indicated that impeller flooding may occur at Na_{js} values greater than 0.03.

The 'attrition speed' was established in a 7l Perspex reactor by way of actual impeller crystal collisions in a mixing set up. Particle size distributions of the attrition product, expressed as number distributions were used to identify the presence of attrition. It was observed that an impeller tip speed of 4.01 m/s is high enough to cause attrition of the nickel crystals. This attrition speed has an equivalent impact energy of $4.90*10^{-7}$ J for feed particles of diameter, d_{50} = 190μm. Breakage tests were performed by use of an ultrafast load cell and a mean fracture energy of 0.18mJ for pure nickel crystals was obtained. This translated to an impeller tip speed of 17.1m/s.

Table of contents

Table of figures

List of tables

Nomenclature

a	aeration constant
A_r	cross-sectional area of the rod (m^2)
B	solid-liquid mass ratio (wt %)
c	concentration (kg/m^3)
c*	equilibrium concentration (kg/m^3)
C	impeller clearance (m)
C_r	wave velocity of the rod (m/s)
d	average diagonal of the plastic indentation (m)
d_p	particle diameter (m)
D	impeller diameter (m)
DT6	Six bladed disc turbine (Rushton Impeller)
E_c	impact energy assumed to be equal to the kinetic energy of the crystals (J)
E_f	fracture energy (J)
E_p	energy required to crush a particle (J)
F	load/force (N)
F_c	Fracture force (N)
$F_{0.5}$	load where 50% of the indentations produced cracks (N)
F_b	force exerted by the particle on the ball (N)
$F_{Hertz,max}$	maximum contact force obtained from Hertz's law of contact (N)
Fr	Froude number
g	acceleration due to gravity (ms^{-2})
GF_{bridge}	ultrafast load cell bridge factor
H	liquid height (m)
H_v	Vickers hardness (N/m^2)
HV	Vickers hardness number (HV)
k	efficiency constant used in equation 2.22
$k_{b,r}$	stiffness of the ball or rod (Pa)
k_p	particle stiffness (Pa)
K	bulk modulus (Pa)
K_e	local deformation coefficient of the Hertzian contact
K_G	constant used in equation 2.9 and 2.10 (min)
K_{SL}	constant used in equation 2.8 and 2.9 (rpm)
K_v	volume shape factor

L	crystal/fragment size (m)
m	constant used in equation 2.14
m_p	mass of particle or crystal (kg)
m_b	mass of the steel ball(kg)
m_0	zeroth moment (#/m^3)
n	constant used in equation 2.14
N	impeller rotational speed (rpm)
N_{js}	critical impeller speed (rpm)
N_{jsu}	critical impeller speed for an ungassed system(rpm)
N_{jsg}	critical impeller speed for a gassed system(rpm)
Na_{js}	just suspension aeration number
$n(L)$	number density of particles (#/m^4)
$N(L)$	cumulative number of particles (#/m^3)
N_p	impeller power number
N_T	total number of particles (#/m^3)
Q	aeration rate (m^3/min)
Re_{imp}	impeller Reynolds number
RJSS	relative just off-bottom suspension speed
s	supersaturation ratio
S	Zwietering constant which is a function of D/T, C/T and impeller type
T	tank diameter (m)
u	impact velocity assumed to be equal to the impeller tip speed (m/s)
u_b	position of the centre of gravity of the ball (m)
u_r	position of the top of the rod (m)
v_0	velocity of the striker at the instant of contact (m/s)
V_a	total volume of fragments
V_c	total effective volume of the reactor (m^3)
V_i	input voltage (V)
V_o	output voltage (V)
W_c	critical work to form cracks (J)
X	solids mass concentration
Y_p	Young's modulus of the particle/crystal (Pa)
Y_r	Young's modulus of the rod (Pa)
z_d	deformation from the loading point (m)

Greek symbols

α	overall contact deformation (m)
ε	impeller dissipated power per unit mass (W/kg)
ε_{axial}	axial strain
ε_{lat}	lateral strain
ρ_c	crystal density (kg/m^3)
ρ_L	liquid density (kg/m^3)
ρ_r	density of the rod (kg/m^3)
ρ_s	solids density (kg/m^3)
Γ	fracture resistance (J/m^2)
τ	Integration variable
μ	shear modulus (Pa)
μ_p	Poisson's ratio
ν	slurry kinematic viscosity (m^2/s)
ν_L	liquid kinematic viscosity (m^2/s)
ν_w	kinematic viscosity of water (m^2/s)
Δ	particle deformation (m)
Δ_c	deformation at fracture (m)
σ	relative supersaturation
σ_p	particle strength (Pa)

CHAPTER 1 : INTRODUCTION

1.1 GENERAL INTRODUCTION

In an industrial application, the process of nickel powder precipitation from aqueous nickel ammoniacal solutions by high pressure hydrogen reduction is conducted in agitated autoclaves (Willis and von Essen, 2000). This technique was first pioneered by Schaufelberger in 1946 and later developed for commercial purposes by Sherrit Gordon Mines between 1950 and 1960 (Ntuli, 2008). The same process has remained essentially unchanged for more than 30 years and is still in use today (Willis and von Essen, 2000).

However, there are various factors that affect the product quality in terms of product particle size, product purity and morphology. These include the supersaturation, pH, hydrogen partial pressure, temperature, impurities, additives and the agitation in the autoclave (Ntuli, 2008). Ntuli and Lewis (2006 and 2007) have studied most of these factors in previous work. However, not much research has been conducted on the role of agitation in systems with high density materials like nickel in an autoclave.

1.2 MOTIVATION

The nickel reduction process is known to occur on the surface of the parent crystals (Ntuli, 2008) such that the rate of reaction is dependent on the available surface area for the reaction (Willis and von Essen, 2000). During nickel crystallisation, the nickel surface on which further reduction occurs is introduced mainly by seeding or attrition and breakage of the parent crystals (Ntuli, 2008). To maximise the available surface area for the reaction, it is therefore important to keep these crystals in complete suspension. Attrition and breakage thus play an important role in the generation of more surface area for reduction and at the same time reducing the size of crystals so that they can be kept in complete suspension.

Agglomeration of nickel crystals is also not desirable and therefore, the turbulent energy in a nickel reduction autoclave should be sufficient to cause shear and thus breakage of the nickel agglomerates. This condition of agglomerates breakage is required to produce smaller sized particles that can be kept in suspension during the reduction process. If particles rapidly get large, they become difficult to suspend forcing the cycle to be terminated after a few densifications than the design requirement (Lewis, 2009).

1.3 PROJECT OBJECTIVES

This study focussed on three key areas:

i. Investigating the concept of 'just suspended impeller speed' for a nickel reduction autoclave taking into consideration the effect of aeration on the critical impeller speed. Two impeller types were used: the Rushton and the pitched blade impeller. The key parameter studied was the critical impeller speed, N_{js} and how it is affected by changes in aeration rates. The experiments were carried out in a 75l elliptically bottomed Perspex reactor and the point of N_{js} was observed visually from the bottom of the tank by use of a video camera.

ii. Establishing the 'attrition speed' for a nickel reduction autoclave. Two methods were employed in this work: the 7l mixing set up and the Vickers microhardness test. The results obtained from these two approaches were compared.

iii. Establishing the 'breakage speed' for a nickel reduction autoclave. Here, a drop weight technique (the ultrafast load cell) was adopted. The fracture energy obtained during single crystal breakage was selected as a suitable measure of particle strength. This fracture energy was then related to the impact energy required to break nickel crystals in a crystalliser.

The suspension experiments were carried out in an attempt to investigate the hypothesis that suspension of particles using a pitched blade impeller in an aerated reactor is largely affected by the aeration rate when gas sparging is performed below the impeller. Attrition and breakage of the nickel particles is also necessary for the successful achievement of a significant number of densifications in the autoclave and therefore, it is important to establish the conditions under which these occur.

1.4 THESES OUTLINE

- Chapter 1 introduces the project.
- Chapter 2 deals with the literature review on all three aspects of the project. The theory behind each experimental technique and the governing equations are discussed.
- In chapter 3, the detailed experimental method, results, discussion and conclusions for the investigation into the just-suspended impeller speed are presented. The effect of aeration rate on the critical impeller speed for both the Rushton and the pitched blade impeller system is investigated.
- Chapter 4 covers the detailed experimental method, results, discussion and conclusions for the investigation into the attrition speed. The 7l mixing set up and the Vickers microhardness test results are presented and the comparison made. The attrition energy obtained in this study is related to the conditions in a crystalliser by use of the kinetic energy equation.
- In chapter 5, the detailed experimental method, results, discussion and conclusions for the investigation into the breakage speed are presented. Both single crystal and bed breakage are covered. Three keys parameters of breakage (fracture energy, particle strength and particle stiffness) were established.
- The overall conclusions are drawn in chapter 6.
- The list of references is presented in chapter 7.

CHAPTER 2 : LITERATURE REVIEW

2.1 GENERAL PRECIPITATION THEORY

Crystallisation or precipitation is defined as the formation of a solid phase out of other phases (solid, liquid or gaseous) as a result of a driving force known as supersaturation (Nyvlt, 1971). The driving force could be a result of cooling, evaporation or chemical reaction between two soluble compounds (Mullin, 2001). To effect the deposition of a crystalline phase from a solution, some degree of supersaturation or supercooling has to be achieved in the system (Mullin, 2001).

Crystallisation can be thought as a two step process: nucleation (birth of new crystals) and growth of these crystals to larger sizes (Biscans, 2004). At an industrial scale, it can be used as a separation or purification process in the production of a wide range of materials, for example chemicals, specialty chemicals, pharmaceuticals or minerals (Biscans, 2004). As the generation step in solid processing, crystallization has a determining influence on the quality of the crystals (product purity, size distribution and morphology of the particles).

2.1.1 Supersaturation

In concentration terms, supersaturation can be referred to as the departure of concentration from the equilibrium (Roberts, 2004). This can be expressed as:

absolute supersaturation, Δc

$$\Delta c = c - c^* \tag{2.1}$$

supersaturation ratio, s

$$s = {}^{c}/_{c^*} \tag{2.2}$$

or relative supersaturation, σ

$$\sigma = {}^{\Delta c}/_{c^*} \tag{2.3}$$

Where c is the concentration,

c^* is the equilibrium concentration

2.1.2 Nucleation

Nucleation is the process with which nanoscopically small formations of the new phase that have the ability for irreversible growth to macroscopically large sizes are randomly generated

in a crystallisation system (Lewis, 2010). Mullin (2001) stated that, nucleation can be induced by agitation, mechanical shock, friction and extreme pressures within the crystallisation solution.

Nucleation can be either primary; nucleation that occurs in the absence of the parent crystals, or secondary; nucleation when crystals of the solute are already present or deliberately added into the system (Mullin, 2001).

Primary nucleation can also be classified as either homogeneous primary nucleation; nucleation in the absence of either solid foreign particles or crystals of its own type, or heterogeneous primary nucleation; nucleation in the presence of foreign particles (Kashchiev, 2000). For primary nucleation to occur in a system, a specific supersaturation known as a metastable supersaturation must be achieved (Mersmann, 2001). A metastable supersaturation refers to an equilibrium supersaturation (not changing with time) but is susceptible to fall into either higher or lower states with only slight interactions (Mersmann, 2001).

Secondary nucleation can be divided into two categories: the first category attributing the origin of the secondary nuclei to the parent crystal and these include initial or dust breeding, needle breeding and collision breeding (Biscans, 2004). The second origin being attributed to the solute and includes impurity concentration gradient nucleation and nucleation due to fluid shear (Biscans, 2004).

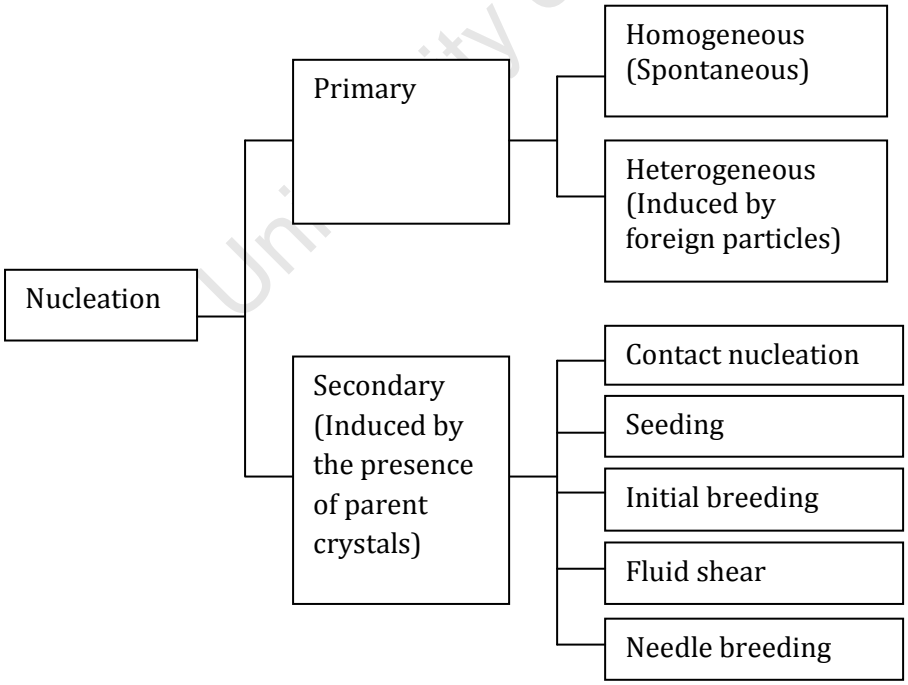

Figure 2.1. Nucleation schemes (Mullin, 2001).

2.1.3 Growth

This is mainly particle enlargement through the consumption of the supersaturation (Lewis, 2010). When particles larger than the critical nuclei have been formed in a supersaturated or super cooled system, crystal growth begins (Nyvlt, 1971). The size enlargement occurs by deposition of growth units from solution, preferably in layers and this happens if the chemical potential of the solid phase is less than that of the corresponding component in solution (Lewis, 2010; Nyvlt, 1971).

2.1.4 Agglomeration

Mullin (2001) described agglomeration as the tendency of small particles to cluster together. If the particles are small enough for the van der Waals forces to exceed the gravitational forces, inter-particle collision may result in permanent attachment (Mullin, 2001). Lewis (2010) also highlighted that, for agglomeration to occur, some supersaturation have to be present to aid the formation of the crystalline bridges between the agglomerating particles.

2.1.5 Precipitation of nickel

In an industrial scale, the process of nickel powder precipitation by high pressure hydrogen reduction is conducted in agitated vessels called autoclaves (Ntuli, 2008). These are normally operated in a semi-batch mode at temperatures between 180 and 210°C and pressures in the range of 2800 to 3500kPa (Willis and von Essen, 2000). Nickel seed on which further reduction occurs is introduced mainly by seeding or nucleation and is kept in suspension by mechanical agitation. Following seeding or nucleation, the autoclave is filled with a batch of the reduction liquor (nickel ammoniacal solution) containing between 50 to 95 g/l of nickel, typically with an ammonia to nickel molar ratio of 1.90 to 2.15 and an ammonium sulphate to nickel ratio of 1.80 to 2.20 (Willis and von Essen, 2000). This liquor is preheated to 180 to 210°C. The reduction process involves introducing pressurised hydrogen gas until the reduction solution is depleted of nickel. The hydrogen supply and the agitators are then stopped and the precipitated nickel powder allowed to settle. The spent solution is then decanted leaving the nickel powder behind which will act as the seed for the subsequent reduction batch. A fresh reduction solution is then introduced and the reduction process repeated for several batches called densifications until the nickel particles are too dense to be kept into suspension by the agitators. On average, about 50 to 60 densifications are conducted per cycle before the powder is finally discharged (Ntuli, 2008) and the cycle normally takes 3 to 5 days (Willis and von Essen, 2000).

The overall reaction for the nickel reduction process is as given by equation 2.4 below

$$Ni(NH_3)SO_4 + H_2 \rightarrow Ni^0 + (NH_4)_2SO_4 \qquad (2.4)$$

At an ammonia to nickel molar ratio of 2.0 to 2.5 for solutions with nickel to cobalt molar ratios of 35 or higher, the reaction is selective for nickel over cobalt (Willis and von Essen, 2000). Ntuli (2008) and Sobol (1993) have also suggested that, the reaction mechanism is electrochemical in nature involving electron transfer between the anodic and cathodic sites on the metal surface.

There are various factors that affect the nickel product quality during the reduction process. These include the reduction solution pH, foreign substances for example additives and impurities, hydrodynamics (agitation) in an autoclave, the rate of reaction and temperature (Ntuli, 2008).

The effects of agitation in an autoclave are discussed in this study. Since nickel precipitation occurs on the surface of the parent crystals (Willis and von Essen, 2000), it is therefore important that these crystals be kept in complete suspension so as to maximise the available surface area for the reaction. In this study, three separate process functions of the agitator were investigated. These include:

- suspension of the nickel crystals,
- attrition, and
- breakage of the nickel crystals.

Attrition and breakage play an important role in a nickel reduction by generating more surface area for the reduction process and at the same time reducing the particle sizes so that crystals can be kept in complete suspension.

2.2 INVESTIGATING THE CONCEPT OF 'JUST-SUSPENDED IMPELLER SPEED' FOR A NICKEL REDUCTION AUTOCLAVE

2.2.1 Aims of solid-liquid mixing

In solid-liquid systems, the primary objectives of mixing are to create and maintain a slurry and/or promote and enhance the rate of mass transfer between the solid and liquid phases (Paul et al., 2004). The mixing operation promotes suspension of solids, mass transfer across the solid-liquid interface, the dispersion of solid aggregates and control of particle size from the action of fluid shear as well as any abrasion due to particle-particle and impeller-particle impacts (Paul et al., 2004).

2.2.2 Hydrodynamics of solid suspension and distribution

Hydrodynamic characteristics in a reactor depend on factors such as the physical properties of the fluid, the operating parameters and the reactor geometry (Paul et al., 2004). One of the main design objectives is to maximize homogeneity at the minimum possible cost. In crystallisation and precipitation, solids are present in high concentrations. The crystallization reactors are usually operated in the semi-batch mode and the purity, productivity, selectivity of the reaction, size distribution and morphology depends on the relative rates of mixing (or homogenisation) compared to chemical reaction (Bujalski et al., 1999). In order to achieve optimum process efficiency, the solid particles must be kept in complete suspension to increase the contact area between the liquid and gas phases. Poor solid suspension reduces the surface area available for chemical reaction and as a result, the apparent density of the suspended particles rapidly increases (Bujalski et al., 1999). An increase in particle density makes it difficult for the particles to remain suspended during the agitation process.

From the hydrodynamics point of view, the most important parameter in reactor design is the minimum agitator speed (Paul et al., 2004). This is the speed at which all particles are in motion and no particles remain on the base of the vessel for more than 1 to 2 seconds (Zwietering, 1958; Zhu and Wu, 2002). This speed is usually called the just off-bottom suspension speed or critical impeller speed (N_{js}). Paul et al. (2004) defines the critical speed as the minimum speed at which the surface area of all the solids in the vessel is in complete contact with the liquid.

Generally, solids suspension studies focus on three aspects: off-bottom solids suspension (Zwietering, 1958), solids cloud height (Bittorf and Kresta, 2003) and solids concentration distribution (Barresi and Baldi, 1987a; Barresi and Baldi, 1987b). Off-bottom solids suspension has been investigated in tanks stirred with single impellers (Barresi and Baldi, 1987a; Barresi

and Baldi, 1987b; Zwietering, 1958; Armenante and Nagamine 1998; Bujalski et al., 1999) and with multiple impellers (Bujalski et al., 1999).

2.2.3 States of solid suspension and distribution

The degree of solids suspension in agitated vessels is generally classified into three levels (Paul et al., 2004):

- On bottom motion or partial suspension,
- Complete off-bottom suspension,
- Uniform suspension.

2.2.3.1 On-bottom motion or partial suspension

For this state, not all the surface area is available for chemical reaction or mass or heat transfer since particles are in constant contact with the base of the vessel (Paul et al., 2004). The complete motion of all particles around the bottom of the vessel is usually characterised by visual observation.

2.2.3.2 Off- bottom or complete suspension

This state of suspension is characterised by the complete motion of all particles in the vessel, with no particle remaining stationary on the base of the tank for more than 1 to 2 seconds (Paul et al., 2004). This condition is commonly known as the Zwietering 1s criterion. Under this condition, the maximum surface area of the particles is available for chemical reaction, mass or heat transfer (Paul et al., 2004).

One criterion that is typically used to investigate off-bottom solids suspension is the critical impeller speed (N_{js}). Armenante and Nagamine (1998) have reported that N_{js} depends on both impeller clearance and the ratio of the impeller diameter to that of the vessel (D/T). Sharma and Shaikh (2003) have shown that the change in the N_{js} with change in the impeller clearance depends on the clearance range. They noted that, at a low clearance, there is higher energy transfer efficiency from the impeller to the solids, and the ratio of the local energy to the overall energy dissipation per unit volume is constant.

2.2.3.3 Uniform suspension

Uniform suspension refers to the state of suspension at which particle concentration and particle size distribution are uniform throughout the vessel (Kasat and Pandit, 2005). Any further increase in agitation speed or power therefore, does not appreciably improve the solids distribution in the fluid (Paul et al., 2004). In process operations where a representative sample

of solids is required or a uniform concentration must be achieved, uniform suspension is often the desired state (Kasat and Pandit, 2005). In crystallization systems, for example, non-uniform solids concentration may lead to unacceptable high local supersaturation levels and subsequent non-uniformity in crystal growth (Paul et al., 2004).

2.2.4 The critical impeller speed, N_{js}

The pioneering, most extensive and influential study on solids suspension in unaerated stirred tanks was done by Zwietering (1958). In this work, the critical impeller speed was employed as a measure of off-bottom solids suspension conditions. Zwietering (1958) developed a correlation for determining the critical impeller speed for a range of system conditions (particle size, d_p, solids-liquid mass ratio, B, liquid kinematic viscosity, ν_L, solids density ρ_s, impeller diameter, D, and tank diameter, T as a scaling parameter) for an ungassed system as indicated in equations 2.5 and 2.6. The correlation was derived from dimensional analysis and the exponents estimated by fitting data for just-suspended impeller speed, N_{js} (Paul et al., 2004).

$$\mathrm{Re}_{\mathrm{imp}}^{0.1}\,\mathrm{Fr}^{0.45}\left(\frac{\mathrm{D}}{\mathrm{d_p}}\right)^{0.2}\mathrm{B}^{0.13}=\mathrm{S} \qquad (2.5)$$

where Re_{imp} is the impeller Reynolds number, $\mathrm{Re}_{\mathrm{imp}}=\mathrm{N_{js}D^2/\nu}$ and Fr the Froude number, $\mathrm{Fr}=\frac{\rho_l}{\rho_s-\rho_l}\,\mathrm{N_{js}^2\,D/g}$

The correlation is often expressed in dimensional form as follows:

$$\mathrm{N_{jsu}}=\mathrm{S}.\mathrm{d_p^{0.20}}.\mathrm{B^{0.13}}.\nu^{0.10}.\mathrm{g^{0.45}}\left(\frac{\rho_S-\rho_L}{\rho_L}\right)^{0.45}.\mathrm{D^{-0.85}} \qquad (2.6)$$

where S is a function of D/T, C/T and impeller type termed the Zwietering constant. This S parameter was given graphically for each impeller type against impeller size and clearance.

2.2.5 Effect of gassing on the critical impeller speed

The original form of the N_{js} correlation as developed by Zwietering (1958) was found to have limited applications. This correlation works well only for an unaerated stirred tank system. However, for an aerated system, it tends to underestimate the N_{js} values. This prompted research on aerated system to extend this correlation for gassed systems by various workers (van der Westhuizen and Deglon, 2007; van der Westhuizen and Deglon, 2008; Chapman et al., 1983a, Dutta and Pangarkar, 1995; Wong et al., 1987). It was noted that gas addition resulted in a linear increase in the critical impeller speed, N_{jsg} as indicted by the relation in equation 2.7.

$$N_{jsg} = N_{jsu} + a.Q \quad (2.7)$$

where Q is the aeration rate (m^3/min),

a is an aeration constant, and

N_{js} is the critical impeller speed (rpm).

Van der Westhuizen and Deglon (2008) developed a Zwietering type correlation for predicting N_{jsg} in a gassed mechanical flotation cell and came up with the correlations shown in equations 2.8 and 2.9. These correlations also show a linear relationship between N_{jsg} and Q.

$$N_{jsg} = K_{SL}.d_p^{0.33}.X^{0.17}.\left(\frac{\rho_s-\rho_L}{\rho_L}\right)^{0.70}.\left(\nu/\nu_w\right)^{0.05} + a.Q \quad (2.8)$$

OR

$$N_{jsg} = K_{SL}.d_p^{0.33}.X^{0.17}.\left(\frac{\rho_s-\rho_L}{\rho_L}\right)^{0.70}.\left(\nu/\nu_w\right)^{0.05} + (1 + K_G.Q) \quad (2.9)$$

where K_{SL} = 52rpm = function of T, D/T, C/T and impeller design

K_G = 0.36min = function of D/T, C/T and impeller design

a = 204 = function of T, D/T, C/T and impeller design.

The Zwietering-type correlations developed by van der Westhuizen and Deglon (2008), predicted their experimental measurements well within 10% of the experimental data. However, it should be noted that Zwietering (1958) used the solid-liquid mass ratio (B) while van der Westhuizen and Deglon (2008) used solids mass concentration (X) as a measure of solids concentration.

Weiss and Schubert (1989) also determined critical impeller speed measurements at different aeration rates in a 54l induced-air mechanical flotation cell, using a double finger impeller at low clearance. They also found a linear increase in critical impeller speed with increased gassing rates. Van der Westhuizen and Deglon (2008) used their data and calculated an 'a' value and found it to be about 144.

Nienow et al. (1992) on the other hand, explored a different approach of incorporating the effect of air on the just off-bottom suspension condition in which the 'a' was taken as being proportional to the ungassed critical impeller speed (a α N_{jsu}). Van der Westhuizen and Deglon (2008) incorporated this into equation 2.7 to give equation 2.10.

$$N_{jsg} = N_{jsu}(1 + K_G.Q) \quad (2.10)$$

where K_G = 0.36min

However, the study conducted by Zhu and Wu (2002) revealed that the difference between the just off-bottom suspension speeds with and without gas sparging is not linearly related to the gassing rate and the relation is system dependant. Several studies had proposed a linear relationship between ΔN_{js} and gas sparging rate, *Q* that is:

$$\Delta N_{js} = N_{jsg} - N_{jsu} = a.Q \quad (2.11)$$

However, the value of '*a*' varied significantly from one study to another (Zhu and Wu, 2002). For the commonly used Rushton impellers (DT6), the value was found to be 0.94, 0.65, 2.03 and 3.75 from the studies by Chapman et al. (1983b), Bujalski et al. (1988), Wong et al. (1987) and Dutta and Pangarkar (1995), respectively (Zhu and Wu, 2002). The large variation in the '*a*' values throws doubt on the validity of equation 2.3 to describe three phase systems and for scale up. Thus Zhu and Wu (2002) developed a non dimensional correlation (the relative just off-bottom suspension speed, *RJSS*).

$$RJSS = {N_{jsg}}/{N_{jsu}} \quad (2.12)$$

This was found to be dependent only on the just suspension aeration number, Na_{js}.

$$Na_{js} = {Q}/{N_{js}D^3} \quad (2.13)$$

And for DT6 impellers, the relation was found to be,

$$RJSS = 1 + mNa_{js}^{n} \quad (2.14)$$

where the values of the constants *m* and *n* were found to be 2.6 and 0.7 respectively

The relation given by equation 2.14 was found to be independent of the impeller size, solids size, solids loading and tank size and can be adopted for scaling up laboratory data to full-scale mixing vessels. When the just off-bottom suspension speed was plotted in the form of RJSS as a function of Na_{js}, data from different experiments almost collapsed into one curve (Figure 2.2). This demonstrates that, regardless of the impeller size, solids size, solids loading and tank size, a similar RJSS value is expected for the same Na_{js} value. However, Na_{js} also depends on the impeller diameter (D) (Zhu and Wu, 2002). The independence of RJSS reflects that the effect of

impeller size, solids concentration, solids density, particle size, tank size and other parameters are combined in the relative just suspension speed N_{jsg}/N_{jsu} (Zhu and Wu, 2002).

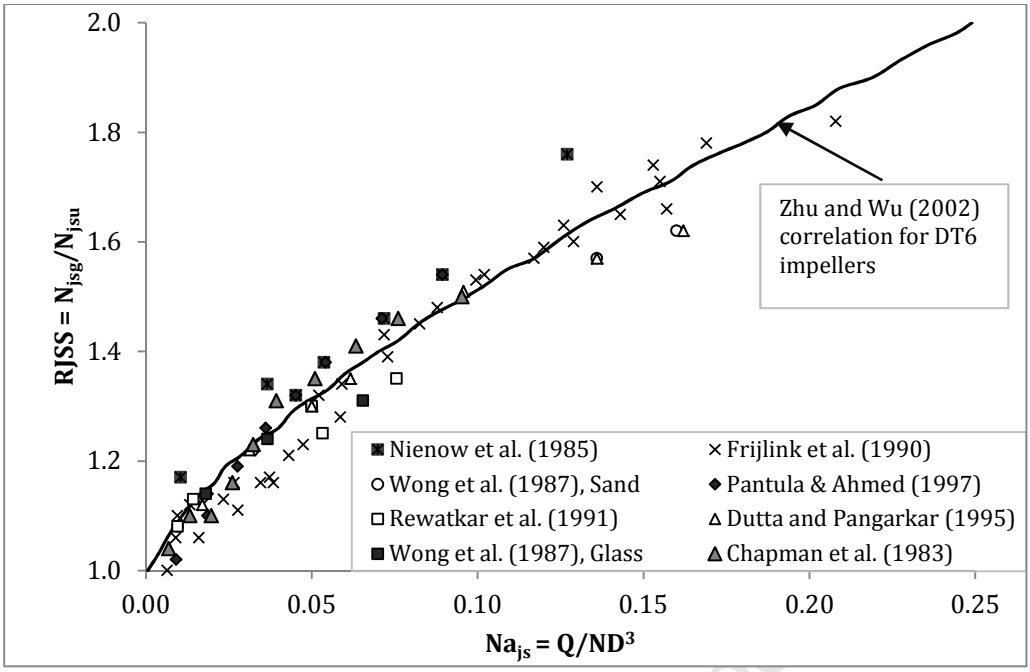

Figure 2.2. RJSS as a function of Na_{js} (Zhu and Wu, 2002)

Chapman et al. (1983b) also studied the effects of impeller geometry on the just-suspended condition. Their study revealed that downward pumping impellers require the least energy to suspend solids at low gas flow rates (Q < 0.3vvm) than disc turbines and upward pumping impellers. However, at high gas rates (Q > 0.5vvm), they were no longer energy efficient and were subject to gross flow instability. Upward pumping impellers, on the other hand, were found to be the least energy efficient at low gassing rates but no instabilities were experienced at higher gas rates. The energy required for particle suspension using upward pumping impellers was found to be independent of the gassing rate and therefore, at high gas rates, these were regarded as the most efficient.

2.2.6 Mixing reactor geometry

A conventional stirred reactor consists of a vessel equipped with a rotating mixer (Paul et al., 2004). The vessel is generally a vertical cylindrical tank which can have a flat or profiled (dished) base. According to Paul et al. (2004), the degree of the bottom base curvature for profiled tanks is dependent on the intended operation. For liquid systems, flat bottomed tanks are commonly used whilst dished or elliptically bottomed tanks are preferred for solid-liquid or solid-liquid-gas systems to aid solids suspension. Most studies on solid-liquid-gas mixing have been conducted in both flat and profiled tanks with conventional Rushton impellers (Armenante

and Nagamine, 1998; Chapman et al., 1983; Bujalski et al., 1988; Wong et al., 1987; Dutta and Pangarkar, 1995; Sharma and Shaikh, 2003).

2.2.6.1 Impeller characteristics

Impellers are classified as either high shear (radial) or high flow (axial) pumping (Ochieng, 2005). Radial flow impellers have been regarded as efficient for gas dispersion and axial flow downward pumping impellers for particle suspension (Armenante and Nagamine, 1998; Ochieng, 2005). For both particle suspension and gas dispersion, Rushton impellers have also been proved to be more efficient compared to axial downward pumping impellers at high aerations (Paul et al., 2004).

Perry et al. (1984) have stated that one of the basic principles of the operation of the impeller is that "a large impeller running at a slow speed gives a large circulating capacity and a low fluid shear rate, while a small impeller running at high speeds gives a high fluid shear and a low total circulating capacity". The choice of the ratio of the impeller diameter (D) to tank diameter (T) determines the way in which the power input is distributed (Perry et al., 1984). However, Paul et al. (2004) highlighted that an optimum impeller D/T ratio for mixing is 1/3.

The impeller clearance also has an influence on the mixing hydrodynamics. An optimum clearance of approximately one third of the liquid height in the mixing tank is recommended (Paul et al., 2004).

2.2.6.2 Baffles

Wall baffles are generally installed for transitional and turbulent mixing. Baffles aid axial mixing between the top and the bottom of the tank by preventing fluid swirl (also called solid body rotation) (Ochieng, 2005). For four baffled reactors, these are normally staggered at 90^{o} to each other, with a baffle width of one twelfth to one tenth of the tank diameter being recommended (Ochieng, 2005).

2.2.6.3 Gas sparging

A ring sparger is generally preferred for uniform gas dispersion throughout the vessel. Typically, the sparger diameter should be less than the impeller diameter and an optimum diameter of 0.8 times the impeller diameter is recommended (Paul et al., 2004).

2.2.7 Mixing and nickel precipitation

The main functions of mixing in a nickel reduction autoclave include (Roberts, 2004):

- to enhance mass transfer of hydrogen from the vapour space into the liquor,

- to suspend nickel solids and expose them to the chemical environment (supersaturation, additives, dissolved hydrogen),
- to supply the turbulent energy required to cause shear and breakage of nickel agglomerates, thus reducing the size of the particles so that they can be easily suspended.

According to Paul et al. (2004), "Successful crystallisation operations depend on identifying the mixing parameters for the most critical aspects of the process and then evaluating whether those parameters will be satisfactory for the other aspects". For a nickel crystallisation system, attrition and homogenous mixing are of importance. It is therefore important to evaluate the respective impeller speeds required for suspension and attrition of the nickel crystals.

2.3 ESTABLISHING THE 'ATTRITION SPEED' FOR A NICKEL REDUCTION AUTOCLAVE

Attrition in crystallisation is defined as the "removal of asperites or fines from the surface of the crystals in solution such that there is only a gradual change in the size of the parent crystal" (Biscans, 2004). The abrasion mechanism of fracture is thus dominant in this case.

2.3.1 Theory of attrition

Attrition is dependent on crystal-crystal impact, crystal-impeller impact and crystal-wall impact (Biscans, 2004). It is assumed to produce a localised fracture of the parent crystal, which is just slightly damaged, generating, at the same time, a number of much smaller fragments (Bravi et al., 2003). During the operation of a crystallizer, when the absolute value of the impact energy between the suspended solids and the impeller tips is low, an elastic deformation of the crystal occurs (Bravi et al., 2003). As the impact energy increases, first the resistance of some spots on the crystal surface is overcome causing attrition by abrasion fracture, after which the resistance of the whole crystal is exceeded, and the crystal is shattered according to the breakage mechanism (Bravi et al., 2003). In modeling studies, the secondary nucleation rate was found to be dependent on the stirrer rotation rate (or the power input), the solid content of the slurry and the supersaturation (Bravi et al., 2003; Gahn and Mersmann, 1995; Biscans, 2004).

The total rate of fine particle generation $(dn/dt)_{tot}$ in a stirred vessel can be expressed as follows (Biscans, 2004):

$$\left(\frac{dn}{dt}\right)_{tot} = \left(\frac{dn}{dt}\right)_{imp} + \left(\frac{dn}{dt}\right)_{turb} \qquad (2.15)$$

where $(dn/dt)_{imp}$ represents the rate of fine particle generation by means of impact, and

$(dn/dt)_{turb}$ is the rate of fine fragment generation by turbulent fluid forces.

Since in dilute suspensions, crystal-crystal and crystal-wall impacts are assumed to have a negligible effect on attrition, the term $(dn/dt)_{imp}$ thus describes the rate of fine particle generation by means of crystal-impeller impact (Synowiec, 2002).

In dilute suspensions, the crystal-crystal interactions can be assumed to be negligible (Gahn and Mersmann, 1995) and as a result, crystal–impeller contacts are the main cause of secondary nucleation. Under the same conditions, attrition will also occur in high density suspensions. The crystal–impeller impact in a stirred vessel depends on several factors (Biscans, 2004):

- the stirring intensity,
- the impact energy applied relative to the unit energy needed to produce one attrition fragment from the crystal surface,
- the impact probability between a crystal of given size and an impeller,
- the material properties of the crystal and the impeller,
- the solids loading which corresponds to the total number of parent particles in the vessel. This influences the relative contribution of crystal–crystal collisions (dominant with high densities of crystals) and crystal–impeller collisions.

According to Bravi et al. (2003) and Gahn and Mersmann (1995), the highest impact velocities of particles in a suspension crystallizer are generally experienced when crystals collide with the impeller. Thus, crystal-impeller impact has the greatest contribution on attrition.

Since all dimensions of the impeller are larger than the crystal, the contact can be assumed to be equivalent to the impact of a crystal on another flat target (Figure 2.3).

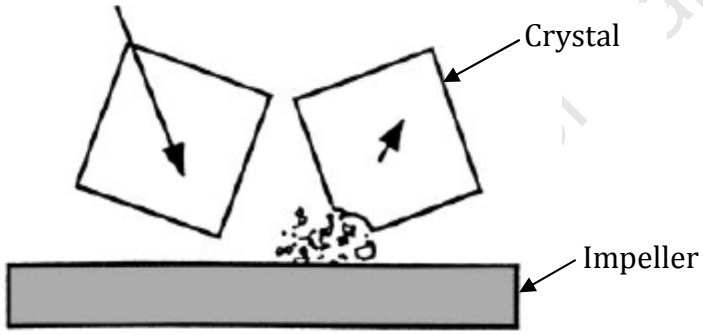

Figure 2.3. Schematic representation of attrition (Gahn and Mersmann, 1995)

Different techniques by various researchers have been used to investigate attrition in different systems (Bravi et al., 2003; Gahn and Mersmann, 1995; Marrot and Biscans, 2001). Gahn and Mersmann (1995) gave a quantitative description of attrition by use of a Vickers indentation test to investigate brittle fracture of solids in a crystallisation process. This was done by comparing the work done to cause breakage on the crystal during loading of the indenter against the impact energy caused by the impellers on the crystals. The impact energy was calculated using the formula,

$$E_c = 0.5\rho_c L^3 u^2. \quad (2.16)$$

where E_c is the impact energy assumed to be equal to the kinetic energy of the crystals (J),

ρ_c is the crystal density (kg/m^3),

L is the fragment size (m), and

u is the velocity assumed to be equal to the impeller tip speed (m/s).

The work done by the indenter to cause onset of breakage on a crystal was calculated from the equations,

$$W_c = 6.0 \times 10^{-2}\left(F_{0.5}^3/H_v\right)^{1/2} \quad (2.17)$$

and, $$H_v = 1.854\frac{F}{d^2} \quad (2.18)$$

where W_c is the critical work to form cracks (J),

$F_{0.5}$ is the load where 50% of the indentations have produced cracks (N),

H_v is the Vickers hardness (N/m^2),

F is the indentation force (N),

d is the average diagonal of the plastic indentation (m),

The factor 1.854 results from the geometry of the indenting diamond.

Bravi et al. (2003) also correlated the attrition behaviour of crystals in a stirred vessel to their mechanical properties based on size distribution of the fragments. In their work, they employed a similar approach to the work of Gahn and Mersmann (1995). Their approach to the attrition problem was based on the evaluation of stress resistance of the material, comparing the impact energy to that required to crush the particles. They also assumed the impact energy to be equal to the kinetic energy, E_c of the crystals. The impact energy was related to the energy required to crush a particle, E_p (J) which was calculated as the product of the loading compression, F (N) and the deformation from the loading point, z_d (m) (Bravi et al., 2003).

$$E_p = Fz_d \quad (2.19)$$

The deformation was taken as:

$$z_d = K_v\frac{F}{LY_p} \quad (2.20)$$

where K_v is a parameter dependent only on the Poisson ratio,

Y_p is the Young's modulus (N/m^2).

In order to determine the stress resistance of the investigated materials, Bravi et al. (2003) performed crush tests on single crystals of each material, using a JJ Loyd instrument, model T20000, at an advancement rate of 0.0083mm/s. The average values of the loading compression, F were obtained from five repeated measurements.

In the work of Marrot and Biscans (2001), the attrition propensity of crystals in suspension was also studied. The impact attrition in crystallizers was simulated by impacting a single crystal in solution, on an immersed target. Two types of parameters were studied and these include those related to the operating conditions (impact velocity, number of impacts and type of target) and those related to the properties of the crystals and of the solution in which they were contained. The controlled parameter was the velocity of impact. This was recorded by use of a high speed camera (Kodak Ektapro with Nikkon macro lens). The rate of attrition was found to increase with an increase in the velocity of impact and the impact energy. The impact energy, E_c (J) was calculated using a similar kinetic energy equation to that used by Gahn and Mersmann (1995).

$$E_c = \frac{1}{2} m_p u^2 \qquad (2.21)$$

where m_p is the mass of crystal (kg),

u is the impact velocity (m/s).

This dependence of the rate of attrition on the velocity of impact was in agreement with the work of Gahn and Mersmann (1999). Gahn and Mersmann (1999) gave a quantitative description of the attrition process in terms of the volume of attrition fragments produced. The total volume, V_a of fragments was found to depend on the impact energy, E_c (J) by the relationship shown in equation 2.22:

$$V_a = \frac{2 H_v^{2/3} k}{3 \mu \Gamma} E_c^{\frac{4}{3}} \qquad (2.22)$$

where H_v is the hardness (Pa),

k is an efficiency constant,

μ is the shear modulus,

Γ is the fracture resistance (J/m^2).

2.3.2 The role of attrition in a nickel reduction autoclave

During the nickel reduction process, nickel seeds on which further reduction occurs are introduced mainly by seeding or attrition of the parent product (Ntuli, 2008). Attrition therefore, plays an important role in a nickel reduction autoclave in the generation of more surface area for the reduction process.

To investigate attrition, two approaches were used in this study: the 7l mixing set up and the Vickers microhardness test.

2.3.3 Measures of attrition in the 7l mixing set up

In the 7l mixing set up, the approach to the problem of attrition was based on the evaluation of the minimum impeller speed required to cause attrition of crystals in a stirred vessel. The presence of attrition was monitored through particle size distribution measurements of the attrition product. The main parameters of interest were the impeller tip speed and the impact energy. This test was based on the assumption that, in crystallisers, "loading occurs by impact, with the maximum impact velocities between impeller and crystals being similar to the velocity of the impeller as measured by the impeller tip speed" (Gahn and Mersmann, 1995).

2.3.3.1 Impact energy

The minimum impeller rotational speed (rpm) sufficient to cause attrition of the crystals was transformed into impeller tip speed, which was then assumed to be the velocity of impact. The impeller tip speed or impact velocity was calculated using the following equation:

$$u = \pi ND \tag{2.23}$$

and the impact energy from the following formula (Bravi et al., 2003):

$$E_c = 0.5\rho_c L^3 u^2 \tag{2.24}$$

Where E_c is the impact energy assumed to be equal to the kinetic energy of the crystals (J),

ρ_c is the crystal density (kg/m^3),

L is the fragment size (m),

u is the impact velocity (m/s),

N is the impeller speed (rps),

D is the impeller diameter (m).

The impeller Reynolds number (Re_{imp}) and the impeller dissipated power per unit mass (ε) were the other two parameters calculated to characterize the attrition.

The impeller Reynolds number was calculated using the following formula:

$$\mathrm{Re_{imp}} = \frac{\mathrm{ND^2}}{\nu} \tag{2.25}$$

where ν is the slurry kinematic viscosity (m^2/s).

The impeller dissipated power per unit mass (ε) (W/kg) was calculated using equation 2.26 (Spicer et al., 1996):

$$\varepsilon = \frac{\mathrm{N_p N^3 D^5}}{\mathrm{V_c}} \tag{2.26}$$

where N_p is the impeller power number, equal to 1.27 for a pitched blade in the turbulent regime and V_c is the total effective volume of the reactor (m^3).

2.3.3.2 Particle size distributions

In order to confirm the existence of attrition, it was necessary to transform the volume % particle size distribution measurements of the product obtained from a laser diffraction instrument into number distributions, using equation 2.27.

$$\mathrm{N(L)} = \frac{\text{vol \%} * \text{conc (vol \%)}}{\mathrm{K_v * L^3}} (\#/\mathrm{m^3}) \tag{2.27}$$

Where K_v is the volume shape factor, assumed to be equal to π/6, L is the average length of an interval (m) and *vol %* and *conc (vol %)* were obtained from the volume distribution measurement (Lewis, 2010).

The number distributions were also transformed into cumulative number distributions and total number evolution (zeroth moment). The cumulative number distribution, *N(L)* was calculated as follows (Lewis, 2010):

$$\mathrm{N(L)} = \int_0^{\mathrm{L}} \mathrm{n(L)dL} \tag{2.28}$$

and the zeroth moment, m_0, as (Lewis, 2010):

$$\mathrm{N_T} = \mathrm{m_0} = \int_0^{\infty} \mathrm{n(L)\, dL} \tag{2.29}$$

where N_T is the total number ($\#/m^3$)

m_0= zeroth moment (equal to total number) ($\#/m^3$)

$n(L)$ = the number density of particles (#/m^4)

dL = the interval size (m).

2.4 ESTABLISHING THE 'BREAKAGE SPEED' FOR A NICKEL REDUCTION AUTOCLAVE

Breakage in this study was taken as the fragmentation of particles into two or more smaller entities of significant size, resulting in a rapid disappearance of the original particles (Biscans, 2004).

2.4.1 The theory of impact breakage

One of the principal size reduction mechanisms in comminution processes is impact breakage (Bbosa, 2007). In conventional engineering, stress/strain curves are generally used to define the material specific elongation (strain) under force per unit area (stress) (Bbosa, 2007). A typical stress/strain curve is illustrated in Figure 2.4. The same graph can be used to describe both the tensile and compressive behavior of a material and traditionally, parameters such as yield stress, Young's modulus, ultimate tensile stress and Poisson's ratio can be extracted (Bbosa, 2007). These parameters are then used to describe measures of material strength properties.

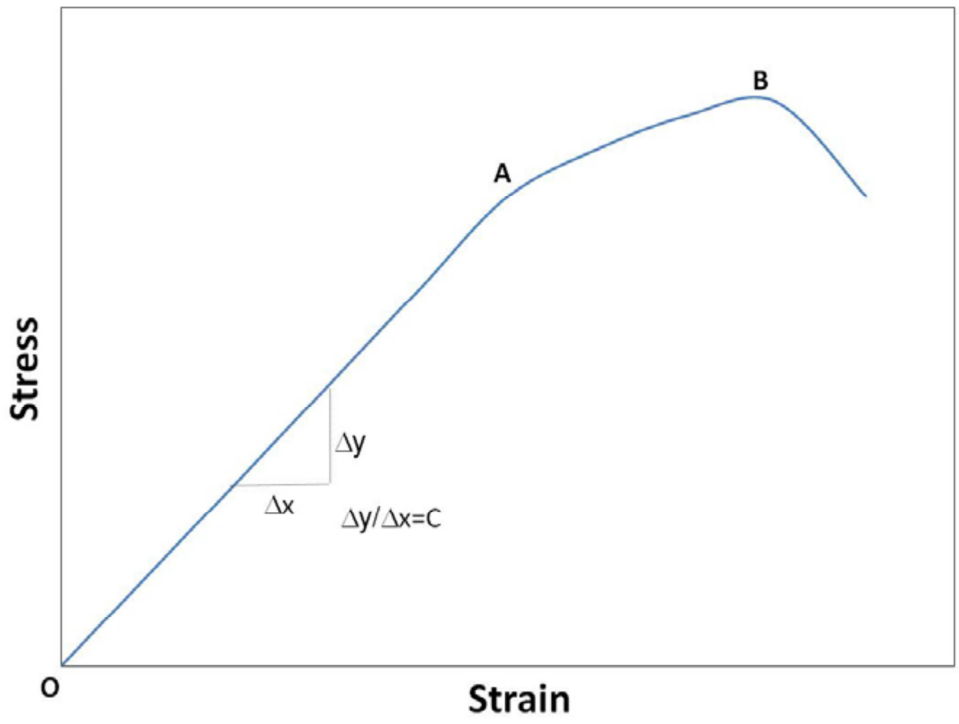

Figure 2.4. Typical stress/strain curve of a material (Bbosa, 2007)

From Figure 2.4, region OA represents the elastic region of a material for which the stress is directly proportional to the strain. The gradient of the region gives a constant known as the Young's modulus (measure of material elasticity). Because metals are ductile in nature, they tend to have lower values compared to rocks which exhibit brittle behavior (Bbosa, 2007).

At point A, the material reaches the stress value known as the yield stress after which it enters a region of plastic deformation AB. In this plastic region, the material experiences permanent deformation without fracturing. This region extends for a brief period until the critical stress value at point B is reached. This value is known as the ultimate compressive stress (UCS) which is the maximum stress a material can withstand before failure.

Another commonly quoted value of interest is the Poisson's ratio which is taken as the ratio of the longitudinal strain to the transverse strain. This value indicates the tendency of a material to displace in the direction of the load when subjected to some stress.

2.4.2 Application of impact breakage research to comminution

A number of parameters have been introduced to describe various characteristics of materials. Based on the work of Tavares and King (1998), particle fracture energy, particle strength and particle stiffness are measures that can be applied to impact breakage.

2.4.2.1 Particle fracture energy (E_f)

This is the total energy absorbed by the particle under impact until first fracture (Bbosa, 2007). It is defined as the area under the force deformation curve until the point of initial breakage. The integral given in equation 2.30 is used to express this relationship (Tavares and King, 1998).

$$E_f = \int_0^{\Delta_c} F_c d\Delta \tag{2.30}$$

where F_c is the fracture force,

Δ is the particle deformation,

Δ_c the deformation at fracture.

2.4.2.2 Particle strength (σ_p)

This is the maximum stress that a particle can withstand before failure (Bbosa, 2007). This can be derived from the ultimate tensile/compressive strength of the material. Since stress is defined as force per unit area, particle strength is thus taken to be the force to failure divided by the cross-sectional area of the particle whose diameter is given by the geometric mean size or distance between loading points (d_p). A simplified equation for this is shown below (Tavares and King, 1998).

$$\sigma_p = \frac{2.8F_c}{\pi d_p^2} \tag{2.31}$$

where F_c is the force to failure (N),

d_p is the geometric mean size or distance between the loading points (m).

2.4.2.3 Particle stiffness (k_p)

Particle stiffness is a material property which is a measure of its resistance to elastic deformation by an applied force (Ashby, 1999). It can also be regarded as a measure of the resistance of a material to crack propagation and is depended on the inter-atomic and inter-molecular bonds within a material (Ashby, 1999). This parameter gives a theoretical estimate of the force deformation relationship for an idealised spherical particle which is useful for modelling and is derived from the Hertzian theory of elastic contact (Tavares and King, 1998). It has been found to show similarity to fracture toughness (Bbosa, 2007) and can be roughly calculated using equation 2.32.

$$k_p = \frac{Y_p}{1-\mu_p^2} \tag{2.32}$$

where Y_p is the Young's modulus of the material, and

μ_p is the Poisson's ratio.

2.4.2.4 Poisson's ratio (μ_b)

The Poisson's ratio is defined as the negative of the ratio of the lateral strain to the axial strain in an axial loading (Bbosa, 2007) (equation 2.33).

$$\mu_b = \frac{-d\varepsilon_{lat}}{d\varepsilon_{axial}} \tag{2.33}$$

Where ε_{lat} is the lateral strain,

ε_{axial} is the axial strain.

Its value is commonly taken as 1/3 for materials with a shear modulus, $G \approx 3/8Y_p$ and a bulk modulus, $K \approx Y_p$. The Poisson's ratio is also used when estimating the bulk and shear modulus from the Young's modulus by simple relationships given in equation 2.34.

$$G = \frac{Y_p}{2(1+\mu_p)} \quad \text{and} \quad K = \frac{Y_p}{3(1-2\mu_p)} \tag{2.34}$$

2.4.3 Previous research

Different techniques have been used by various researchers to investigate breakage of mineral ores under compressive and tensile stresses (Tavares and King, 1998; Bourgeois and Banini,

2002; Kapur et al., 1997; King and Bourgeois, 1993; Tavares, 2004; Tavares, 1999; Al-Mousawi et al., 1997).

Al-Mousawi et al. (1997) used a split Hopkinson pressure bar technique for dynamic testing of mineral ores under both compressive and tensional stresses. The split Hopkinson pressure bar contains some strain gauges installed to record the strain histories during the impact tests. During a compression test, the specimen was positioned between two long uniform cylindrical pressure bars and subjected to a load. The strain experienced by the specimen during loading was recorded by the strain gauges and the breakage parameters were extracted from the strain histories.

Genc et al. (2004) on the other hand characterised single particle impact breakage by drop weight testing. From their study, it was concluded that drop weight test methods are a useful and practical way of evaluating the impact strengths of materials. Their results were found to be useful in the mathematical modelling of autogenous and ball milling.

Tavares and King (1998) also investigated the effect of material type, particle size and particle shape on the three fundamental fracture characteristics (particle fracture energy, particle strength and particle stiffness) of brittle materials during single particle fracture. An impact drop weight tester (ultrafast load cell) was used in this test. The results of these breakage parameters showed a scatter which was attributed to the fact that "particle fracture energy and particle strength are structure-sensitive properties that are strongly affected by the presence of critical flaws and cracks in the zones of high stress in the material" (Tavares and King, 1998). The typical results obtained for fracture energy are shown in Figure 2.5. Particle size was also found to influence these parameters. The argument was that, "as particle size decreases, cracks progressively disappear which results in increases in both strength and particle fracture energy" (Tavares and King, 1998).

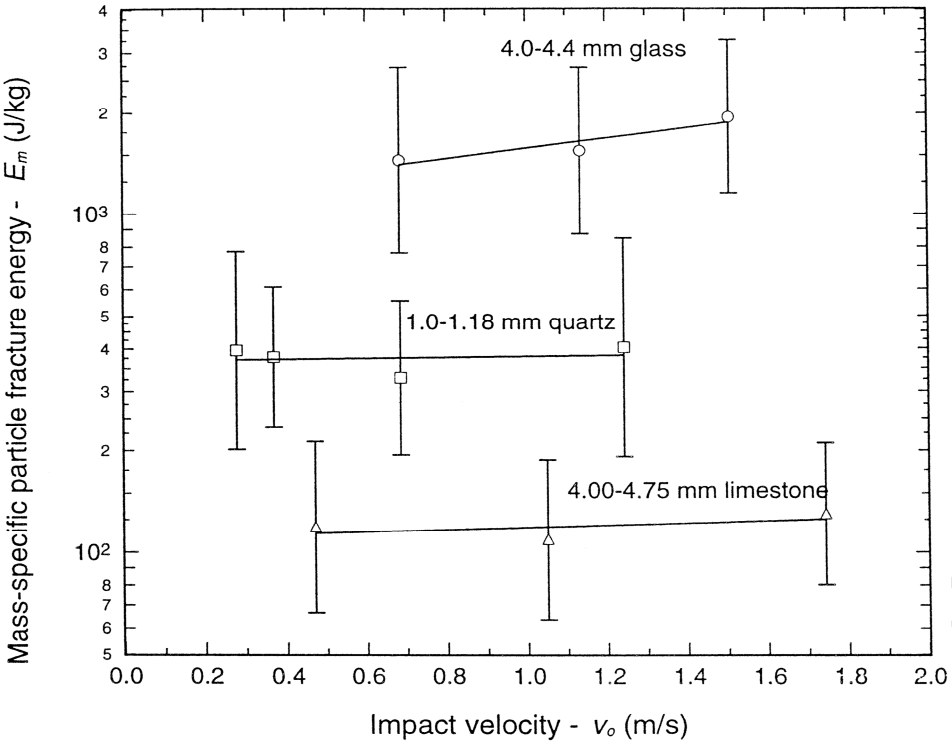

Figure 2.5. Fracture energy distribution of different materials. Vertical lines represent the standard deviations of the distributions (Tavares and King, 1998).

However, particle stiffness at a microscale level is not a structure-sensitive property as it depends on the atomic and molecular structure of the material and therefore, is an intrinsic property of the material (Tavares and King, 1998). In that case, consistent results are expected. At macroscale level, however, it was found to be affected by the microstructural features such as pores and cracks within the material (Tavares and King, 1998). This argument explained the scattered results that were obtained in their study.

2.4.4 The ultrafast load cell (UFLC)

The UFLC is a drop weight tester consisting of a long steel rod equipped with strain gauges on which a single particle or a bed of particles is placed and impacted by a falling steel ball (Figure 2.6) (Tavares and King, 1998). The compressive wave resulting from the impact travels down the rod and is sensed by the solid state strain gauges resulting in a voltage change in the Wheatstone bridge circuit. The voltage change is then recorded as a function of time using a digital oscilloscope. Given that the mechanical and physical properties of the rod as well as the bridge and gauge factors are known, the measured voltage outputs are then transformed into force-time histories (Tavares and King, 1998).

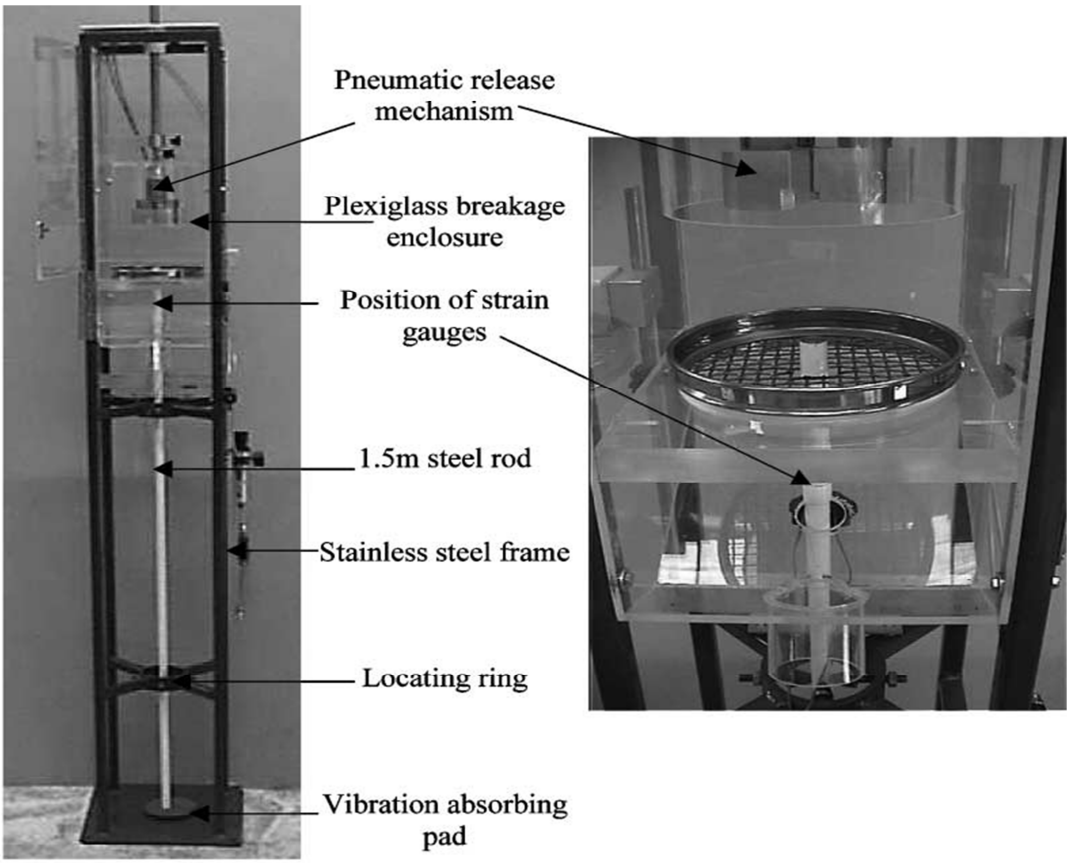

Figure 2.6. Ultrafast load cell layout (Bourgeois and Banini, 2002)

The compression experienced by a particle due to impact is not determined directly. It is calculated from the momentum balance of the falling steel ball and the deformation of the steel rod (Tavares and King, 1998). The momentum balance that is used to determine the motion of the striking ball during impact is shown below (Tavares and King, 1998):

$$m_b \frac{d^2 u_b}{dt^2} = -F_b + m_b g \qquad (2.35)$$

where u_b is the position of the centre of gravity of the ball,

m_b is the ball mass,

F_b is the force exerted by the particle on the ball,

g is the acceleration due to gravity.

When equation 2.35 is integrated subject to initial conditions at the instant of contact (t=0):

$$\frac{du_b}{dt} = v_0 \text{ and } F_b = 0 \tag{2.36}$$

gives:

$$\frac{du_b}{dt} = v_0 + gt - \frac{1}{m_b}\int_0^t F_b(t)\,dt \tag{2.37}$$

where v_0 is the velocity of the striker at the instant of contact.

The velocity of the striker is calculated as $v_0 = (2gh)^{1/2}$ since free-fall conditions prevail where h is the initial distance between the bottom of the ball and the top of the particle (Tavares and King, 1998).

Assuming that there is one-dimensional wave propagation in the rod, the forces and deformations of the top of the rod are related by equation 2.38 (Tavares and King, 1998):

$$\frac{du_r}{dt} = \frac{1}{\rho_r A_r C_r} F_r(t) \tag{2.38}$$

where ρ_r is the density of the rod,

A_r is the cross-sectional area of the rod,

C_r is the wave velocity of the rod.

By neglecting the inertia of the particle during impact, force continuity exists at the surfaces in contact ($F_r = F_b = F$) and subtraction of equations 3.10 and 3.11 and integration yields the following expression (Tavares and King, 1998):

$$\alpha(t) = v_0 t + \frac{gt^2}{2} - \frac{1}{m_b}\int_0^t\int_0^\tau F(T)\,dT d\tau - \frac{1}{\rho_r A_r C_r}\int_0^t F(\tau)\,d\tau \tag{2.39}$$

where $\alpha = u_b - u_r$ as illustrated in Figure 2.7,

The net approach between the centre of gravity of the falling ball and a point in the rod distant from point of impact is given by equation 2.39 (Tavares, King 1998). α therefore, represents the overall deformation in the vicinity of the contact as a result of the compression of the particle and the local indentations of the ball and the anvil. It is calculated using the initial impact velocity, the ball mass and the experimentally determined force-time histories (Tavares and King, 1998).

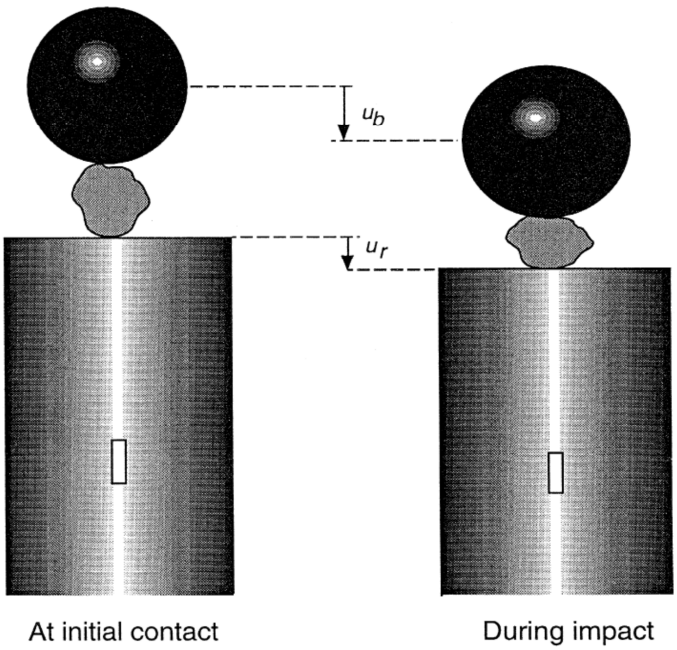

Figure 2.7. Illustration of the principle used to calculate the deformation experienced by a particle during impact breakage on the UFLC (Tavares and King, 1998).

2.4.5 Fracture characteristics obtained from the UFLC

2.4.5.1 Fracture energy (E_f)

Substituting equation 2.39 for Δ=α into equation 2.30, the expression for the energy required to break the particle will be given as:

$$E_f = \nu_0 \int_0^{t_c} F(\tau)d\tau + g\int_0^{t_c} F(\tau)\,\tau d\tau - \frac{1}{2m_b}\left(\int_0^{t_c} F(\tau)\,d\tau\right)^2 - \frac{1}{\rho_r A_r C_r}\int_0^{t_c} F^2(\tau)d\tau \qquad (2.40)$$

where τ is an integration variable.

Setting α=Δ requires that the local indentations in the ball and the UFLC rod are negligible (Tavares and King, 1998).

The output voltage, V_0 from the strain gauges is transformed into force by the relationship given in equation 2.41 where F is the contact force (N), A_r is the cross sectional area of the rod (m^2), Y_r is the Young's modulus of the rod (Pa), V_i and V_o are the input and output voltages of the Wheatstone bridge respectively (V), GF_{bridge} is the proportionality constant known as the bridge factor which is function of the gauge factor of the strain gauges used.

$$F(N) = \frac{A_r Y_r}{GF_{bridge}}\frac{V_0}{V_i} \qquad (2.41)$$

The GF_{bridge} is obtained during calibration by conducting an impact between the ball bearing and the impact load cell in the absence of a sample and recording the maximum output voltage, $V_{o,max}$ obtained. The Hertz's law of contact described by equation 2.42 is used to predict the maximum contact force, $F_{Hertz,max}$. The GF_{bridge} will then be estimated from equation 2.43.

$$F_{Hertz,max} = k\alpha^{3/2} \tag{2.42}$$

where α is the contact deformation and k the proportionality constant that depends on geometry and the elastic property of the materials in contact.

$$GF_{bridge} = \frac{A_r Y_r}{V_i} \frac{V_{0,max}}{F_{Hertz,max}} \tag{2.43}$$

2.4.5.2 Particle strength (σ_p)

Since the crystals are assumed to be spherical in this work, the particle strength is calculated as fracture force divided by particle cross-sectional area.

$$\sigma_p = \frac{4F_c}{\pi d_p^2} \tag{2.44}$$

2.4.5.3 Particle stiffness (k_p)

Equation 2.21 can be used to directly calculate the particle stiffness if the Young's modulus and the Poisson's ratio are known. However, they are not known and therefore the procedure described below is used.

From the Hertzian law of contact, the relationship between force and deformation for a spherical or nearly spherical particle compressed between falling ball and the rod is given by (Tavares and King, 1998):

$$F = \frac{K_e d_p^{1/2}}{3} \alpha^{3/2} \tag{2.45}$$

where K_e is the local deformation coefficient of the Hertzian contact given by (Tavares, King 1998),

$$K_e = \frac{k_p k_{b,r}}{k_p + k_{b,r}} \tag{2.46}$$

where $k_{b,r}$ is the stiffness of the ball or rod and k_p is the particle stiffness .

The particle fracture energy can be related to the deformation at fracture and the local deformation coefficient by substituting equation 2.45 into 2.30 and integrating to obtain the following expression:

$$E_f = \frac{2}{15} d_p^{1/2} K_e \alpha_c^{5/2} \quad (2.47)$$

By substituting equation 2.45 into 2.47 and rearranging, K_e can be related to the critical load and the particle fracture energy by (Tavares and King, 1998),

$$K_e = \left(0.576 \frac{F_c^5}{d_p E_f^3}\right)^{1/2} \quad (2.48)$$

The stiffness of the particle can then be calculated by solving equation 2.46 giving,

$$k_p = \frac{K_e k_{b,r}}{K_e - k_{b,r}} \quad (2.49)$$

where $k_{b,r} = \frac{Y_{b,r}}{1-\mu_{b,r}^2}$

CHAPTER 3 : INVESTIGATING THE CONCEPT OF 'JUST-SUSPENDED IMPELLER SPEED' FOR A NICKEL REDUCTION AUTOCLAVE

3.1 EXPERIMENTAL DESIGN

The objective of this study was to investigate the effect of aeration on the just-suspended impeller speed for a nickel reduction autoclave. A Rushton and a pitched blade impeller were employed in this work. An experimental design shown in Table 3.1 was followed.

Table 3.1. Just-suspended impeller speed experimental design

Reactor	Aim	Conditions
75L Perspex tank	Investigating N_{js}	- Two impeller configurations (Rushton and 30^o pitched blade) - Varying solids density (using nickel crystals and glass beads) - Varying solids loading (from 5wt % to 20wt %) - Varying aeration rate (from 0vvm to 1.5vvm)

3.2 MATERIALS AND METHODS

A 75l, 4 baffled, elliptically-bottomed Perspex vessel with a diameter (T) of 0.378m was employed in this work. The 4 baffles had a radial width of 0.1T (37.8mm), a thickness of 8mm and were staggered at 90^o to each other along the vessel wall. The effects of using a Rushton and a 4-bladed downward pumping pitched blade impeller having a 30^o pitch, with a diameter (D) of 0.14m were investigated. A pitched blade impeller was chosen because most nickel reduction autoclaves employ pitched blade impellers. A Rushton impeller was used as the standard since most mixing studies have identified radial impellers as ideal for simultaneously accomplishing both gas dispersion and solids suspension (Perry et al., 1973; Paul et al., 2004). An impeller clearance of H/3 (where H is the height of the liquid in the tank) was used. The impeller clearance was taken as the distance from the bottom of the tank to the middle of the impeller

blade. A ring sparger with a diameter of 0.8 times the impeller diameter and 1.5mm holes was also used for uniform gas dispersion throughout the vessel. The sparger was situated at a clearance of H/6 from the bottom of the tank. To observe the suspension of the solids from the vessel bottom through the clear tank, a video camera (Sony: model DCR-SX44E) was fitted below the tank. A schematic representation of the experimental set up is as shown in Figure 3.1.

Pure nickel powder of 8912kg/m^3 density and 2500kg/m^3 glass beads were used as the solid phases throughout the experiment. Tap water was used as the liquid medium, and a static liquid height equal to the diameter of the tank (0.378m) was maintained throughout the experiment. Compressed air was used to simulate pressurized hydrogen and a variable gas-mass flow meter (Universal Flow Monitors, Inc: model OFM-EF-2P56-B-X1A-D3) was used to measure the different flow rates of the air.

Dry sieving was employed to segregate the nickel samples into different size fractions. A nickel particle size range of 100-300μm was used. Two sub-ranges of 106-180 and 180-300 μm were identified from the size range. Glass beads (supplied by Blastrite Manufacturers, Cape Town, South Africa) were obtained in two different size ranges: 200-400 and 400-600 μm and used as received.

All the experiments were carried out at room temperature. The nickel crystals / glass beads were introduced into the vessel, which already contained tap water, to achieve a predetermined solids loading in the range of 5-20 wt%. To determine the just-suspended impeller speed at various aeration rates, the impeller speed was increased gradually until no particle remained static at the bottom of the tank for more than 1-2s (Zwietering 1s criterion). A visual method using the installed camera was used to establish the just- suspended condition.

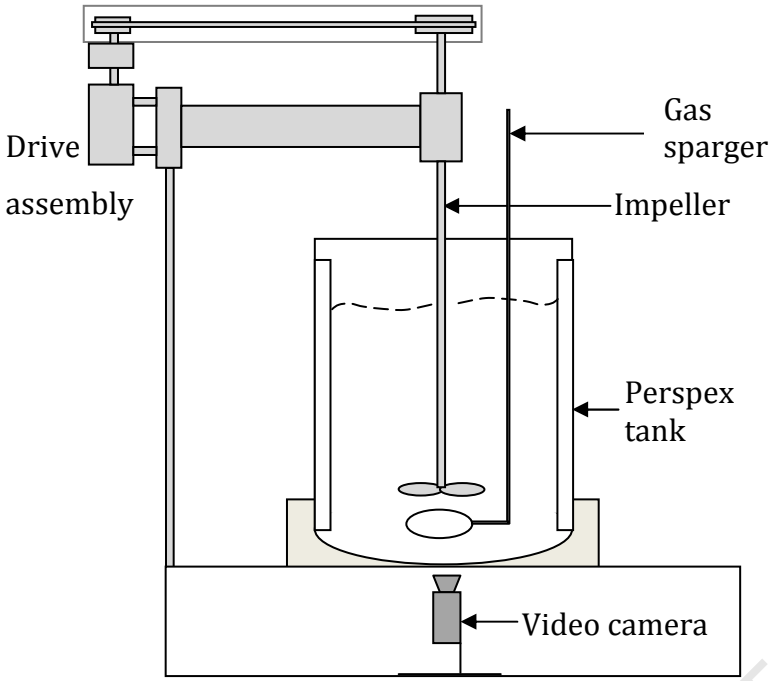

Figure 3.1. Just-suspended impeller speed experimental rig.

To investigate the effect of aeration rate, Q on the just-suspended impeller speed, N_{jsg}, the following procedure was followed:

i. Determining N_{jsu} experimentally,
ii. Introducing air and determining N_{jsg} at various aeration rates,
iii. Investigating how aeration rate affects N_{jsg}.

3.3 RESULTS AND DISCUSSION

3.3.1 The influence of aeration rate, Q on the critical impeller speed, N_{jsg}

The results for the Rushton impeller system are shown in Figure 3.2. From the graph, it can be observed that, even though the relationship between N_{jsg} and Q for the Rushton impeller system is slightly parabolic, it can be approximated by a linear relation in the form of equation 2.7. However, the 'a' values differ for the nickel (a = 156.37) and the glass beads (a = 89.21) systems highlighting that the relationship is system specific. A lower 'a' value was obtained for the glass beads compared to the nickel system. This means that for higher density materials, higher increases in impeller speeds are required to re-suspend particles with an increase in aeration rates.

This is in agreement with Zhu and Wu (2002) who highlighted that the linear relationship between N_{jsg} and Q is system specific and the 'a' value varies from one study to another. This variation throws doubt on the validity of equation 2.7 to describe three phase systems and for the purpose of scale up. Zhu and Wu (2002) also highlighted that 'a' cannot be a constant, since both N_{jsg} and N_{jsu} are dependent on operating conditions such as impeller type, impeller size, solids concentration, solids size and tank geometry. Furthermore, the relation is in a dimensional form which is system-dependent, thereby limiting its use for scale-up.

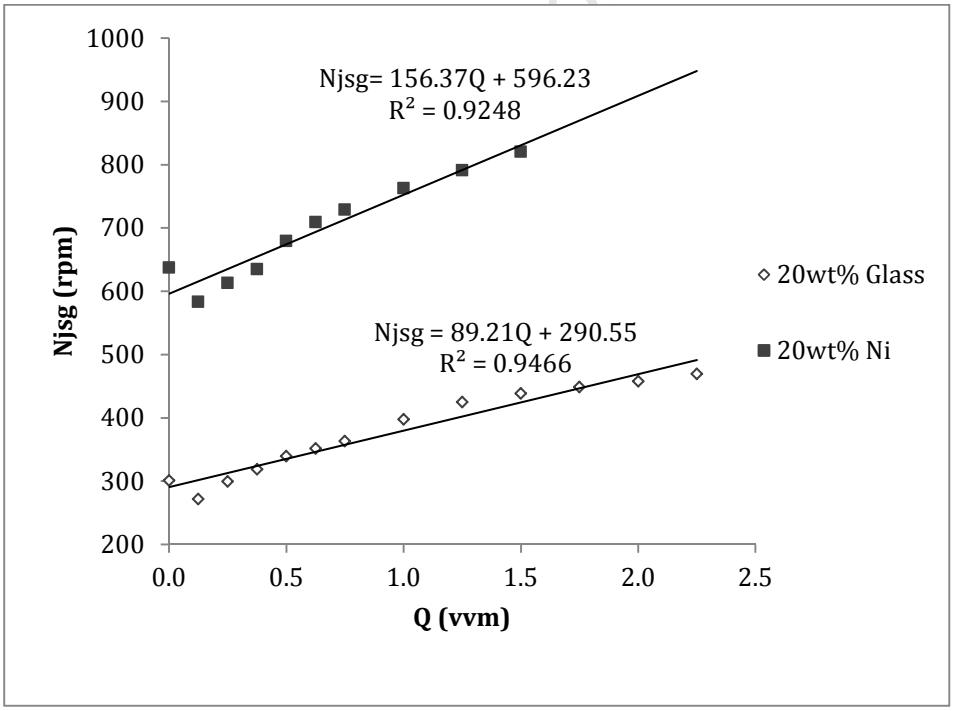

Figure 3.2. N_{jsg} as a function of Q for a Rushton impeller system: effect of solids density on the 'a' value.

The relationship between N_{jsg} and Q was also tested for the pitched blade impeller system and the results in Figure 3.3 were obtained for various wt% of glass beads. From the results, it was found that the linear relationship no longer held. A much greater increase in impeller speed was required to re-suspend the particles compared to the Rushton impeller under the same aeration condition (Figure 3.4). This can be supported by the findings of Kasat and Pandit (2005) who mentioned that solid suspension in a three-phase system is mainly determined by the gas liquid hydrodynamics of the impeller. A pitched blade impeller tends to flood at increased gassing rates. An impeller under flooding conditions does not generate any significant liquid phase circulation in the vessel, resulting in the sedimentation of the suspended particles. Figure 3.4 shows the comparison between a pitched blade and a Rushton impeller system for 20wt% glass beads.

Chapman et al. (1983) also highlighted that a greater power input is required to cause suspension of particles under aerated conditions. The argument was that the presence of gas has an additional effect other than the reduction of flow from the impeller region, in the form of damping local turbulence and velocities near the vessel base. This effect is more pronounced for a pitched blade impeller pumping downwards against the rising gas. Hence, much higher speeds were required for a pitched blade impeller system to counter these damping effects.

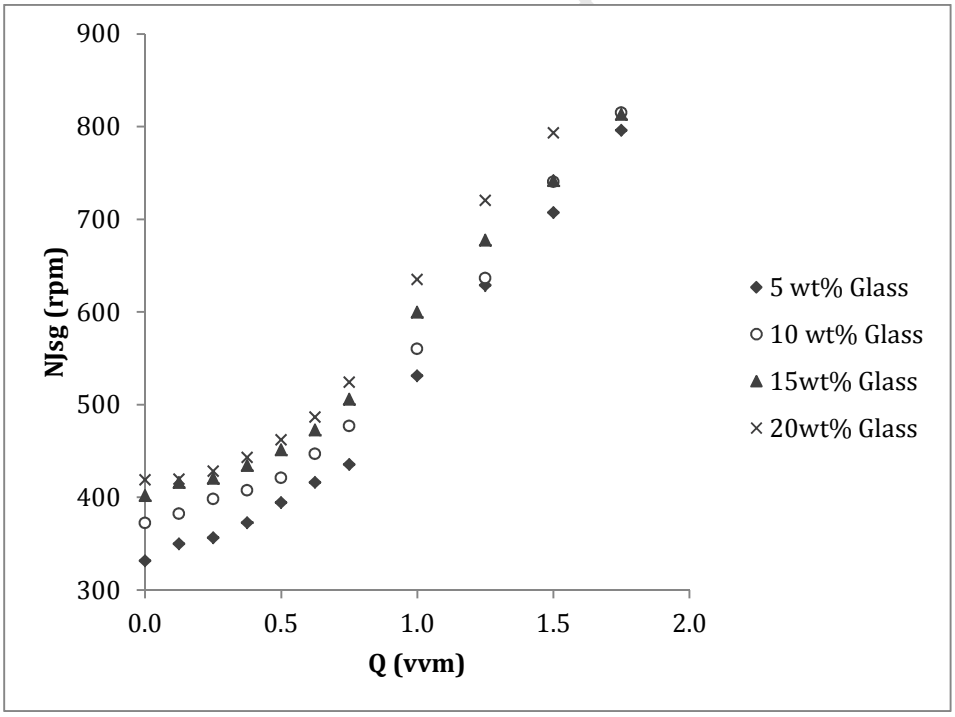

Figure 3.3. N_{jsg} as a function of Q for a 4-bladed pitched blade impeller system at various solids loading

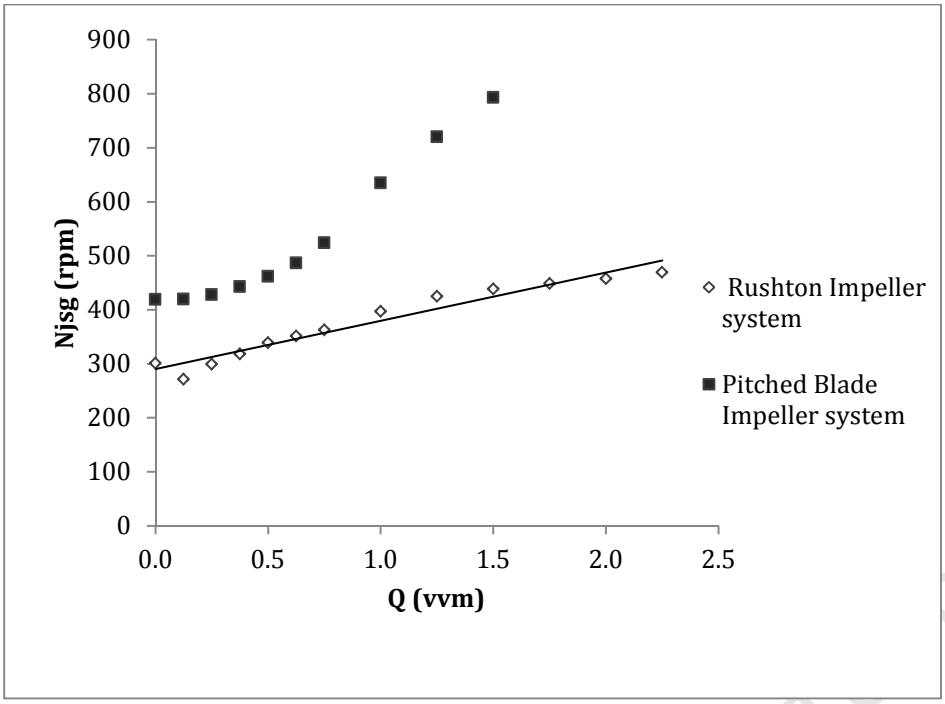

Figure 3.4. N_{jsg} as a function of Q for 20wt% glass beads for a Rushton and a pitched blade impeller system

From Figure 3.5, it can be observed that, for the same system of glass beads, regardless of the solids loading, aeration has a similar effect on the N_{jsg} and the same increase in impeller speed is required to re-suspend the particles. This is in agreement with Chapman et al. (1983), who highlighted that, for a wide range of solid loadings, density differences and independent of the gas-liquid mixing condition, the same increase in impeller speed is necessary to restore the just-suspended condition on increased gassing rate. For the nickel system, however, a much higher increase in impeller speed was required to re-suspend the particles especially at higher aerations compared to the glass beads system. This finding therefore, contradicts the work of Chapman et al. (1983). The possible explanation could be that Chapman et al. (1983) studied with solid densities in the range of 1050 to 2900 kg/m^3 and therefore their results were not applicable to higher densities.

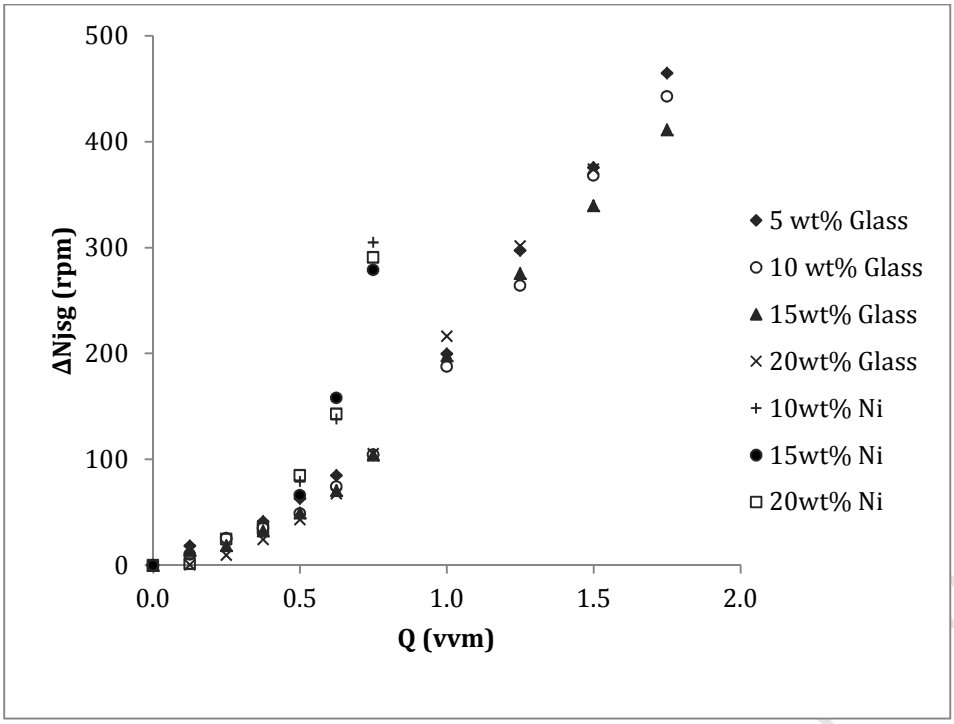

Figure 3.5. ΔN_{jsg} vs. Q for a pitched blade impeller system: effect of density

3.3.2 The influence of aeration number, Na_{js} on the critical impeller speed, N_{jsg}

In response to the short comings of Q, the results in Figure 3.2 for the Rushton impeller system were plotted in the form of RJSS as a function of Na_{js} and then related to the Zhu and Wu (2002) correlation (equation 2.14). The results in Figure 3.6 were obtained. Although this correlation was developed with solid particles of a density of around 2500 to 2700kg/m^3, it can however, also be used to approximate N_{jsg} for higher density materials like nickel which has a density of approximately 8912kg/m^3. This demonstrates that RJSS depends only on Na_{js} and is independent of impeller size, solids density and concentration as highlighted by Zhu and Wu (2002). The data from this study for both the nickel and the glass beads systems almost collapsed onto one curve along the correlation. This demonstrates that the non-dimensional correlation by Zhu and Wu (2002) can be used to describe three phase systems for a Rushton impeller system, even for high density materials and therefore can be adopted for scale up.

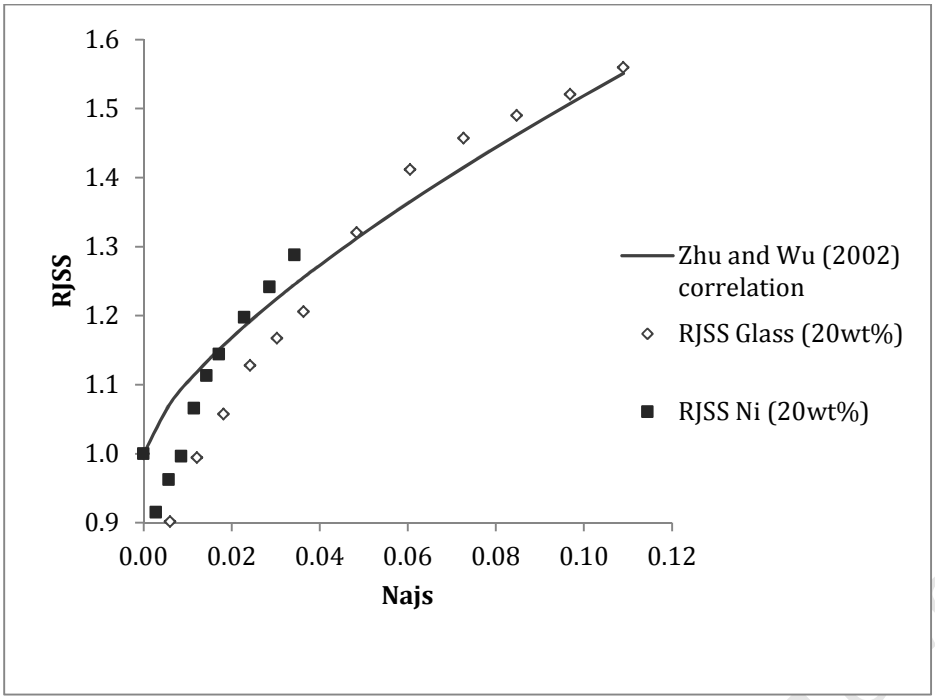

Figure 3.6. RJSS as a function of Na_{js} for a Rushton impeller system: testing the validity of the Zhu and Wu (2002) correlation on high density materials

Though the Zhu and Wu (2002) correlation was developed using Rushton impellers as agitators, it was also tested for the pitched blade impeller system in both the nickel and the glass beads systems and the results obtained are shown in Figure 3.7. The results confirmed that this correlation does not hold for a pitched blade impeller system since it underestimates the N_{jsg} at high aerations. The effects of impeller flooding on solids suspension can also be attributed to this, since much higher speeds were required under aerated conditions in pitched blade impeller systems.

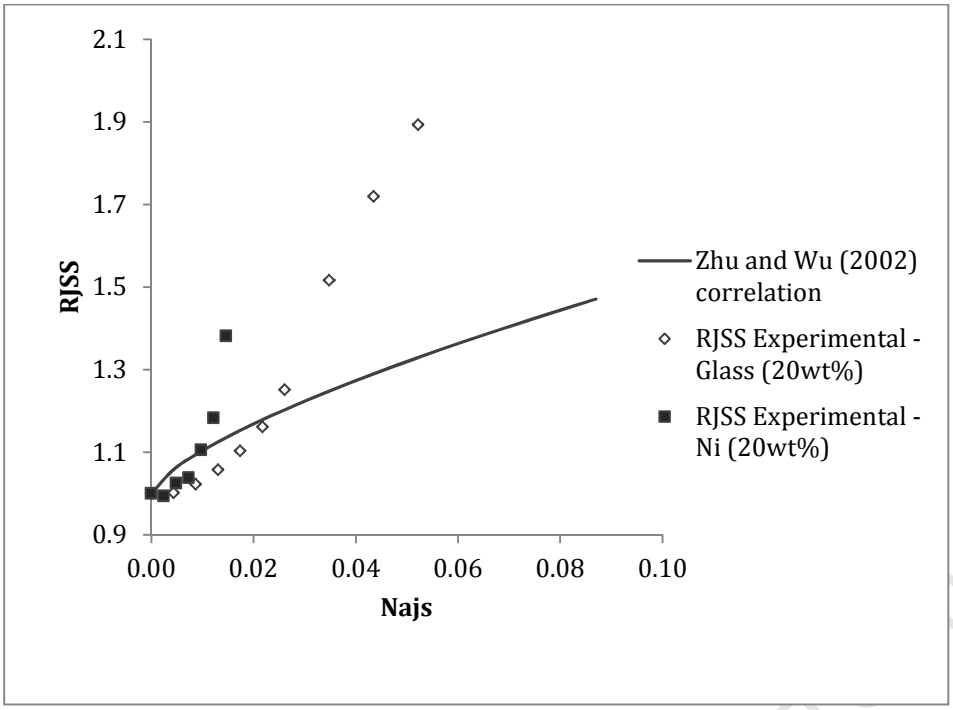

Figure 3.7. RJSS as a function of Na_{js}: testing the validity of the Zhu and Wu (2002) correlation for a pitched blade impeller system

Perry et al. (1973) indicated that impeller flooding may occur at Na_{js} values greater than 0.03. This argument was obtained from results where solids of densities lower than 5000kg/m^3 were used. In the current study, it was found that the same argument holds for the glass beads system. However, for the high density nickel system, flooding occurred at Na_{js} values less than 0.015. This finding was expected because the N_{jsu} values for the nickel system are high (about twice those of glass beads), and since Na_{js} is inversely related to N_{jsu}, it is therefore required that much higher values of the aeration rates, Q be supplied before the Na_{js} of 0.03 are met. Hence a much greater resistance to solids pick up would be experienced as a result of the damping effects of the rising air.

However, when the RJSS values for the glass beads were plotted against Na_{js} as shown in Figure 3.8, the data almost collapsed onto the same curve especially at low aeration rates. This means that for the same density, RJSS vs. Na_{js} follows a similar trend.

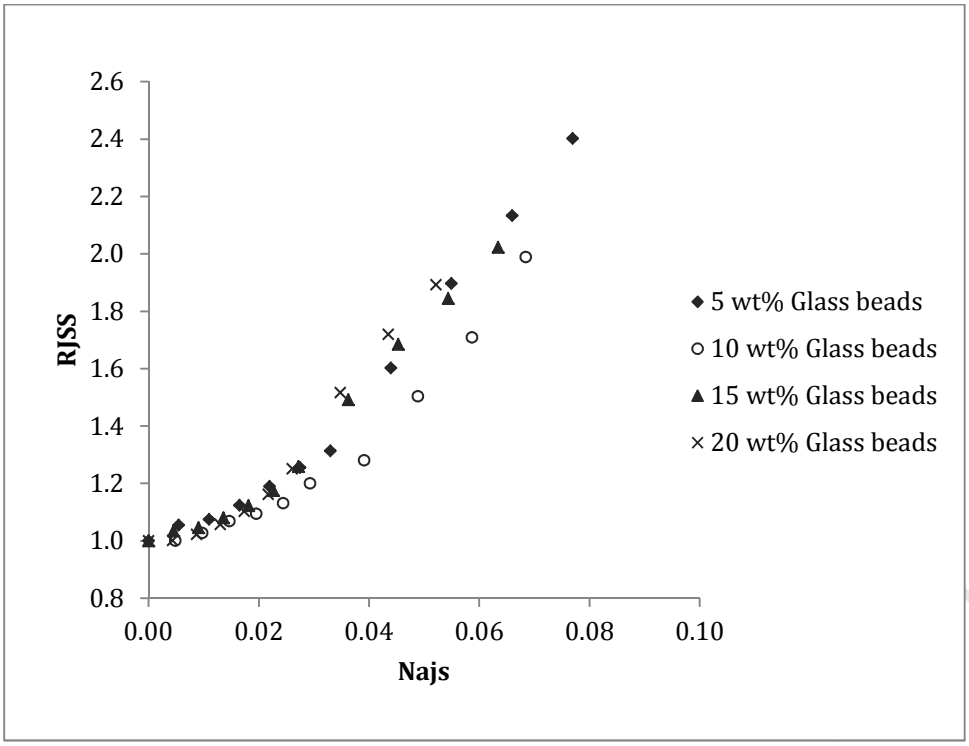

Figure 3.8. RJSS as a function of Na_{js} for a pitched blade impeller system: using glass beads as solids

On the other hand, changing the number of impeller blades also has an effect on impeller flooding; resulting in higher gassing rates being needed before flooding occurs. This was observed when the results of the glass beads from this study using a 4-bladed pitched blade impeller were compared to those of a similar system by Nienow et al. (1986) with 6-bladed pitched blade impeller as can be seen on Figure 3.9. These results were in agreement with Nienow et al. (1986) who highlighted that, at a constant impeller speed, increasing the number of blades on the impeller reduces the rate at which gassed power falls with increasing gassing rate and a higher gassing rate is needed before flooding occurs.

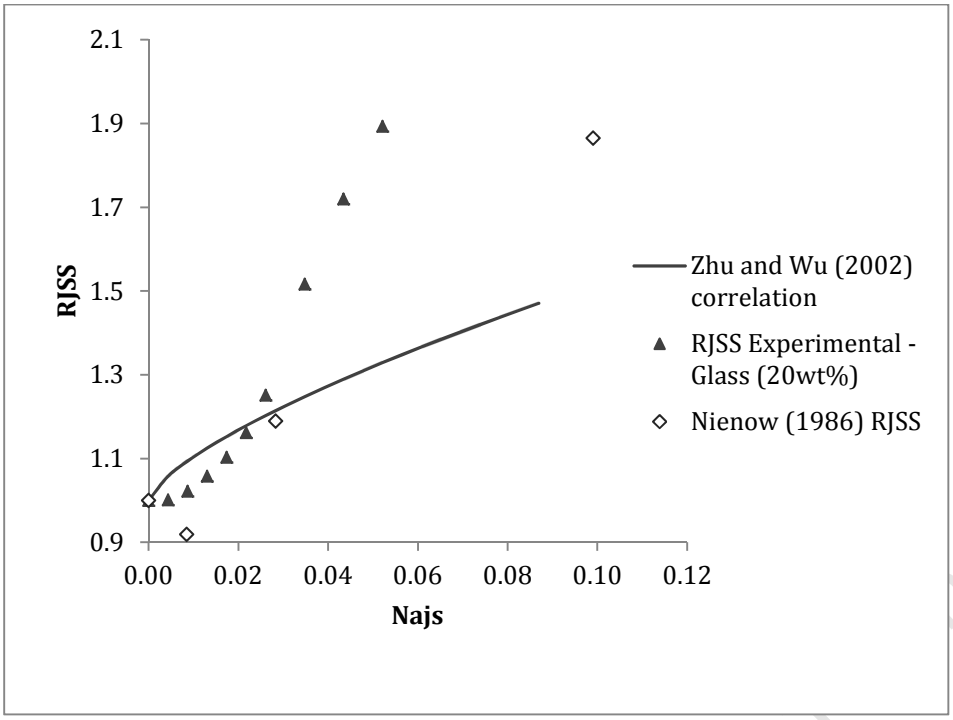

Figure 3.9. RJSS as a function of Na_{js} for a pitched blade impeller system: effect of increasing the number of impeller blades.

3.4 CONCLUSIONS

3.4.1 Rushton impeller system

- The influence of aeration rate on the just-suspended impeller speed for a Rushton impeller system can be approximated by a linear equation, $N_{jsg} = N_{jsu} + aQ$. This relationship however, was found to be system specific and therefore could neither be used to describe three phase systems nor for the purpose of scale up. This is mainly because the 'a' values vary from one system to another.
- The non-dimensional correlation $RJSS = 1 + mNa_{js}^{n}$ developed by Zhu and Wu (2002) was found to be useful, where m and n are constants with values of 2.6 and 0.7 respectively.

3.4.2 Pitched blade impeller system

- The linear relationship between N_{jsg} and Q disappeared for the pitched blade impeller system since a pitched blade impeller is very sensitive to gassing rates and tends to flood under high aeration rates. This led to much higher requirements of N_{jsg} to re-suspend the particles.
- However, increasing the number of blades resulted in higher gassing rates being needed before flooding occurs. This was also supported by the work of Nienow et al. (1986) and that of Kasat and Pandit (2005).
- When compared to Rushton impellers, pitched blade impellers are less efficient for simultaneous gas dispersion and solids suspension under high gassing rates.

3.4.3 The impeller flooding

Perry et al. (1973) indicated that impeller flooding may occur at Na_{js} values greater than 0.03. This argument also held for the glass beads system. However, it was identified that for high density materials like nickel, flooding may occur at Na_{js} values of less than 0.015 for a pitched blade impeller system.

3.5 RECOMMENDATION

For a nickel reduction autoclave using pitched blade impellers as agitators, sparging hydrogen below the impellers will cause impeller flooding, leading to nickel solids sedimentation. It is therefore recommended that hydrogen feeding be performed into the headspace and then use a dual impeller system for mixing. The top impeller would be for hydrogen induction and the bottom for nickel suspension. This was also recommended by Willis and von Essen (2000).

CHAPTER 4 : ESTABLISHING THE 'ATTRITION SPEED' FOR A NICKEL REDUCTION AUTOCLAVE

4.1 THE 7L MIXING SETUP

The aim of this study was to establish the impeller speed required to cause attrition of nickel crystals in a nickel reduction autoclave. An experimental design shown in Table 4.1 was followed.

Table 4.1. The 'attrition speed' experimental design

Reactor	Aim	Conditions
7L Perspex tank	Establish attrition speed	- 90mm Pitched blade impeller - 105µm to 250µm nickel crystals - Varying impeller rotational speed (from 0 to 1050rpm)

4.1.1 Materials and Method

A 7L fully baffled, elliptically-bottomed Perspex vessel with a diameter (T) of 0.22m and a 90mm diameter (D), 45^{o} pitched blade impeller was used in these experiments. This choice of impeller was because most nickel reduction autoclaves employ pitched blade impellers. An impeller clearance of H/3 (where H is the height of the liquid in the tank) was used. A schematic representation of the experimental set up is shown in Figure 4.1.

Pure nickel powder supplied by Impala (South Africa) was used as the solid phase in this experiment. Since nickel is insoluble in water and to avoid nucleation, growth, aggregation and all other phenomena capable of modifying the crystal size distribution and habit (Bravi et al., 2003), tap water was used as the liquid medium.

Wet sieving was used to segregate the nickel samples into different size fractions, within which the particle size distribution was measured using a Malvern Mastersizer laser diffraction instrument (model: S-Long bench). Wet sieving was required so as to minimise the dust and fine particles outside the required feed size range. The preferred nickel particle size range was 100-300µm, within which two sub-ranges were identified: 106-180 and 180-300 µm.

All the experiments were carried out at room temperature. The nickel crystals were introduced into the vessel, which already contained tap water, to achieve a predetermined solids loading of 500g crystals in 5l of water (mass fraction 0.1). The impeller speed was varied from 0 to 1050rpm at 20rpm increments and the experiment was allowed to run for one hour at each impeller speed. After every one hour run, sampling was done offline by use of a 50ml syringe at three different positions in the tank. The upper third of the reactor was targeted for sampling as fines are known to segregate to the top during mixing. Fines generation was investigated by measuring the particle size distribution (PSD) of the attrition product using a Malvern Mastersizer laser diffraction instrument. The emergence of a new peak of smaller diameter particles in the particle size distribution was used as an indication of the presence of attrition. The minimum impeller speed resulting in fines generation was then considered as the minimum attrition speed.

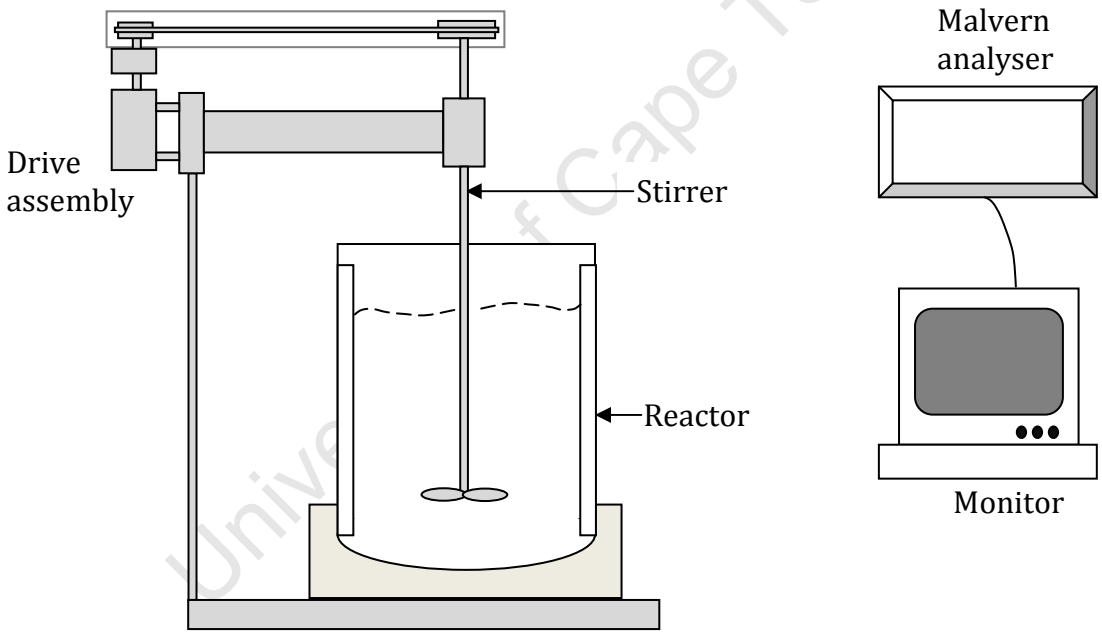

Figure 4.1. Experimental setup for the attrition experiments

4.1.2 Results and discussion

The particle size distributions of the attrition product, expressed as number distributions are shown in Figure 4.2. The number distribution was preferred as it has a higher resolution at smaller sizes compared to the volume distribution (Lewis, 2010). From the graph, it can be observed that as the impeller tip speed of 4.01m/s was reached, some fragments smaller than the original crystals were produced. A bimodal size distribution in which the resulting larger particles have almost the same size distribution as the parent crystals indicates that attrition was the dominant mechanism of the crystal fracture.

This is in agreement with Biscans (2004), who highlighted that attrition gives rise to a bimodal size distribution. Attrition is assumed to produce a localised fracture of the parent crystal, which is just slightly damaged, generating, at the same time, a number of much smaller fragments (Bravi et al., 2003). During the operation of a crystalliser, when the absolute value of the impact energy between the suspended solids and the impeller tips is low, an elastic deformation of the crystal occurs. As the impact energy increases, first the resistance of some spots on the crystal surface is overcome, causing attrition by abrasion fracture, then the resistance of the whole crystal is exceeded, and the crystal is shattered according to the breakage mechanism (Bravi et al., 2003). This means that during this work, the abrasion fracture mechanism of attrition was studied since only the onset of attrition was considered.

It can also be observed from Figure 4.2, Figure 4.3 and Figure 4.4 that increasing the impeller tip beyond the minimum attrition speed also increases the attrition rate and at the same time producing bigger attritioned particles.

The minimum impeller tip speed required to cause attrition of the crystals was then taken as the minimum attrition speed. The impeller tip speed represented the impact velocity since attrition is known from previous researchers (Bravi et al., 2003; Gahn and Mersmann, 1995) to be dominant on the impeller tip region. This impeller tip speed corresponded to an impact energy of $4.90*10^{-7}$ J for feed particles of a diameter d_{50} of 190μm. The impact energy was calculated using equation 2.16.

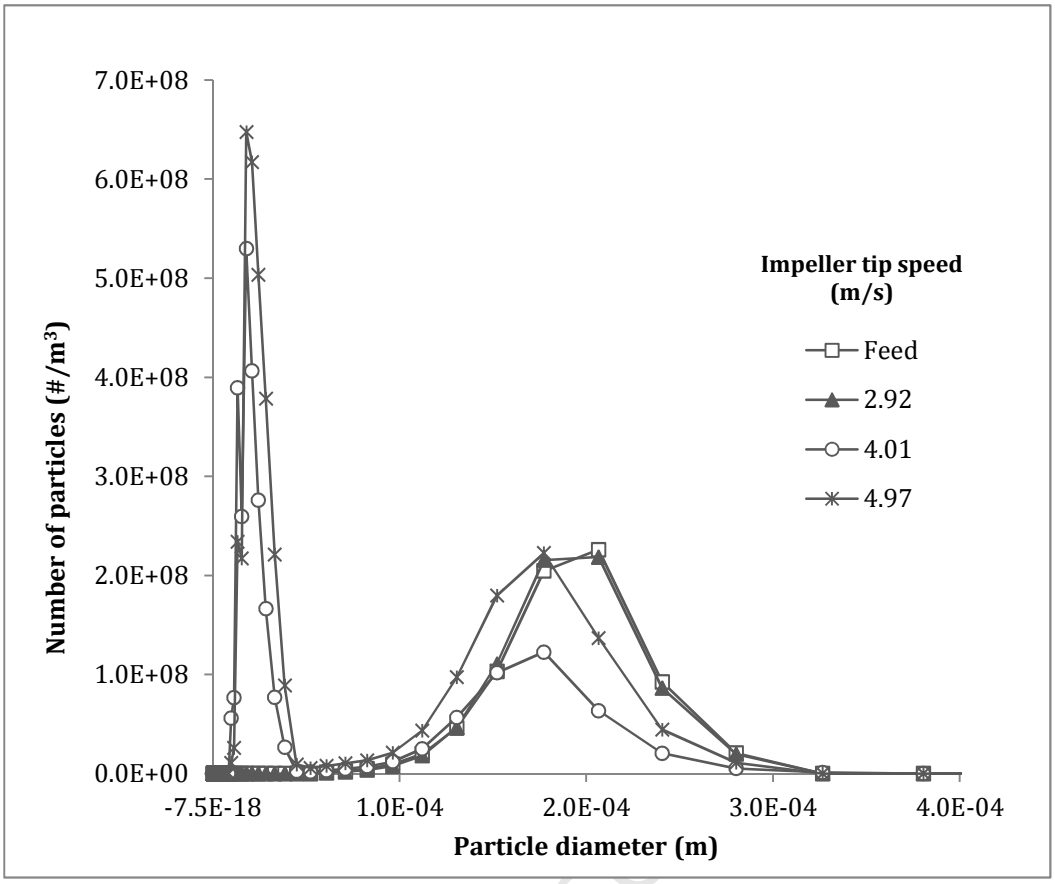

Figure 4.2. Particle number distribution for the attrition experiment at various impeller tip speeds

The cumulative number distribution (Figure 4.3) and the evolution of the total number of particles (zeroth moment) (Figure 4.4) curves of the fragments also gave some indication of the attrition resistance of the nickel crystals. In the absence of attrition, the total number of particles at any given time in the reactor should remain constant and equal to the number in the feed. Since attrition results in an increase in the total number of particles in the vessel, the fact that the total number of particles increased as the impeller tip speed reached 4.01m/s meant that this impeller speed (4.01m/s) could be defined as the minimum attrition speed.

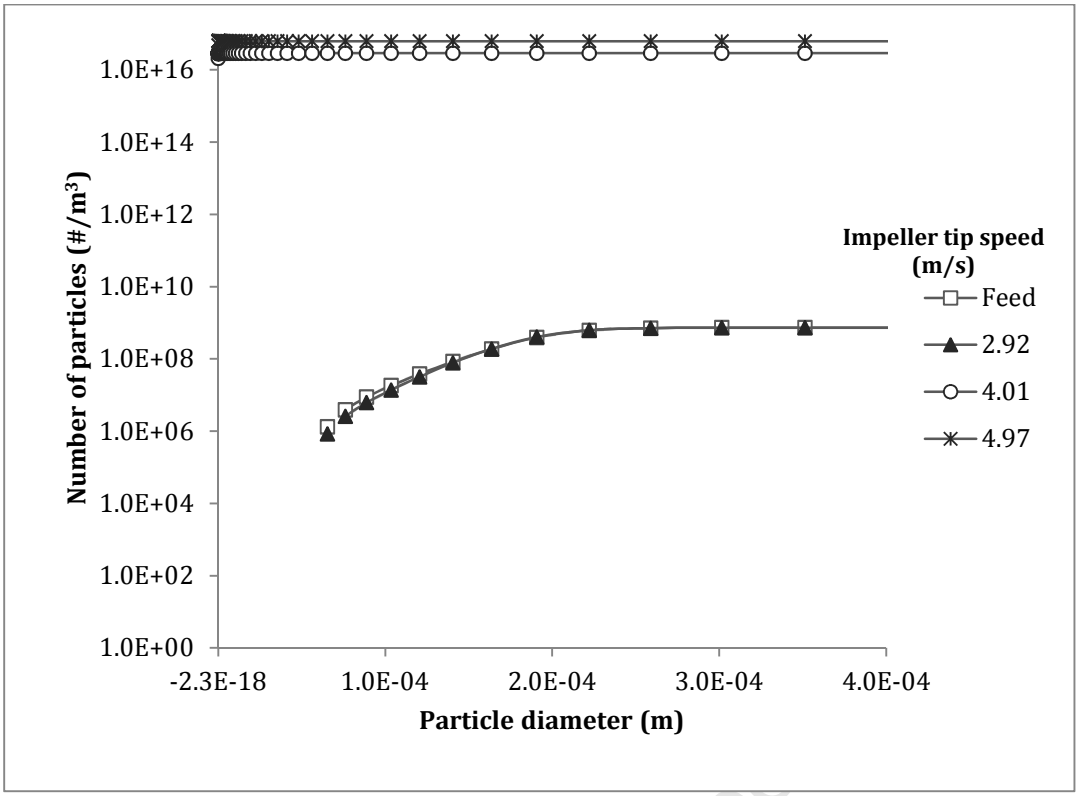

Figure 4.3. Cumulative number distribution at various impeller tip speeds

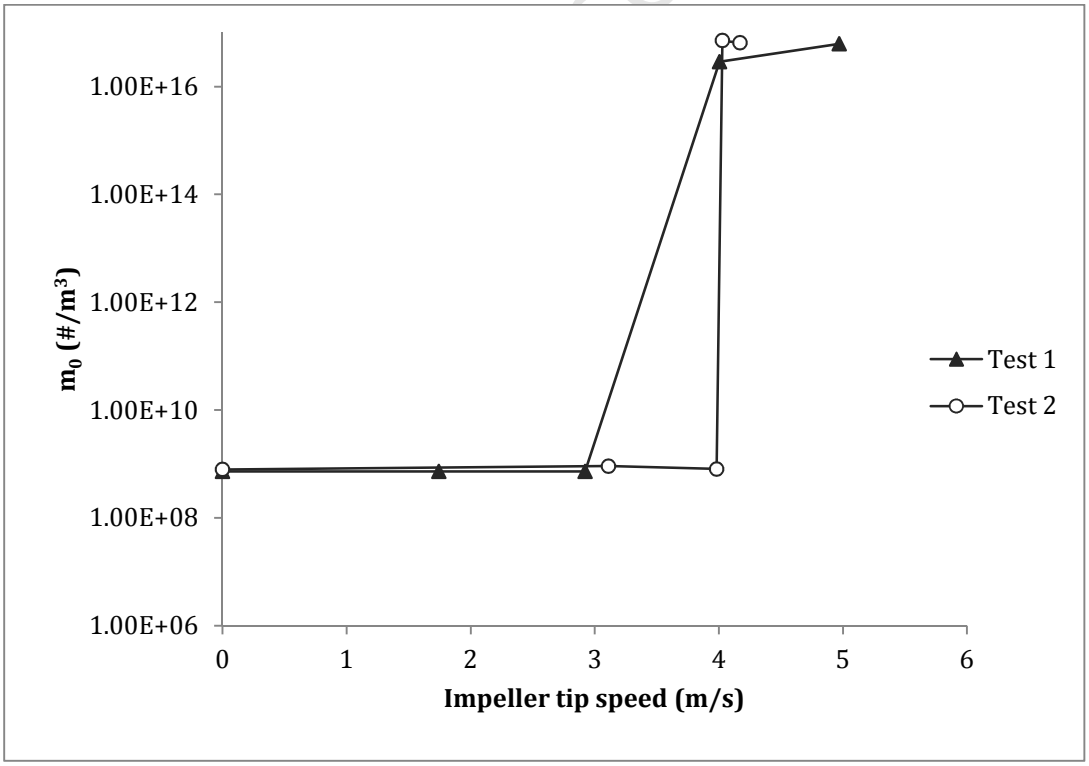

Figure 4.4. The change in total number of particles with change in impeller tip speed

The calculated and measured parameters for the experiment using the particle fraction with d_{50} = 190μm are shown in Table 4.2.

Table 4.2. Calculated parameters for the attrition experiments

PARAMETER	LABORATORY SET UP					INDUSTRIAL CASE STUDY
Impeller diameter (m)	0.09	0.09	0.09	0.09	0.09	0.94
Impeller speed (rpm)	Feed	370rpm	620rpm	850rpm	1055rpm	233rpm
Impeller tip speed, u (m/s)	0	1.74	2.92	4.01	4.97	11.46
Impact energy, E_c (J)	0	$9.29*10^{-8}$	$2.61*10^{-7}$	$4.90*10^{-7}$	$7.55*10^{-7}$	$4.01*10^{-6}$
Impeller Reynolds number, Re	0	$5.26*10^{4}$	$8.82*10^{4}$	$1.21*10^{5}$	$1.50*10^{5}$	$3.04*10^{7}$
Impeller dissipated power per unit mass, ε (W/kg)	0	0.35	1.64	4.22	8.06	1.36
Result	← No attrition →			← Attrition →		

From the results presented in Table 4.2, it can be argued that for the purpose of scale up, the impeller tip speed, the impact energy and the impeller Reynolds number can give a better prediction of the conditions required to cause attrition in a crystalliser, compared to the impeller dissipated power per unit mass, *ε*. This was observed when the experimental results were compared with an industrial case study. It was found that, the impeller dissipated power per unit mass from the industrial case study (ε = 1.36 W/kg) when used for scaling down to the 7L experimental set up, an impeller tip speed of 2.75m/s would be required to maintain the same ε (1.36 W/kg) and this impeller speed is not sufficient to cause attrition. However, the impeller tip speed of 11.46m/s in the industrial case study is sufficient to cause attrition. This is because; the impeller dissipated power per unit mass represents the volume averaged power dissipated into the reactor and therefore, is also depended on the reactor volume. However, most of the energy will be dissipated around the impeller region.

4.2 THE VICKERS MICROHARDNESS TEST

This test aimed to establish the critical work required for the formation of a crack on a nickel crystal using the approach by Gahn and Mersmann (1995). The main objective was to compare the results obtained from the microhardness test with those obtained from the 7L mixing set up. The critical work for the formation of cracks obtained from the microhardness test was compared to the impact energy required to cause attrition in the 7L mixing set up.

4.2.1 Materials and method

A microhardness tester (ZHV1 micro Vickers hardness tester HWDM–3 series) equipped with a standard measuring microscope with a X100 and X400 magnification was used in this study. The tester is also coupled with a diamond indenter in the form of a right pyramid with a square base and an angle of 360 degrees between opposite faces. The device is capable of performing tests using forces: 10, 25, 50, 100, 200, 300, 500, 1000 gf.

Pure nickel crystals of 2mm diameter (supplied by Impala, South Africa) were used in this test. These crystals were fixed onto the microhardness tester allowing the alignment of a given face under a microscope. The test was done by indenting the nickel crystals with the diamond indenter for 10 to 15 seconds. The two diagonals of the indentation left in the surface of the material after removal of the load were measured using a microscope. This measurement was done by adjusting two lines controlled by large diameter thumb wheels. The lines enable the corners of the diamond shaped indentation to be precisely located. The average of the two diagonals (d_1 and d_2) and the area of sloping surface of the indentation were calculated.

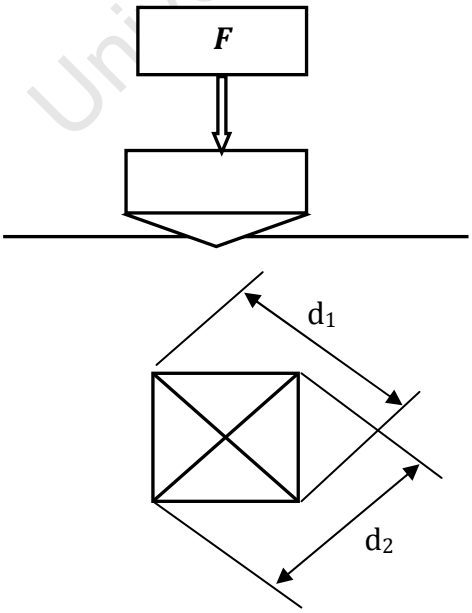

Figure 4.5. Microhardness test technique

The Vickers hardness number (HV) was calculated as the applied load (kgf) divided by the surface area of the indentation (mm^2).

$$HV = \frac{2F\sin\frac{136}{2}}{d^2} \qquad HV = 1.854\frac{F}{d^2} \text{ approximately} \qquad (4.1)$$

Where F = load in kgf

d = arithmetic mean of the two diagonals, d_1 and d_2 in mm

HV = Vickers hardness number

4.2.2 Results and discussion

To test for repeatability, experiments were repeated under the same indentation load and about 12 tests were performed at the critical force of 50gf. Findings from these tests indicate a low degree of repeatability in terms of the hardness values which range from 0.62 to 2.30GPa. Results of these tests are presented in Table 4.3.

The typical indents that were obtained from the microhardness test are shown in Figure 4.6.

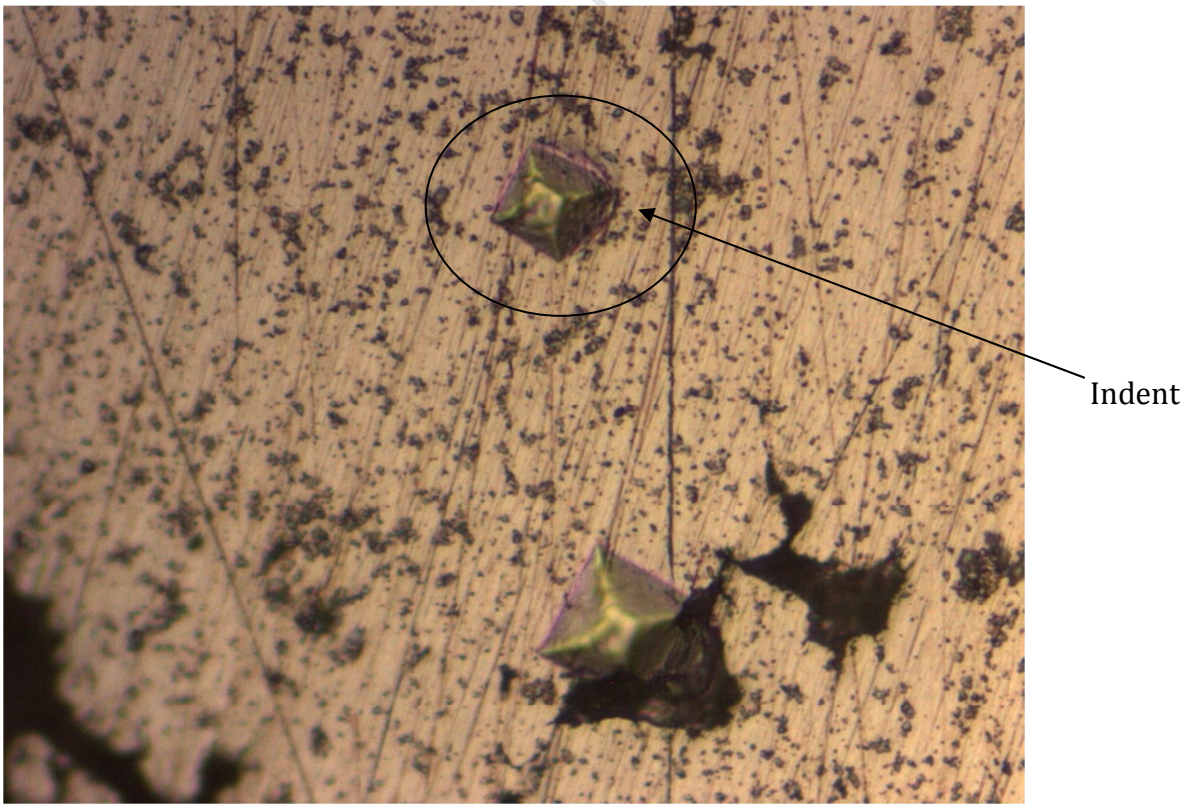

Figure 4.6. Indents from the Vickers microhardness test

During the tests, the critical force which is the load at which 50% of the indentations produced cracks (Gahn and Mersmann, 1995), was found to be 50gf. The corresponding hardness values were averaged and a mean H_v value of 1.7GPa was obtained.

The hardness values obtained from the microhardness tests are summarised in Table 4.3. These values are within the range of the theoretical values for pure nickel obtained from literature, which are in the range of 0.8 to 3.0GPa.

Table 4.3. Hardness values obtained from Vickers microhardness test

Force (gf)	Hardness (HV)	Hardness (GPa)
100	182.2	1.79
100	161.3	1.58
50	63.2	0.62
50	200.0	1.96
50	206.0	2.02
50	214.3	2.10
50	220.6	2.16
50	178.3	1.75
50	204.3	2.00
50	191.5	1.88
50	214.3	2.10
50	234.1	2.30
50	114.1	1.12
50	121.7	1.19
1000	108.0	1.06
3000	90.0	0.88

Using equation 2.17 by Gahn and Mersmann (1995) to determine the critical work to cause onset of fracture (attrition energy) and an average hardness value of 1.7GPa obtained at an applied force of 50gf, an attrition energy of $5.10*10^{-7}$J was obtained. This value is close to that obtained from the 7L mixing setup ($4.90*10^{-7}$J), highlighting that, under these experimental conditions, both methods are suitable for approximating the attrition energy in a crystalliser.

4.3 CONCLUSIONS

4.3.1 The 7L mixing set up

If the assumption that attrition is primarily due to crystal-impeller collisions in a mixing environment is correct, then the 7L mixing set up and the PSD measurement method used in this study can be regarded as an effective method to quantify the attrition speed for a nickel reduction autoclave.

Under these conditions, attrition by an abrasion mechanism was believed to be the dominant mechanism for the fines generation as observed from the bimodal PSDs of the attrition product.

From the results, it can be concluded that an impeller tip speed of 4.01 m/s is sufficient to cause attrition of the nickel crystals in the laboratory scale reactor. This attrition speed has an equivalent impact energy of $4.90*10^{-7}$J for feed particles of diameter d_{50} = 190 µm.

4.3.2 The Vickers microhardness test

The model by Gahn and Mersmann (1995) was also tested in this work. From the results, it can be concluded that the model is an effective way of quantifying the attrition energy in a crystalliser. This is mainly because, the critical work for the formation of a crack obtained from the microhardness test using the Gahn and Mersmann (1995) model ($5.10*10^{-7}$J) was close to that obtained from the 7L mixing set up ($4.90*10^{-7}$J).

CHAPTER 5 : ESTABLISHING THE 'BREAKAGE SPEED' FOR A NICKEL REDUCTION AUTOCLAVE

5.1 EXPERIMENTAL DESIGN

The aim of this study was to establish the impeller speed required to cause breakage of nickel crystals in a nickel reduction autoclave. An ultrafast load cell was employed in this work and the experimental design which was followed is given in Table 5.1.

Table 5.1. The 'breakage speed' experiment design

Type of test	Aim	Conditions
Experiment 1 (Single crystal breakage)	Measure fracture energy	- 2mm nickel crystals - Varying input energy (from 0.72J to 1.48J)
Experiment 2 (bed breakage)	Measure fracture energy	- 2mm nickel crystals (bed height of 4.75mm) - Varying input energy (from 0.72J to 1.48J)

5.2 MATERIALS AND METHODS

An ultrafast load cell, consisting of a 1.5m long, 19.90mm diameter steel impact rod coupled to an oscilloscope with 12-bit, 10MHz digitizers was used in this study. The rod is made of TG&P 140 steel, and the complete unit weighs approximately 50kgs, including its stainless steel frame.

The device is equipped with two strain gauges (Kulite S/UGP-1000-090 semiconductor gauges with a nominal unbounded resistance of 1000Ω and gauge factor of +155) mounted in the classic Wheatstone bridge arrangement as shown in Figure 5.1. These strain gauges are located approximately 104mm below the top of the impact rod.

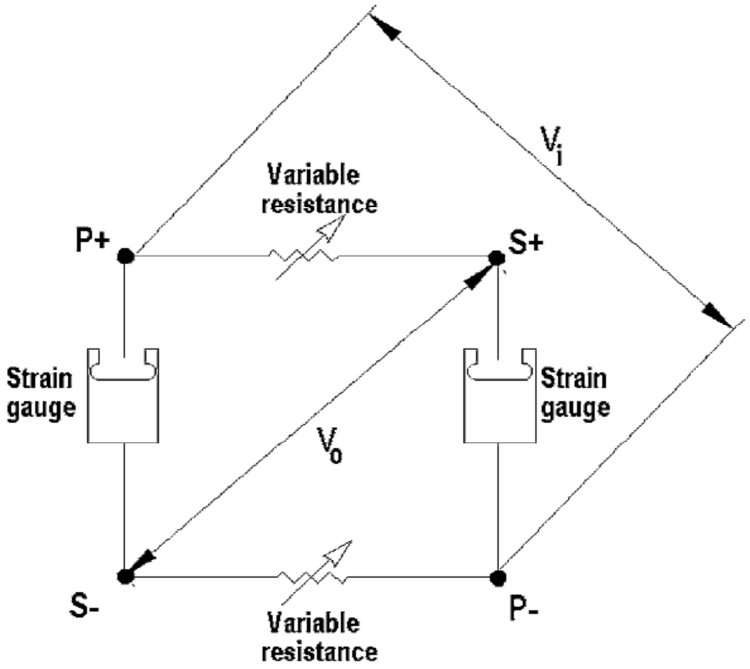

Figure 5.1. Wheatstone bridge configuration (Bourgeois and Banini, 2002)

The input voltage to the bridge, V_i was set at 2.466V. The output voltage, V_0 was affected dynamically by the strain exerted on the strain gauges.

A laser-photodiode triggering mechanism is installed across the impact region to completely separate the triggering event from the impact signal output by the strain gauges. Its height can be adjusted so that the laser passes through a 1mm height on top of the test particle as shown in Figure 5.2. As the drop weight cuts across the laser beam during an impact test, it cuts the signal to the photodiode, thus signalling the onset of data acquisition.

The equipment also consists of a 3-point pneumatic gripper with adjustable gripping fingers that permit testing with 0.5", 1", 2" and 3" diameter ball bearings giving access to different drop weights depending on the operator's needs. A graduated 300mm steel ruler is mounted onto the side of the plexiglass enclosure to precisely measure the drop height by use of a sliding marker giving a maximum drop height of 300mm.

Pure nickel crystals with a diameter, d_p of approximately 2mm and a mass of approximately 0.02g were used in this study. The density of these crystals was assumed to be 8912kg/m^3 (Lewis, 2009).

When setting the drop height before the test, the ball was placed in the pneumatic gripper, and the drop weight system with the ball gripped initially lowered to touch the top of the impact rod. The height marker was then set to zero. The drop weight was then raised to the desired

height, reading the drop height off the ruler from the new position of the marker. The drop height was recorded for subsequent data analysis.

Two types of breakage tests were performed in this work: single crystal breakage and bed breakage. The nickel crystal of known mass and diameter or a bed of crystals of known mass and height was placed on top of the impact rod and the laser beam adjusted so as to shoot just above the particle. The drop weight was then released from the pneumatic grippers by turning the pneumatic valve and thus breaking the crystal/crystals. The voltage signal due to the strain experienced by the strain gauges during impact was recorded for analysis.

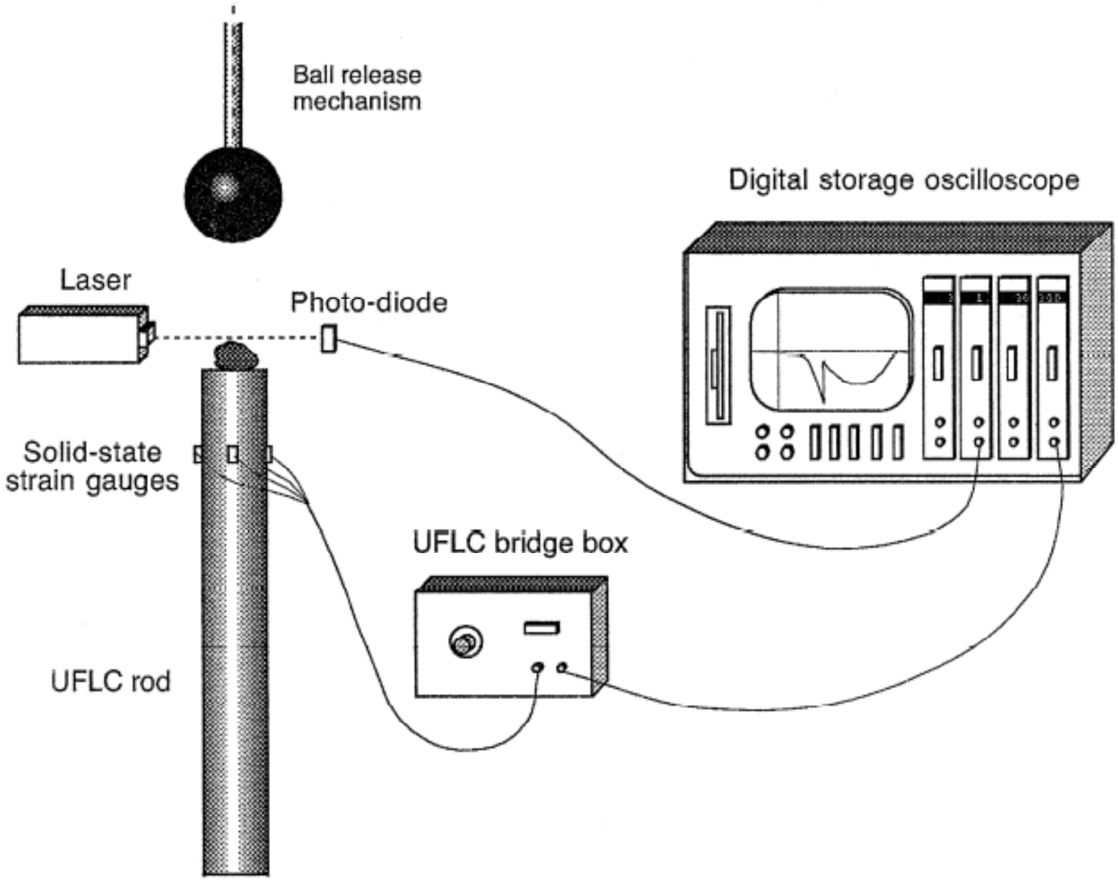

Figure 5.2. Schematic outline of the UFLC set up (Tavares and King, 1998)

5.3 RESULTS AND DISCUSSION

To test for repeatability of the results, three runs were performed during single crystal breakage at each drop height (input energy) and five runs during bed breakage. The typical force and energy signal analysis for a breakage test is as shown in Figure 5.3.

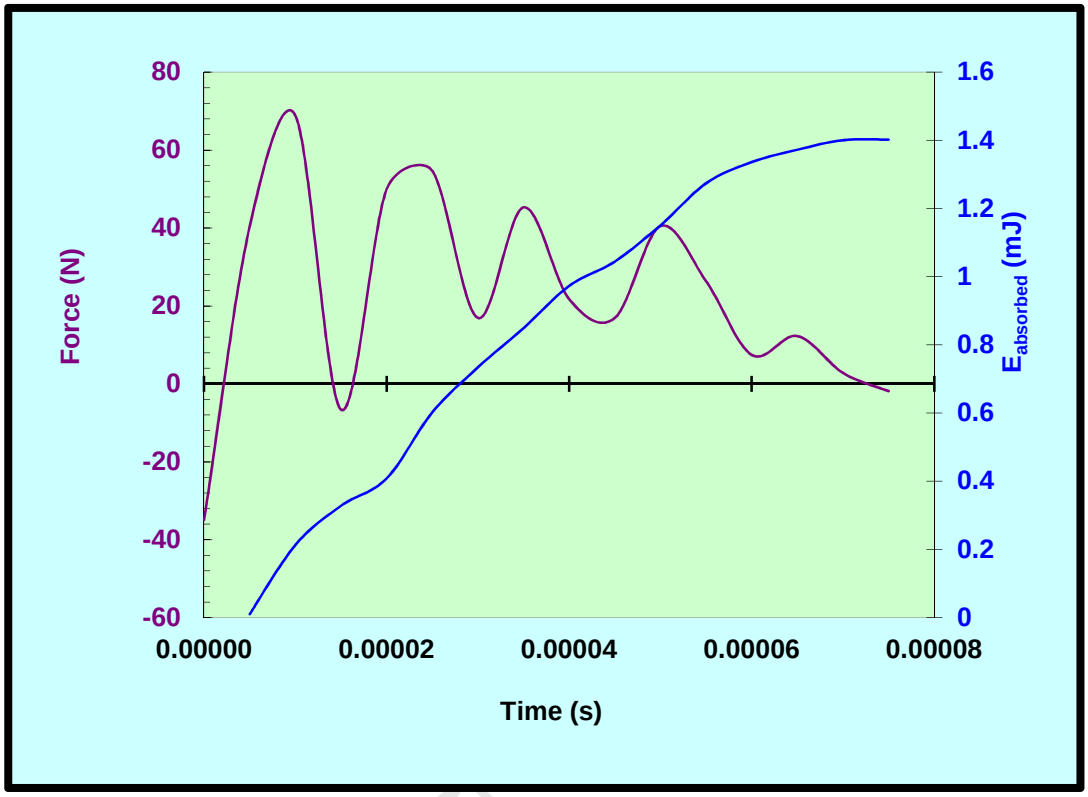

Figure 5.3: Impact signal obtained during single crystal breakage: impact carried out with 510g steel ball and from a 30mm drop height on a 2mm single nickel crystal

The analysis of Figure 5.3 gave the fracture characteristics presented in Table 5.2. During the breakage test, the strain experienced by the strain gauges tends to increase from the point of initial contact between the drop weight (steel ball) and the nickel crystal until the crystal breaks. This increase in strain leads to an increase in the output voltage and hence, the force also increases. From Figure 5.3, the point of initial breakage was determined from the first peak on the force time profile whilst the successive peaks were obtained from the secondary breakage (further breakage of the progeny crystals). The force exerted on the crystal at the point of initial breakage (68.9 N) was taken as the fracture force and the total energy absorbed by the particle until the point of initial fracture (0.213 mJ) as the fracture energy.

Table 5.2. Fracture characteristics obtained from the signal analysis of Figure 5.3

Impact analysis results		
Impact duration	0.080	ms
Fracture force	68.9	N
Fracture energy	0.213	mJ
Spec. fracture energy	0.00296	kWh/t
Particle strength	21.92	MPa
Particle stiffness	215.04	GPa
Energy absorbed by particle	1.40	mJ
% Energy used for breakage	1.00	%

5.3.1 Single crystal breakage

When the fracture characteristics of the individual nickel crystals were measured, a large scatter of results were obtained as shown in Figure 5.4, Figure 5.5 and Figure 5.6 for particle fracture energy, particle strength and particle stiffness respectively.

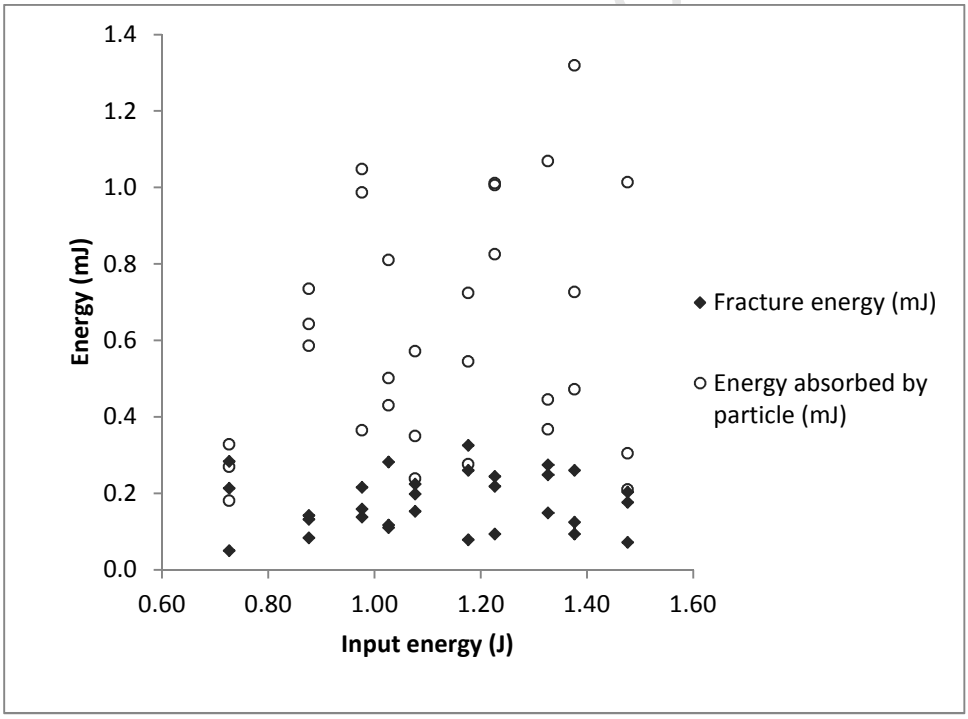

Figure 5.4. Fracture energy and energy absorbed by particles during single crystal breakage

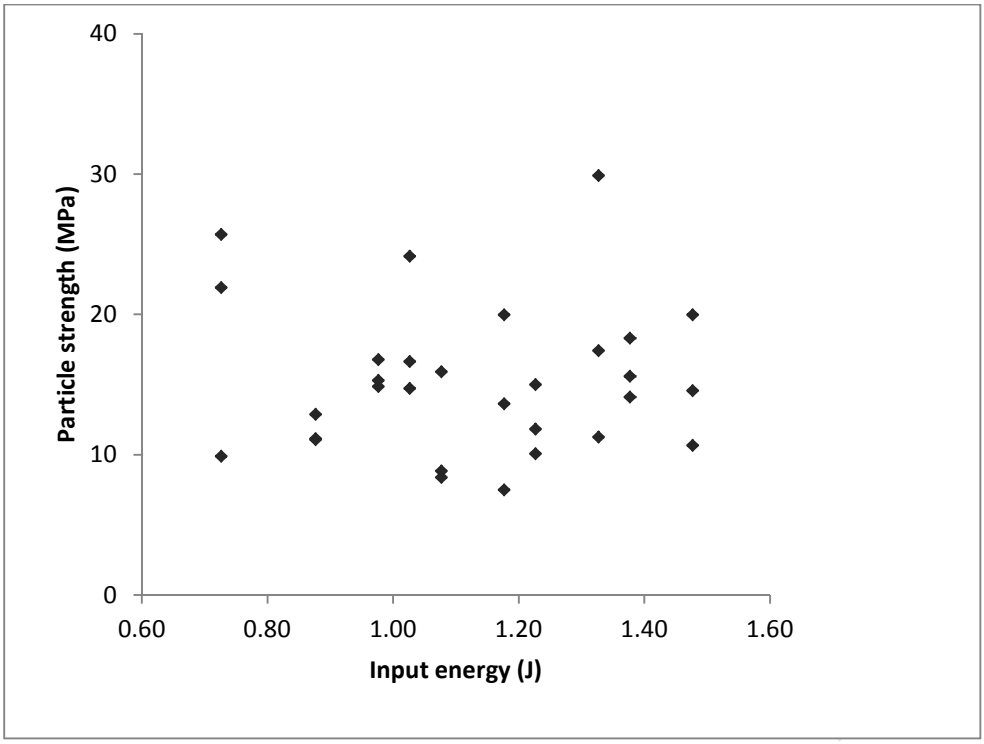

Figure 5.5. Particle strength during single nickel crystal breakage

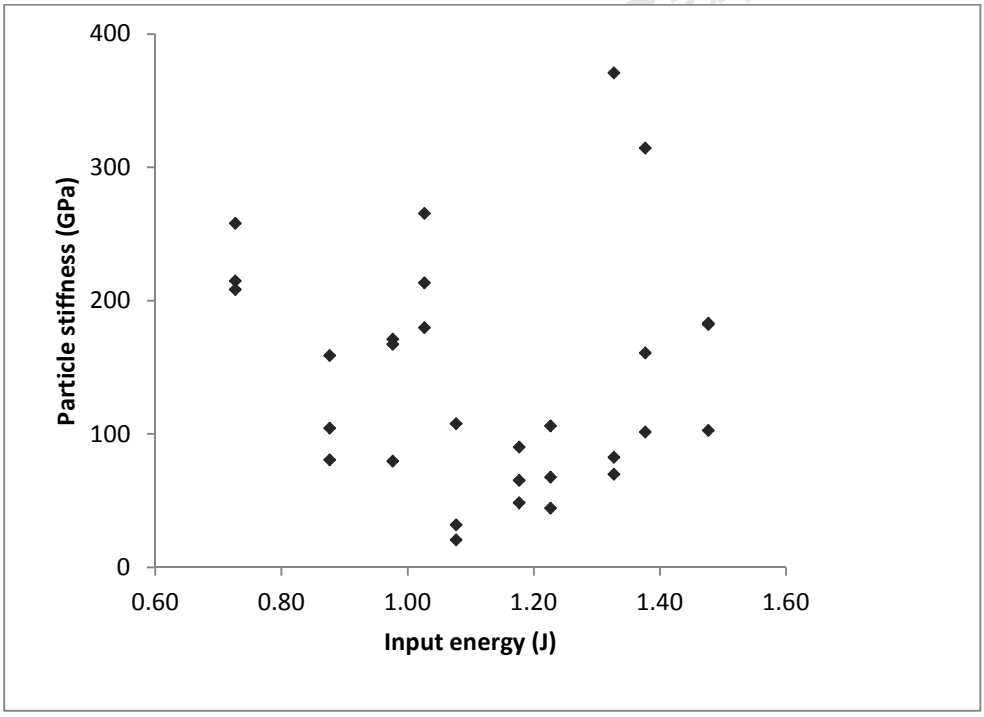

Figure 5.6. Particle stiffness values obtained during single nickel crystal breakage test

The variations in particle fracture energy and particle strength are in agreement with Tavares and King (1998) who attributed the variations of these properties to the fact that they are structure sensitive properties which are strongly affected by the presence of critical flaws and

cracks in zones of high stress in the material. Tavares and King (1998) also stated that particle size has an effect on both particle fracture energy and particle strength, and they highlighted that, as particle size decreases, cracks within the material progressively disappear. This results in an increase in both the particle strength and the particle fracture energy.

Although particle stiffness is known to be an intrinsic property of a material at a microscale level (Tavares and King, 1998), at macroscopic level, however, it is also affected by microstructural features such as pores, cracks and grain boundaries in the material. This resulted in variations in the stiffness values obtained in this study.

The breakage tests were also carried out at different input energies (drop heights). The breakage parameters extracted were found to be independent of the input energy since increasing the input energy did not have an effect on the breakage parameters (fracture energy, particle strength and particle stiffness).

5.3.2 Bed breakage

Particle fracture characteristics of the nickel crystals were also measured during bed breakage at various input energies. The results are summarised in Figure 5.7, Figure 5.8, and Figure 5.9 for particle fracture energy, particle strength and particle stiffness respectively. Similar trends to those of single crystal breakage were also obtained.

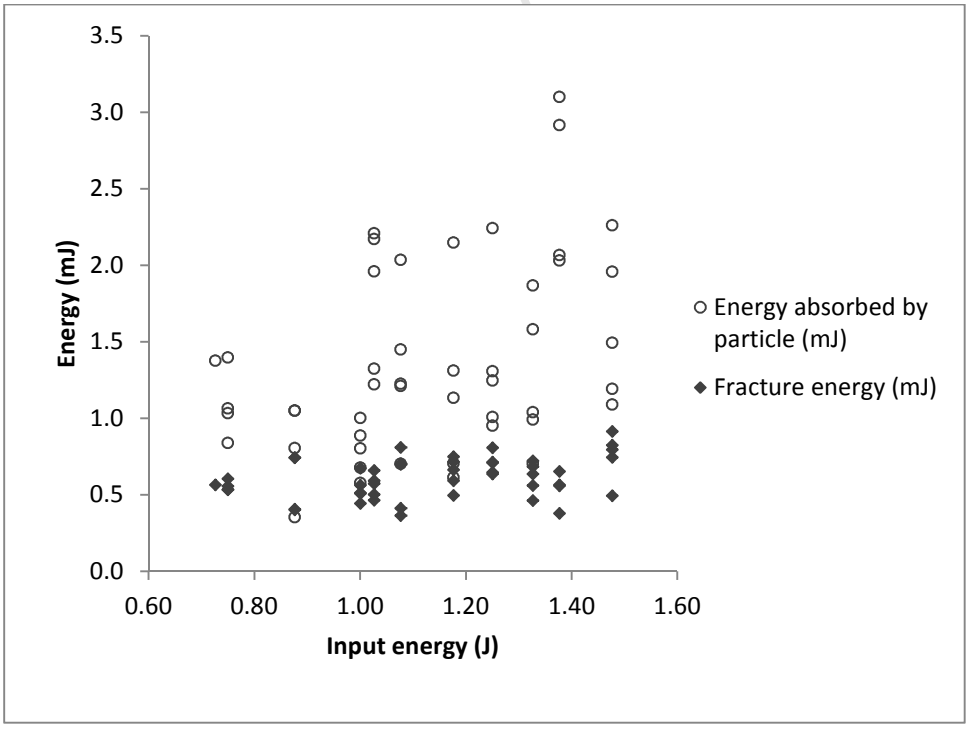

Figure 5.7. Fracture energy and energy absorbed by particles during bed breakage

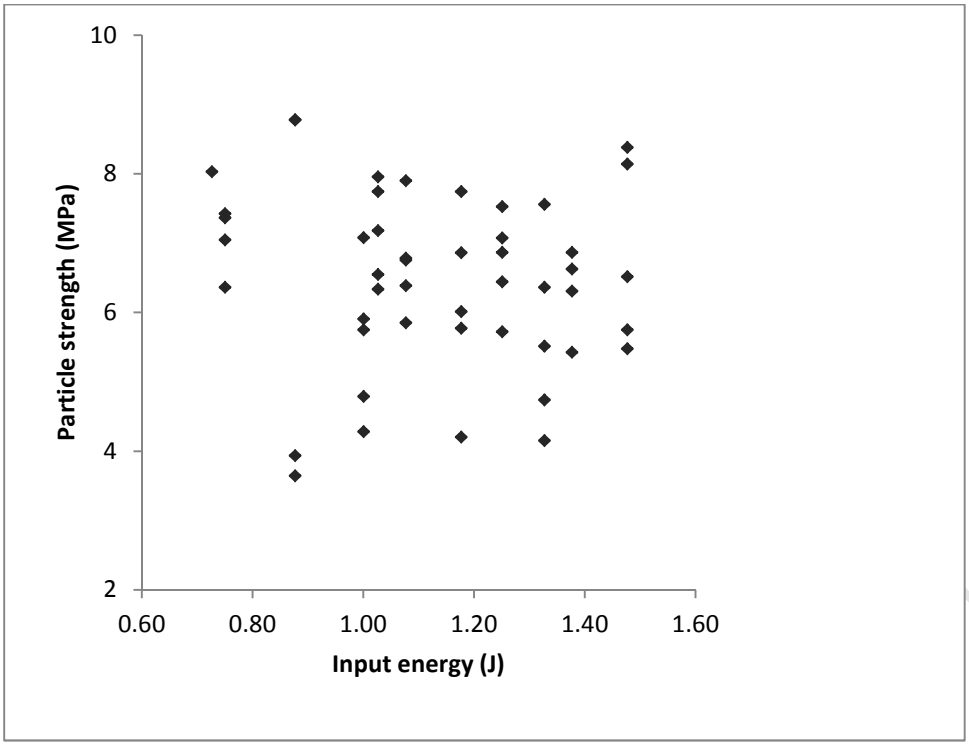

Figure 5.8. Particle strength values obtained during nickel bed breakage

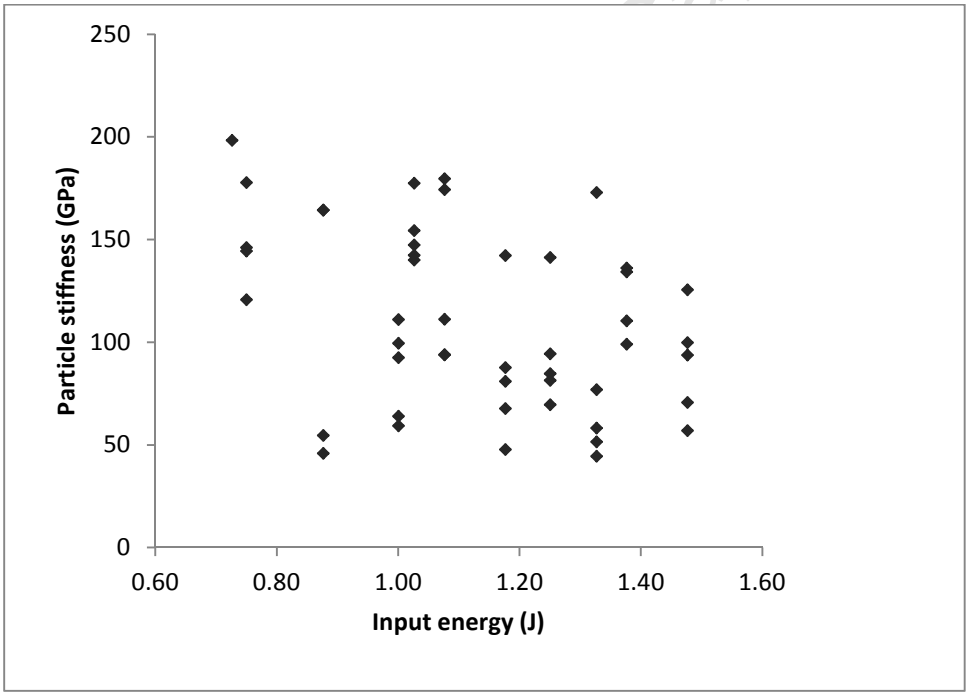

Figure 5.9. Particle stiffness values obtained during nickel bed breakage

5.3.3 Single crystal vs. bed breakage

To analyse the fracture characteristics of the nickel crystals, the individual measurements were converted to frequency distributions. This was done by identifying the number of observations falling within certain ranges of values in the results and then expressing the counts in each interval in terms of percentage of observations. Table 5.3, Table 5.4 and Table 5.5 show the frequency distribution data for particle fracture energy, particle strength and particle stiffness respectively.

Table 5.3. Fracture energy distribution data for single crystal and bed breakage

Single crystal breakage			**Bed breakage**		
Bin	No. of observations	% distribution	Bin	No. of observations	% distribution
0.05	0	0	0.36	0	0
0.15	13	48	0.48	8	17
0.24	9	33	0.60	16	33
0.28	5	19	0.72	14	29
0.32	2	7	0.84	9	19
0.33	1	4	0.96	1	2
			0.97	0	0

Table 5.4. Particle strength distribution data for single crystal and bed breakage

Single crystal breakage			**Bed breakage**		
Bin	No. of observations	% distribution	Bin	No. of observations	% distribution
7	0	0	3.5	0	0
12	10	33	4.2	5	10
19	14	47	4.8	5	10
26	5	17	6.8	18	38
30	1	3	7.9	13	27
32	0	0	8.8	7	15
			9.0	0	0

Table 5.5. Particle stiffness distribution data for single crystal and bed breakage

Single crystal breakage			Bed breakage		
Bin	No. of observations	% distribution	Bin	No. of observations	% distribution
20	0	0	40	0	0
120	16	53	80	13	27
220	10	33	120	15	31
320	3	10	160	12	25
371	1	3	200	8	17
380	0	0	240	0	0

The corresponding frequency distribution curves of the particle fracture energy, particle strength and particle stiffness are shown in Figure 5.10, Figure 5.11 and Figure 5.12 respectively.

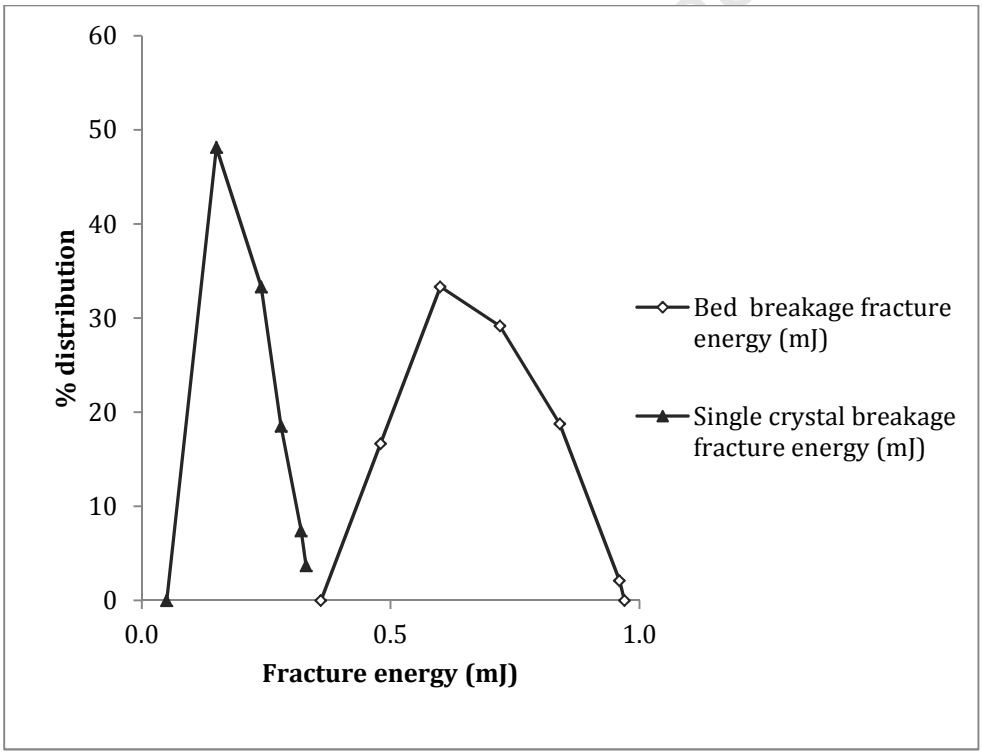

Figure 5.10. Frequency distribution for particle fracture energy during nickel breakage test

Figure 5.10 shows that the fracture energies obtained during bed breakage are higher than those for single crystal breakage. This is because during bed breakage, more than one particle will get into contact with the falling steel ball such that the input energy is distributed into all

the impacted particles. This means a higher resistance to breakage will be experienced resulting in more energy being absorbed before the point of initial breakage.

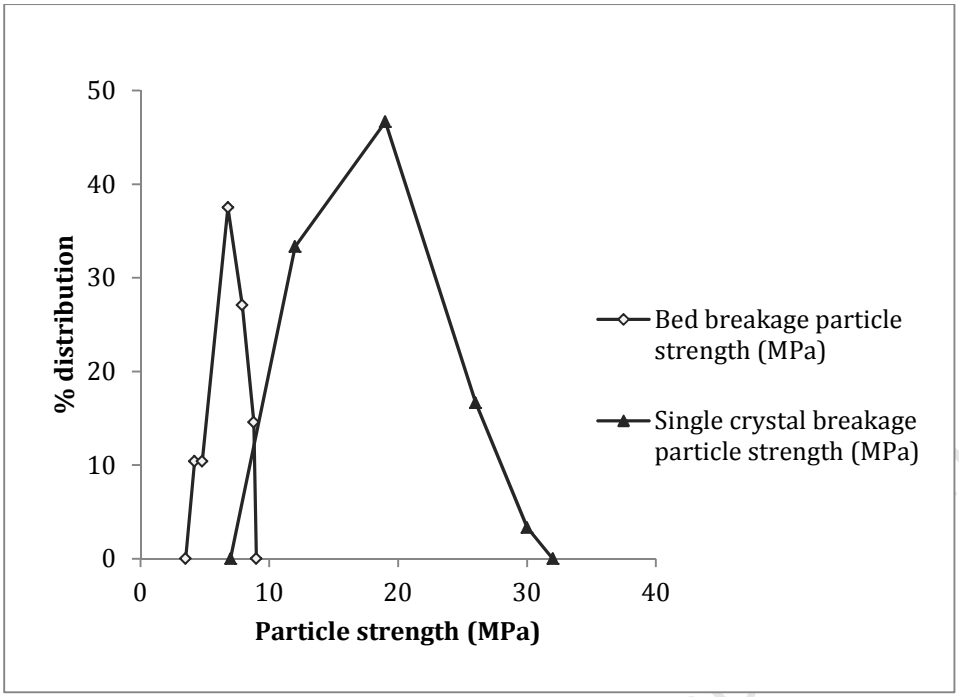

Figure 5.11. Frequency distribution for particle strength during nickel breakage test

From Figure 5.11, however, the particle strength values obtained during bed breakage were lower than those for single crystal breakage. This is because a bed of crystals has voids between particles which reduce the resistance to compression of the particles during the impact test.

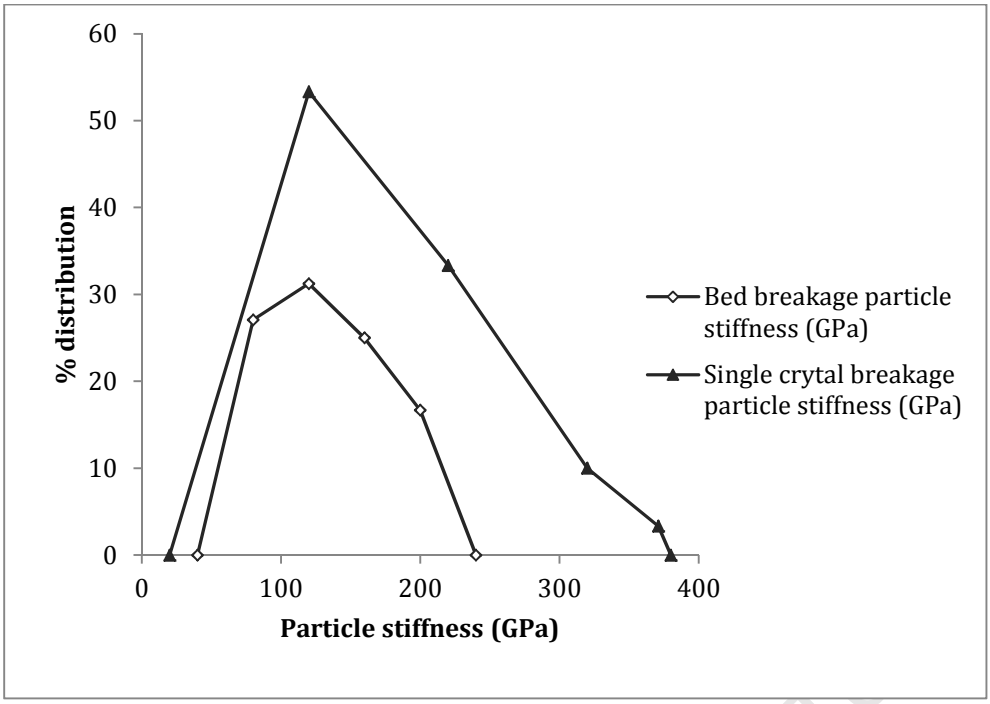

Figure 5.12. Frequency distribution for particle stiffness during nickel breakage test

Figure 5.12 indicates that, unlike particle fracture energy and particle strength, particle stiffness data for both bed and single crystal breakage falls within the same range, suggesting that stiffness is a material property. This is also supported by the work of Tavares and King (1998) who highlighted that particle stiffness is an intrinsic property which depends mainly on the atomic and molecular structure of the material.

The mean values obtained from the breakage tests are given in Table 5.6 and these were considered as the average material fracture characteristics for this study.

Table 5.6. Average material properties obtained during the breakage tests

Property	Single crystal breakage	Bed breakage
Particle fracture energy (mJ)	0.18	0.61
Particle strength (MPa)	15.27	6.47
Particle stiffness (GPa)	142	110

For the purpose of determining the "breakage speed" in a nickel reduction autoclave, the fracture characteristics obtained during single crystal breakage were used since the impact in a crystalliser is between each individual crystal and the impeller. The particle strengths obtained in this study (Table 5.6) have lower values than expected (compressive strength) for pure nickel from literature (Table 5.7). This variation can be attributed to the fact that these properties are

structure sensitive, and therefore, since the nickel crystals have an open structure (Figure 5.13); their resistance to breakage can be expected to be lower than that of pure nickel blocks with a closed structure. Also, because the nickel crystals used for this test were obtained from an industrial product, flaws and cracks may have already existed prior to the breakage tests.

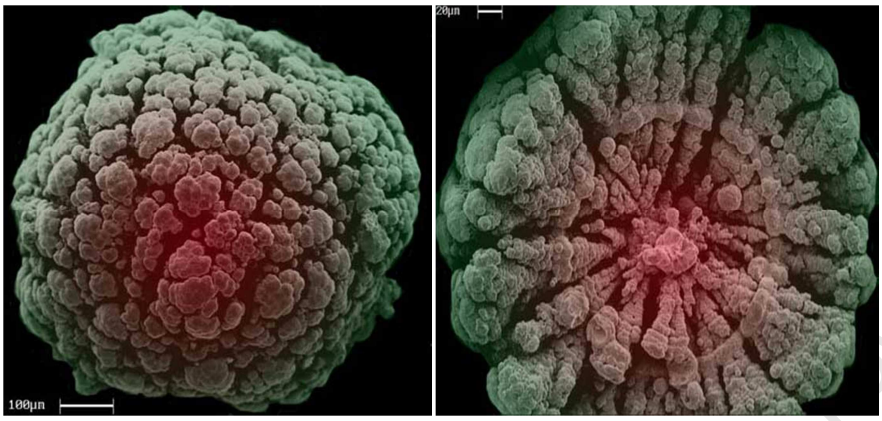

Figure 5.13. Open structure of the nickel crystals

Table 5.7. Pure nickel properties from literature

Property	Minimum value	Maximum value
Hardness (GPa)	0.8	3
Bulk modulus (GPa)	162	200
Young's modulus (GPa)	190	220
Shear modulus (GPa)	72	86
Compressive strength (MPa)	70	935
Poisson's ratio	0.305	0.315

When the mean fracture energy (0.18 mJ) was related to the impact energy in a nickel crystalliser using equation 2.24, a required impeller tip speed of 17.98m/s in order to fracture particles with a diameter of 500µm was obtained.

5.4 CONCLUSIONS

If the theory that particle fracture energy and particle strength are structure sensitive properties that are affected by the macrostructure of the material is correct, then the ultrafast load cell breakage test can be regarded as an effective method to quantify the fracture characteristics of the nickel crystals.

The material fracture properties (particle fracture energy, particle strength and particle stiffness) show a scatter and these variations can be attributed to the fact that they are structure sensitive properties which are strongly affected by the presence of critical flaws and cracks in zones of high stress in the material.

From the results, it can be concluded that a mean fracture energy of 0.18mJ is sufficient to cause breakage of the nickel crystals. Using the kinetic energy equation, this fracture energy translates to an impeller tip speed of 17.99m/s for particles of diameter d_{50} = 500μm.

CHAPTER 6 : OVERALL CONCLUSIONS

6.1 Suspension tests

For a nickel reduction autoclave using pitched blade impellers as agitators, sparging hydrogen below the impellers will cause impeller flooding, leading to nickel solids sedimentation. An impeller under flooding conditions does not generate any significant liquid phase circulation in the vessel, resulting in the sedimentation of the suspended particles. To reduce the effects of flooding and ensure optimum operation of the autoclave, it is therefore concluded that, hydrogen feeding should be performed into the headspace and then use a dual impeller system for mixing. The top impeller would be for hydrogen induction and the bottom for nickel suspension.

6.2 Attrition tests

Industrial autoclaves are normally operated at impeller tip speeds around 10m/s (Willis and von Essen, 2000). Based on the attrition studies in chapter 4 of this work, this impeller tip speed (10m/s) is sufficient to cause attrition of the nickel crystals since the minimum attrition speed for nickel crystals was found to be 4.01m/s. It can therefore be concluded that attrition is always present during the nickel reduction process under the standard mixing conditions (impeller tip speeds of around 10m/s).

6.3 Breakage tests

The breakage tests performed by use of an ultrafast load cell were single impact breakage and these have indicated that an impeller tip speed of 17.99m/s is required to cause breakage of nickel crystal. This impeller tip speed (17.99m/s), however, according to Willis and von Essen (2000), may lead to impeller blade erosion. Willis and von Essen (2000) highlighted that impeller blade erosion becomes a problem at impeller tip speeds in excess of 10m/s. It is therefore important to operate an autoclave at impeller tip speeds that do not lead to excessive blade erosion.

Because the nickel crystals used for these tests were too small (maximum size was 2mm), repeated impact breakage tests were therefore difficult to perform using the ultrafast load cell. It is therefore possible that breakage as a result of repeated impacts can occur at tip speeds lower than 17.99m/s. Further investigation using a different technique for measuring the fracture energy under repeated impacts is therefore still required.

CHAPTER 7 : REFERENCES

Al-Mousawi, M.M., Reid, S.R. & Deans, W.F. 1997, "The use of the split Hopkinson pressure bar techniques in high strain rate material testing", *Proceedings of the Institution of Mechanical Engineers, Part C: Journal of Mechanical Engineering Science,* vol. 211, no. 4, pp. 273.

Armenante, P.M. & Nagamine, E.U. 1998, "Effect of low off-bottom impeller clearance on the minimum agitation speed for complete suspension of solids in stirred tanks", *Chemical Engineering Science,* vol. 53, no. 9, pp. 1757-1775.

Ashby, M.F. 1999, *Materials selection in mechanical design,* Second edn, Butterworth Heinemann, Linacre House, Jordan Hill, Oxford.

Barresi, A. & Baldi, G. 1987a, "Solid dispersion in an agitated vessel", *Chemical Engineering Science,* vol. 42, no. 12, pp. 2949-2956.

Barresi, A. & Baldi, G. 1987b, "Solid dispersion in an agitated vessel: effect of particle shape and density", *Chemical Engineering Science,* vol. 42, no. 12, pp. 2969-2972.

Bbosa, L. 2007, *Measurement of impact breakage properties of ore particles using a series of devices*, Msc edn, University of Cape Town, Western Cape, South Africa.

Biscans, B. 2004, "Impact attrition in crystallization processes. Analysis of repeated impacts events of individual crystals", *Powder Technology,* vol. 143-144, pp. 264-272.

Bittorf, K.J. & Kresta, S.M. 2003, "Prediction of Cloud Height for Solid Suspensions in Stirred Tanks", *Chemical Engineering Research and Design,* vol. 81, no. 5, pp. 568-577.

Bourgeois, F.S. & Banini, G.A. 2002, "A portable load cell for in-situ ore impact breakage testing", *International Journal of Mineral Processing,* vol. 65, no. 1, pp. 31-54.

Bravi, M., Di Cave, S., Mazzarotta, B. & Verdone, N. 2003, "Relating the attrition behaviour of crystals in a stirred vessel to their mechanical properties", *Chemical Engineering Journal,* vol. 94, no. 3, pp. 223-229.

Bujalski, W., konno, M. & Nienow, A.W. 1988, "Scale-up of 45^{o} Pitch Blade Agitators for Gas Dispersion and Solid Suspension", *6th European conference on mixing*Pavia, Italy, pp. 389.

Bujalski, W., Takenaka, K., Paolini, S., Jahoda, M., Paglianti, A., Takahashi, K., Nienow, A.W. & Etchells, A.W. 1999, "Suspension and Liquid Homogenisation in High Solids Concentration Stirred Chemical Reactors", vol. 77.

Chapman, C.M., Nienow, A.W., Cooke, M. & Middleton, J.C. 1983, "Particle-gas-liquid mixing in stirred vessels. Part III: Three phase mixing", *Chemical Engineering Research and Design,* vol. 61, pp. 167.

Dutta, N.N. & Pangarkar, V.G. 1995, "Critical Impeller speed for solid suspension in multi-impeller three phase agitated contactors", *The Canadian Journal of Chemical Engineering,* vol. 73, no. 3, pp. 273-283.

Gahn, C. & Mersmann, A. 1999, "Brittle fracture in crystallization processes Part A. Attrition and abrasion of brittle solids", *Chemical Engineering Science,* vol. 54, no. 9, pp. 1273-1282.

Gahn, C. & Mersmann, A. 1995, "The brittleness of substances crystallized in industrial processes", *Powder Technology,* vol. 85, no. 1, pp. 71-81.

Genc, O., Ergun, L. & Benzer, H. 2004, "Single particle impact breakage characterisation of materials by drop weight testing", *Physicochemical problems of mineral processing,* vol. 38, pp. 241.

Kapur, P.C., Pande, D. & Fuerstenau, D.W. 1997, "Analysis of single-particle breakage by impact grinding", *International Journal of Mineral Processing,* vol. 49, no. 3-4, pp. 223-236.

Kasat, G.R. & Pandit, A.B. 2005, "Review on mixing characteristics in solid-liquid and solid-liquid-gas reactor vessels", *The Canadian journal of Chemicl Engineering,* vol. 83, pp. 618-618-643.

Kashchiev, D. 2000, *Nucleation: Basic theory with applications,* 1st edn, Butterworth Heinemann, Binacre House, Jordan Hill, Oxford OX2 8DP.

King, R.P. & Bourgeois, F. 1993, "Measurement of fracture energy during single-particle fracture", *Minerals Engineering,* vol. 6, no. 4, pp. 353-367.

Lewis, A.E. 2010, *Understanding Industrial Crystallisation Processes*, Lecture Notes edn, University of Cape Town, Department of Chemical Engineering, University of Cape Town, Western Cape, South Africa.

Lewis, A.E. 2009, *Report to Murrin Murrin: Feedback on Plant Trials March 2009. Part 2: Solids Suspension and Attrition*, University of Cape Town, South Africa.

Marrot, B. & Biscans, B. 2001, "Impact of a single crystal in solution, on an immersed target, in conditions which simulate impact attrition in crystallizers", *Powder Technology,* vol. 120, no. 3, pp. 141-150.

Mersmann, A. 2001, "Crystallisation technology handbook. Second Edition", *Marcel Dekker, Inc. United States of America,* .

Montante, G., Pinelli, D. & Magelli, F. 2003, "Scale-up criteria for the solids distribution in slurry reactors stirred with multiple impellers", *Chemical Engineering Science,* vol. 58, no. 23-24, pp. 5363-5372.

Mullin, J.W. 2001, *Crystallisation,* 4th edn, Reed Educational and Professional Publishing ltd, Butterworth Heinemann, Binacre House, Jordab Hill, Oxford OX2 8DP.

Nienow, A.W., Edwards, M.F. & Harnby, N. 1992, "The suspension of solid particles", *Mixing in the Process Industries second edition,* vol. 2, pp. 364-393.

Nienow, A.W., konno, M. & Bujalski, W. 1986, "Studies on three phase mixing: A review and recent studies", *Chemical Engineering Research and Design,* vol. 64, no. 1, pp. 35-35-42.

Ntuli, F. 2008, *Nickel powder precipitation by high-pressure hydrogen reduction*, PHD edn, University of Cape Town, Western Cape, South Africa.

Ntuli, F. & Lewis, A.E. 2007, "The influence of iron on the precipitation behaviour of nickel powder", *Chemical Engineering Science,* vol. 62, no. 14, pp. 3756-3766.

Ntuli, F. & Lewis, A.E. 2006, "The effect of a morphology modifier on the precipitation behaviour of nickel powder", *Chemical Engineering Science,* vol. 61, no. 17, pp. 5827-5833.

Nyvlt, J. 1971, *Industrial crystallisation from solutions,* 1st edn, Butterworth and Co. ltd, 33/35 Beach Grove, Durban, South Africa.

Ochieng, A. 2005, *A hydrodynamic study of nickel suspension in stirred tanks*, PHD edn, University of Cape Town, Western Cape, South Africa.

Paul, E.L., Atiemo-Obeng, V.A. & Kresta, S.M. (eds) 2004, *Handbook of Industrial Mixing: Science and Practice*, 1st edn, John Wiley & sons, Inc., Hoboken, New Jersey, Canada.

Perry, R.H. & Chilton, H.C. 1973, *Perry's Chemical Engineers Handbook,* 5th edn, McGraw-Hill, New York.

Perry, R.H., Green, D.W. & Maloney, J.O. 1984, *Perry's Chemical Engineers' handbook,* 6th edn, McGraw-Hill, New York.

Roberts, M. 2004, *The hydrodynamics studies, morphology quantification and kinetics studies of nickel powder produced via high-pressure hydrogen reduction*, MSc edn, University of Cape Town, Western Cape, South Africa.

Sharma, R.N. & Shaikh, A.A. 2003, "Solids suspension in stirred tanks with pitched blade turbines", *Chemical Engineering Science,* vol. 58, no. 10, pp. 2123-2140.

Sobol, S.I. 1993, "The problems of study of thermodynamics and kinetics of nickel and cobalt reduction by hydrogen from solutions", *The Paul E. Queneau International Symposium, Extractive metallurgy of copper, nickel and cobalt, Vol 1. Fundamental Aspects*, eds. R.G. Reddy & R.N. Weizenbach, The Minerals, Metals and Materials Society, , pp. 803.

Spicer, P.T., Keller, W. & Pratsinis, S.E. 1996, "The Effect of Impeller Type on Floc Size and Structure during Shear-Induced Flocculation", *Journal of colloid and interface science,* vol. 184, no. 1, pp. 112-122.

Synowiec, P. 2002, "How to improve the crystal size distribution (CSD) in crystallizers with the inner suspension circulation", *Chemical Engineering and Processing,* vol. 41, no. 7, pp. 585-593.

Tavares, L.M. 2004, "Optimum routes for particle breakage by impact", *Powder Technology,* vol. 142, no. 2-3, pp. 81-91.

Tavares, L.M. 1999, "Energy absorbed in breakage of single particles in drop weight testing", *Minerals Engineering,* vol. 12, no. 1, pp. 43-50.

Tavares, L.M. & King, R.P. 1998, "Single-particle fracture under impact loading", *International Journal of Mineral Processing,* vol. 54, no. 1, pp. 1-28.

van der Westhuizen, A.P. & Deglon, D.A. 2008, "Solids suspension in a pilot-scale mechanical flotation cell: A critical impeller speed correlation", *Minerals Engineering,* vol. 21, no. 8, pp. 621-629.

van der Westhuizen, A.P. & Deglon, D.A. 2007, "Evaluation of solids suspension in a pilot-scale mechanical flotation cell: The critical impeller speed", *Minerals Engineering,* vol. 20, no. 3, pp. 233-240.

Weiss, T. & Schubert, H. 1989, "On optimum hydrodynamics of coarse particle flotation", *Aufbereitungs-Technik,* vol. 30, pp. 657-663.

Willis, B. & von Essen, J. 2000, "Precipitation of nickel metal by hydrogen reduction: A new perspective", *Ni/Co conference*ALTA, Perth, Australia.

Wong, C.W., Wang, J.P. & Huang, S.T. 1987, "Investigations of fluid dynamics in mechanically stirred slurry reactors", *The Canadian Journal of Chemical Engineering,* vol. 65, no. 3, pp. 412-419.

Wu, J., Zhu, Y. & Pullum, L. 2001, "Impeller Geometry Effect on Velocity and Solids Suspension", *Chemical Engineering Research and Design,* vol. 79, no. 8, pp. 989-997.

Zhu, Y. & Wu, J. 2002, "Critical impeller speed for suspending solids in aerated tanks", *The Canadian Journal of Chemical Engineering,* vol. 80, no. 4, pp. 1-6.

Zwietering, T.N. 1958, "Suspending of solid particles in liquid by agitators", *Chemical Engineering Science,* vol. 8, no. 3-4, pp. 244-253.

Appendix

ATTRITION EXPERIMENTS

Raw PSD data in volume % obtained from the Malvern Mastersizer laser diffraction technique.

Attrition test 1:

Result: Analysis Table

ID: Attrition | Run No: 1 | Measured: 5/3/2010 12:03PM
File: NOBERT | Rec. No: 9 | Analysed: 5/3/2010 12:03PM
Path: C:\SIZERS\DATA\ | Source: Analysed

Range: 300RF mm | Beam: 2.40 mm | Sampler: MS1 | Obs': 11.1 %
Presentation: 3OAD | Analysis: Polydisperse | Residual: 0.424 %
Modifications: None

Conc. = 0.2820 %Vol | Density = 8.910 g/cm^3 | S.S.A.= 0.0039 m^2/g
Distribution: Volume | D[4, 3] = 178.79 um | D[3, 2] = 173.09 um
D(v, 0.1) = 141.66 um | D(v, 0.5) = 177.61 um | D(v, 0.9) = 218.66 um
Span = 4.336E-01 | Uniformity = 1.294E-01

Size (um)	Volume In %	Size (um)	Volume In %	Size (um)	Volume In %	Size (um)	Volume In %
0.05	0.00	0.58	0.00	6.63	0.00	76.32	0.16
0.06	0.00	0.67	0.00	7.72	0.00	88.91	0.52
0.07	0.00	0.78	0.00	9.00	0.00	103.58	1.91
0.08	0.00	0.91	0.00	10.48	0.00	120.67	6.76
0.09	0.00	1.06	0.00	12.21	0.00	140.58	21.16
0.11	0.00	1.24	0.00	14.22	0.00	163.77	36.97
0.13	0.00	1.44	0.00	16.57	0.00	190.80	23.96
0.15	0.00	1.68	0.00	19.31	0.00	222.28	8.50
0.17	0.00	1.95	0.00	22.49	0.00	258.95	0.00
0.20	0.00	2.28	0.00	26.20	0.00	301.68	0.00
0.23	0.00	2.65	0.00	30.53	0.00	351.46	0.00
0.27	0.00	3.09	0.00	35.56	0.00	409.45	0.00
0.31	0.00	3.60	0.00	41.43	0.00	477.01	0.00
0.36	0.00	4.19	0.00	48.27	0.00	555.71	0.00
0.42	0.00	4.88	0.00	56.23	0.01	647.41	0.00
0.49	0.00	5.69	0.00	65.51	0.02	754.23	0.00
0.58	0.00	6.63	0.00	76.32	0.05	878.67	0.00

Result: Analysis Table

ID: Attrition | Run No: 2 | Measured: 5/3/2010 1:01PM
File: NOBERT | Rec. No: 10 | Analysed: 5/3/2010 1:01PM
Path: C:\SIZERS\DATA\ | Source: Analysed

Range: 300RF mm | Beam: 2.40 mm | Sampler: MS1 | Obs': 11.0 %
Presentation: 3OAD | Analysis: Polydisperse | Residual: 0.406 %
Modifications: None

Conc. = 0.2773 %Vol | Density = 8.910 g/cm^3 | S.S.A.= 0.0039 m^2/g
Distribution: Volume | D[4, 3] = 177.64 um | D[3, 2] = 171.99 um
D(v, 0.1) = 140.58 um | D(v, 0.5) = 176.15 um | D(v, 0.9) = 217.74 um
Span = 4.381E-01 | Uniformity = 1.305E-01

Size (um)	Volume In %	Size (um)	Volume In %	Size (um)	Volume In %	Size (um)	Volume In %
0.05	0.00	0.58	0.00	6.63	0.00	76.32	0.13
0.06	0.00	0.67	0.00	7.72	0.00	88.91	0.48
0.07	0.00	0.78	0.00	9.00	0.00	103.58	1.97
0.08	0.00	0.91	0.00	10.48	0.00	120.67	7.37
0.09	0.00	1.06	0.00	12.21	0.00	140.58	22.67
0.11	0.00	1.24	0.00	14.22	0.00	163.77	36.37
0.13	0.00	1.44	0.00	16.57	0.00	190.80	22.76
0.15	0.00	1.68	0.00	19.31	0.00	222.28	8.20
0.17	0.00	1.95	0.00	22.49	0.00	258.95	0.00
0.20	0.00	2.28	0.00	26.20	0.00	301.68	0.00
0.23	0.00	2.65	0.00	30.53	0.00	351.46	0.00
0.27	0.00	3.09	0.00	35.56	0.00	409.45	0.00
0.31	0.00	3.60	0.00	41.43	0.00	477.01	0.00
0.36	0.00	4.19	0.00	48.27	0.00	555.71	0.00
0.42	0.00	4.88	0.00	56.23	0.00	647.41	0.00
0.49	0.00	5.69	0.00	65.51	0.01	754.23	0.00
0.58	0.00	6.63	0.00	76.32	0.04	878.67	0.00

Result: Analysis Table

ID: Attrition | Run No: 5 | Measured: 5/3/2010 2:11PM
File: NOBERT | Rec. No: 11 | Analysed: 5/3/2010 2:11PM
Path: C:\SIZERS\DATA\ | Source: Analysed

Range: 300RF mm | Beam: 2.40 mm | Sampler: MS1 | Obs': 8.4 %
Presentation: 3OAD | Analysis: Polydisperse | Residual: 0.537 %
Modifications: None

Conc. = 0.1778 %Vol | Density = 8.910 g/cm^3 | S.S.A.= 0.0498 m^2/g
Distribution: Volume | D[4, 3] = 162.57 um | D[3, 2] = 13.51 um
D(v, 0.1) = 122.12 um | D(v, 0.5) = 159.33 um | D(v, 0.9) = 210.34 um
Span = 5.537E-01 | Uniformity = 1.857E-01

Size (um)	Volume In %	Size (um)	Volume In %	Size (um)	Volume In %	Size (um)	Volume In %
0.05	0.23	0.58	0.00	6.63	0.00	76.32	0.48
0.06	0.12	0.67	0.00	7.72	0.00	88.91	1.57
0.07	0.03	0.78	0.00	9.00	0.00	103.58	5.63
0.08	0.00	0.91	0.00	10.48	0.04	120.67	15.94
0.09	0.00	1.06	0.00	12.21	0.04	140.58	30.37
0.11	0.00	1.24	0.00	14.22	0.14	163.77	24.90
0.13	0.00	1.44	0.00	16.57	0.16	190.80	12.70
0.15	0.00	1.68	0.00	19.31	0.18	222.28	5.06
0.17	0.00	1.95	0.00	22.49	0.17	258.95	1.73
0.20	0.00	2.28	0.00	26.20	0.12	301.68	0.00
0.23	0.00	2.65	0.00	30.53	0.07	351.46	0.00
0.27	0.00	3.09	0.00	35.56	0.01	409.45	0.00
0.31	0.00	3.60	0.00	41.43	0.01	477.01	0.00
0.36	0.00	4.19	0.00	48.27	0.03	555.71	0.00
0.42	0.00	4.88	0.00	56.23	0.08	647.41	0.00
0.49	0.00	5.69	0.00	65.51	0.18	754.23	0.00
0.58		6.63		76.32		878.67	

Result: Analysis Table

ID: Attrition | Run No: 6 | Measured: 5/3/2010 2:19PM
File: NOBERT | Rec. No: 12 | Analysed: 5/3/2010 2:19PM
Path: C:\SIZERS\DATA\ | Source: Analysed

Range: 300RF mm | Beam: 2.40 mm | Sampler: MS1 | Obs': 12.9 %
Presentation: 3OAD | Analysis: Polydisperse | Residual: 0.450 %
Modifications: None

Conc. = 0.2897 %Vol | Density = 8.910 g/cm^3 | S.S.A.= 0.0493 m^2/g
Distribution: Volume | D[4, 3] = 162.82 um | D[3, 2] = 13.65 um
D(v, 0.1) = 122.90 um | D(v, 0.5) = 161.51 um | D(v, 0.9) = 208.12 um
Span = 5.277E-01 | Uniformity = 1.757E-01

Size (um)	Volume In %	Size (um)	Volume In %	Size (um)	Volume In %	Size (um)	Volume In %
0.05	0.24	0.58	0.00	6.63	0.00	76.32	0.55
0.06	0.12	0.67	0.00	7.72	0.00	88.91	1.64
0.07	0.02	0.78	0.00	9.00	0.00	103.58	5.40
0.08	0.00	0.91	0.00	10.48	0.01	120.67	14.96
0.09	0.00	1.06	0.00	12.21	0.01	140.58	28.90
0.11	0.00	1.24	0.00	14.22	0.06	163.77	27.46
0.13	0.00	1.44	0.00	16.57	0.09	190.80	14.09
0.15	0.00	1.68	0.00	19.31	0.11	222.28	5.61
0.17	0.00	1.95	0.00	22.49	0.12	258.95	0.00
0.20	0.00	2.28	0.00	26.20	0.10	301.68	0.00
0.23	0.00	2.65	0.00	30.53	0.07	351.46	0.00
0.27	0.00	3.09	0.00	35.56	0.01	409.45	0.00
0.31	0.00	3.60	0.00	41.43	0.02	477.01	0.00
0.36	0.00	4.19	0.00	48.27	0.05	555.71	0.00
0.42	0.00	4.88	0.00	56.23	0.11	647.41	0.00
0.49	0.00	5.69	0.00	65.51	0.23	754.23	0.00
0.58		6.63		76.32		878.67	

Result: Analysis Table

ID: Attrition	Run No: 8	Measured: 5/3/2010 3:02PM
File: NOBERT	Rec. No: 14	Analysed: 5/3/2010 3:02PM
Path: C:\SIZERS\DATA\		Source: Analysed

Range: 300RF mm	Beam: 2.40 mm	Sampler: MS1
Presentation: 3OAD	Analysis: Polydisperse	Obs': 10.3 %
Modifications: None		Residual: 0.393 %

Conc. = 0.2258 %Vol	Density = 8.910 g/cm^3	S.S.A.= 0.0540 m^2/g
Distribution: Volume	D[4, 3] = 163.13 um	D[3, 2] = 12.48 um
D(v, 0.1) = 123.90 um	D(v, 0.5) = 162.17 um	D(v, 0.9) = 208.43 um
Span = 5.213E-01	Uniformity = 1.762E-01	

Size (um)	Volume In %	Size (um)	Volume In %	Size (um)	Volume In %	Size (um)	Volume In %
0.05		0.58		6.63		76.32	
0.06	0.28	0.67	0.00	7.72	0.00	88.91	0.44
0.07	0.12	0.78	0.00	9.00	0.00	103.58	1.42
0.08	0.02	0.91	0.00	10.48	0.00	120.67	5.03
0.09	0.00	1.06	0.00	12.21	0.01	140.58	14.68
0.11	0.00	1.24	0.00	14.22	0.02	163.77	28.77
0.13	0.00	1.44	0.00	16.57	0.09	190.80	27.96
0.15	0.00	1.68	0.00	19.31	0.13	222.28	14.35
0.17	0.00	1.95	0.00	22.49	0.17	258.95	5.67
0.20	0.00	2.28	0.00	26.20	0.20	301.68	0.00
0.23	0.00	2.65	0.00	30.53	0.19	351.46	0.00
0.27	0.00	3.09	0.00	35.56	0.12	409.45	0.00
0.31	0.00	3.60	0.00	41.43	0.02	477.01	0.00
0.36	0.00	4.19	0.00	48.27	0.02	555.71	0.00
0.42	0.00	4.88	0.00	56.23	0.04	647.41	0.00
0.49	0.00	5.69	0.00	65.51	0.09	754.23	0.00
0.58	0.00	6.63	0.00	76.32	0.18	878.67	0.00

Result: Analysis Table

ID: Attrition	Run No: 7	Measured: 5/3/2010 2:30PM
File: NOBERT	Rec. No: 13	Analysed: 5/3/2010 2:30PM
Path: C:\SIZERS\DATA\		Source: Analysed

Range: 300RF mm	Beam: 2.40 mm	Sampler: MS1
Presentation: 3OAD	Analysis: Polydisperse	Obs': 9.2 %
Modifications: None		Residual: 0.690 %

Conc. = 0.2341 %Vol	Density = 8.910 g/cm^3	S.S.A.= 0.0039 m^2/g
Distribution: Volume	D[4, 3] = 181.83 um	D[3, 2] = 174.33 um
D(v, 0.1) = 137.44 um	D(v, 0.5) = 179.25 um	D(v, 0.9) = 229.76 um
Span = 5.150E-01	Uniformity = 1.567E-01	

Size (um)	Volume In %	Size (um)	Volume In %	Size (um)	Volume In %	Size (um)	Volume In %
0.05		0.58		6.63		76.32	
0.06	0.00	0.67	0.00	7.72	0.00	88.91	0.18
0.07	0.00	0.78	0.00	9.00	0.00	103.58	0.68
0.08	0.00	0.91	0.00	10.48	0.00	120.67	2.51
0.09	0.00	1.06	0.00	12.21	0.00	140.58	8.01
0.11	0.00	1.24	0.00	14.22	0.00	163.77	20.15
0.13	0.00	1.44	0.00	16.57	0.00	190.80	31.15
0.15	0.00	1.68	0.00	19.31	0.00	222.28	23.58
0.17	0.00	1.95	0.00	22.49	0.00	258.95	11.78
0.20	0.00	2.28	0.00	26.20	0.00	301.68	1.89
0.23	0.00	2.65	0.00	30.53	0.00	351.46	0.00
0.27	0.00	3.09	0.00	35.56	0.00	409.45	0.00
0.31	0.00	3.60	0.00	41.43	0.00	477.01	0.00
0.36	0.00	4.19	0.00	48.27	0.00	555.71	0.00
0.42	0.00	4.88	0.00	56.23	0.00	647.41	0.00
0.49	0.00	5.69	0.00	65.51	0.01	754.23	0.00
0.58	0.00	6.63	0.00	76.32	0.05	878.67	0.00

Attrition test 2:

Result: Analysis Table

ID: Attrition	Run No: 9	Measured: 5/4/2010 10:28AM
File: NOBERT	Rec. No: 15	Analysed: 5/4/2010 10:28AM
Path: C:\SIZERS\DATA\		Source: Analysed

Range: 300RF mm	Beam: 2.40 mm	Sampler: MS1
Presentation: 3OAD	Analysis: Polydisperse	Obs': 8.7 %
Modifications: None		Residual: 0.483 %

Conc. = 0.2129 %Vol	Density = 8.910 g/cm^3	S.S.A.= 0.0040 m^2/g
Distribution: Volume	D[4, 3] = 176.63 um	D[3, 2] = 168.83 um
D(v, 0.1) = 133.42 um	D(v, 0.5) = 171.78 um	D(v, 0.9) = 225.01 um
Span = 5.332E-01	Uniformity = 1.668E-01	

Size (um)	Volume In %	Size (um)	Volume In %	Size (um)	Volume In %	Size (um)	Volume In %
0.05		0.58		6.63		76.32	
0.06	0.00	0.67	0.00	7.72	0.00	88.91	0.19
0.07	0.00	0.78	0.00	9.00	0.00	103.58	0.71
0.08	0.00	0.91	0.00	10.48	0.00	120.67	2.92
0.09	0.00	1.06	0.00	12.21	0.00	140.58	10.25
0.11	0.00	1.24	0.00	14.22	0.00	163.77	25.48
0.13	0.00	1.44	0.00	16.57	0.00	190.80	31.64
0.15	0.00	1.68	0.00	19.31	0.00	222.28	18.03
0.17	0.00	1.95	0.00	22.49	0.00	258.95	7.26
0.20	0.00	2.28	0.00	26.20	0.00	301.68	2.67
0.23	0.00	2.65	0.00	30.53	0.00	351.46	0.77
0.27	0.00	3.09	0.00	35.56	0.00	409.45	0.00
0.31	0.00	3.60	0.00	41.43	0.00	477.01	0.00
0.36	0.00	4.19	0.00	48.27	0.00	555.71	0.00
0.42	0.00	4.88	0.00	56.23	0.00	647.41	0.00
0.49	0.00	5.69	0.00	65.51	0.02	754.23	0.00
0.58	0.00	6.63	0.00	76.32	0.05	878.67	0.00

Result: Analysis Table

ID: Attrition	Run No: 10	Measured: 5/4/2010 11:25AM
File: NOBERT	Rec. No: 16	Analysed: 5/4/2010 11:25AM
Path: C:\SIZERS\DATA\		Source: Analysed

Range: 300RF mm	Beam: 2.40 mm	Sampler: MS1
Presentation: 3OAD	Analysis: Polydisperse	Obs': 9.7 %
Modifications: None		Residual: 0.435 %

Conc. = 0.2238 %Vol	Density = 8.910 g/cm^3	S.S.A.= 0.0043 m^2/g
Distribution: Volume	D[4, 3] = 163.88 um	D[3, 2] = 157.39 um
D(v, 0.1) = 126.87 um	D(v, 0.5) = 160.90 um	D(v, 0.9) = 208.23 um
Span = 5.056E-01	Uniformity = 1.605E-01	

Size (um)	Volume In %	Size (um)	Volume In %	Size (um)	Volume In %	Size (um)	Volume In %
0.05		0.58		6.63		76.32	
0.06	0.00	0.67	0.00	7.72	0.00	88.91	0.39
0.07	0.00	0.78	0.00	9.00	0.00	103.58	1.33
0.08	0.00	0.91	0.00	10.48	0.00	120.67	4.97
0.09	0.00	1.06	0.00	12.21	0.00	140.58	15.32
0.11	0.00	1.24	0.00	14.22	0.00	163.77	31.74
0.13	0.00	1.44	0.00	16.57	0.00	190.80	27.58
0.15	0.00	1.68	0.00	19.31	0.00	222.28	13.44
0.17	0.00	1.95	0.00	22.49	0.00	258.95	5.02
0.20	0.00	2.28	0.00	26.20	0.00	301.68	0.00
0.23	0.00	2.65	0.00	30.53	0.00	351.46	0.00
0.27	0.00	3.09	0.00	35.56	0.00	409.45	0.00
0.31	0.00	3.60	0.00	41.43	0.01	477.01	0.00
0.36	0.00	4.19	0.00	48.27	0.02	555.71	0.00
0.42	0.00	4.88	0.00	56.23	0.05	647.41	0.00
0.49	0.00	5.69	0.00	65.51	0.14	754.23	0.00
0.58	0.00	6.63	0.00	76.32		878.67	

Result: Analysis Table

ID: Attrition | Run No: 11 | Measured: 5/4/2010 12:24PM
File: NOBERT | Rec. No: 17 | Analysed: 5/4/2010 12:24PM
Path: C:\SIZERS\DATA\ | Source: Analysed

Range: 300RF mm | Beam: 2.40 mm | Sampler: MS1 | Obs': 11.7 %
Presentation: 3OAD | Analysis: Polydisperse | Residual: 0.388 %
Modifications: None

Conc. = 0.2761 %Vol | Density = 8.910 g/cm^3 | S.S.A.= 0.0042 m^2/g
Distribution: Volume | D[4, 3] = 166.57 um | D[3, 2] = 160.30 um
D(v, 0.1) = 127.88 um | D(v, 0.5) = 164.60 um | D(v, 0.9) = 206.99 um
Span = 4.806E-01 | Uniformity = 1.557E-01

Size (um)	Volume In %	Size (um)	Volume In %	Size (um)	Volume In %	Size (um)	Volume In %
0.05	0.00	0.58	0.00	6.63	0.00	76.32	0.33
0.06	0.00	0.67	0.00	7.72	0.00	88.91	1.11
0.07	0.00	0.78	0.00	9.00	0.00	103.58	4.19
0.08	0.00	0.91	0.00	10.48	0.00	120.67	13.34
0.09	0.00	1.06	0.00	12.21	0.00	140.58	29.69
0.11	0.00	1.24	0.00	14.22	0.00	163.77	31.19
0.13	0.00	1.44	0.00	16.57	0.00	190.80	14.82
0.15	0.00	1.68	0.00	19.31	0.00	222.28	5.14
0.17	0.00	1.95	0.00	22.49	0.00	258.95	0.00
0.20	0.00	2.28	0.00	26.20	0.00	301.68	0.00
0.23	0.00	2.65	0.00	30.53	0.00	351.46	0.00
0.27	0.00	3.09	0.00	35.56	0.00	409.45	0.00
0.31	0.00	3.60	0.00	41.43	0.00	477.01	0.00
0.36	0.00	4.19	0.00	48.27	0.00	555.71	0.00
0.42	0.00	4.88	0.00	56.23	0.02	647.41	0.00
0.49	0.00	5.69	0.00	65.51	0.04	754.23	0.00
0.58	0.00	6.63	0.00	76.32	0.12	878.67	0.00

Result: Analysis Table

ID: Attrition | Run No: 12 | Measured: 5/4/2010 1:23PM
File: NOBERT | Rec. No: 18 | Analysed: 5/4/2010 1:23PM
Path: C:\SIZERS\DATA\ | Source: Analysed

Range: 300RF mm | Beam: 2.40 mm | Sampler: MS1 | Obs': 10.7 %
Presentation: 3OAD | Analysis: Polydisperse | Residual: 0.408 %
Modifications: None

Conc. = 0.2601 %Vol | Density = 8.910 g/cm^3 | S.S.A.= 0.0041 m^2/g
Distribution: Volume | D[4, 3] = 172.67 um | D[3, 2] = 165.00 um
D(v, 0.1) = 131.78 um | D(v, 0.5) = 168.68 um | D(v, 0.9) = 218.03 um
Span = 5.114E-01 | Uniformity = 1.684E-01

Size (um)	Volume In %	Size (um)	Volume In %	Size (um)	Volume In %	Size (um)	Volume In %
0.05	0.00	0.58	0.00	6.63	0.00	76.32	0.28
0.06	0.00	0.67	0.00	7.72	0.00	88.91	0.96
0.07	0.00	0.78	0.00	9.00	0.00	103.58	3.66
0.08	0.00	0.91	0.00	10.48	0.00	120.67	11.62
0.09	0.00	1.06	0.00	12.21	0.00	140.58	27.01
0.11	0.00	1.24	0.00	14.22	0.00	163.77	31.09
0.13	0.00	1.44	0.00	16.57	0.00	190.80	16.44
0.15	0.00	1.68	0.00	19.31	0.00	222.28	6.16
0.17	0.00	1.95	0.00	22.49	0.00	258.95	2.10
0.20	0.00	2.28	0.00	26.20	0.00	301.68	0.53
0.23	0.00	2.65	0.00	30.53	0.00	351.46	0.00
0.27	0.00	3.09	0.00	35.56	0.00	409.45	0.00
0.31	0.00	3.60	0.00	41.43	0.00	477.01	0.00
0.36	0.00	4.19	0.00	48.27	0.01	555.71	0.00
0.42	0.00	4.88	0.00	56.23	0.03	647.41	0.00
0.49	0.00	5.69	0.00	65.51	0.09	754.23	0.00
0.58	0.00	6.63	0.00	76.32	0.09	878.67	0.00

Result: Analysis Table

ID: Attrition | Run No: 13 | Measured: 5/4/2010 2:23PM
File: NOBERT | Rec. No: 19 | Analysed: 5/4/2010 2:23PM
Path: C:\SIZERS\DATA\ | Source: Analysed

Range: 300RF mm | Beam: 2.40 mm | Sampler: MS1 | Obs': 9.6 %
Presentation: 3OAD | Analysis: Polydisperse | Residual: 0.535 %
Modifications: None

Conc. = 0.2197 %Vol | Density = 8.910 g/cm^3 | S.S.A.= 0.0043 m^2/g
Distribution: Volume | D[4, 3] = 163.66 um | D[3, 2] = 156.40 um
D(v, 0.1) = 125.08 um | D(v, 0.5) = 159.64 um | D(v, 0.9) = 209.11 um
Span = 5.264E-01 | Uniformity = 1.686E-01

Size (um)	Volume In %	Size (um)	Volume In %	Size (um)	Volume In %	Size (um)	Volume In %
0.05	0.00	0.58	0.00	6.63	0.00	76.32	0.46
0.06	0.00	0.67	0.00	7.72	0.00	88.91	1.51
0.07	0.00	0.78	0.00	9.00	0.00	103.58	5.49
0.08	0.00	0.91	0.00	10.48	0.00	120.67	16.14
0.09	0.00	1.06	0.00	12.21	0.00	140.58	31.74
0.11	0.00	1.24	0.00	14.22	0.00	163.77	26.24
0.13	0.00	1.44	0.00	16.57	0.00	190.80	12.27
0.15	0.00	1.68	0.00	19.31	0.00	222.28	4.42
0.17	0.00	1.95	0.00	22.49	0.00	258.95	1.46
0.20	0.00	2.28	0.00	26.20	0.00	301.68	0.00
0.23	0.00	2.65	0.00	30.53	0.00	351.46	0.00
0.27	0.00	3.09	0.00	35.56	0.00	409.45	0.00
0.31	0.00	3.60	0.00	41.43	0.01	477.01	0.00
0.36	0.00	4.19	0.00	48.27	0.03	555.71	0.00
0.42	0.00	4.88	0.00	56.23	0.07	647.41	0.00
0.49	0.00	5.69	0.00	65.51	0.17	754.23	0.00
0.58	0.00	6.63	0.00	76.32	0.17	878.67	0.00

Result: Analysis Table

ID: Attrition | Run No: 14 | Measured: 5/4/2010 3:21PM
File: NOBERT | Rec. No: 20 | Analysed: 5/4/2010 3:21PM
Path: C:\SIZERS\DATA\ | Source: Analysed

Range: 300RF mm | Beam: 2.40 mm | Sampler: MS1 | Obs': 11.5 %
Presentation: 3OAD | Analysis: Polydisperse | Residual: 0.553 %
Modifications: None

Conc. = 0.2700 %Vol | Density = 8.910 g/cm^3 | S.S.A.= 0.0042 m^2/g
Distribution: Volume | D[4, 3] = 167.07 um | D[3, 2] = 159.92 um
D(v, 0.1) = 125.85 um | D(v, 0.5) = 165.08 um | D(v, 0.9) = 211.05 um
Span = 5.161E-01 | Uniformity = 1.656E-01

Size (um)	Volume In %	Size (um)	Volume In %	Size (um)	Volume In %	Size (um)	Volume In %
0.05	0.00	0.58	0.00	6.63	0.00	76.32	0.44
0.06	0.00	0.67	0.00	7.72	0.00	88.91	1.40
0.07	0.00	0.78	0.00	9.00	0.00	103.58	4.82
0.08	0.00	0.91	0.00	10.48	0.00	120.67	13.89
0.09	0.00	1.06	0.00	12.21	0.00	140.58	27.51
0.11	0.00	1.24	0.00	14.22	0.00	163.77	29.48
0.13	0.00	1.44	0.00	16.57	0.00	190.80	15.86
0.15	0.00	1.68	0.00	19.31	0.00	222.28	6.33
0.17	0.00	1.95	0.00	22.49	0.00	258.95	0.00
0.20	0.00	2.28	0.00	26.20	0.00	301.68	0.00
0.23	0.00	2.65	0.00	30.53	0.00	351.46	0.00
0.27	0.00	3.09	0.00	35.56	0.00	409.45	0.00
0.31	0.00	3.60	0.00	41.43	0.01	477.01	0.00
0.36	0.00	4.19	0.00	48.27	0.02	555.71	0.00
0.42	0.00	4.88	0.00	56.23	0.07	647.41	0.00
0.49	0.00	5.69	0.00	65.51	0.17	754.23	0.00
0.58	0.00	6.63	0.00	76.32	0.17	878.67	0.00

Result: Analysis Table

ID: Attrition | Run No: 15 | Measured: 5/4/2010 4:20PM
File: NOBERT | Rec. No: 21 | Analysed: 5/4/2010 4:21PM
Path: C:\SIZERS\DATA\ | Source: Analysed

Range: 300RF mm | Beam: 2.40 mm | Sampler: MS1 | Obs': 10.5 %
Presentation: 3OAD | Analysis: Polydisperse | Residual: 0.470 %
Modifications: None

Conc. = 0.2404 %Vol | Density = 8.910 g/cm^3 | S.S.A.= 0.0043 m^2/g
Distribution: Volume | D[4, 3] = 163.82 um | D[3, 2] = 156.71 um
D(v, 0.1) = 124.86 um | D(v, 0.5) = 161.03 um | D(v, 0.9) = 209.72 um
Span = 5.270E-01 | Uniformity = 1.665E-01

Size (um)	Volume In %	Size (um)	Volume In %	Size (um)	Volume In %	Size (um)	Volume In %
0.05	0.00	0.58	0.00	6.63	0.00	76.32	0.52
0.06	0.00	0.67	0.00	7.72	0.00	88.91	1.61
0.07	0.00	0.78	0.00	9.00	0.00	103.58	5.47
0.08	0.00	0.91	0.00	10.48	0.00	120.67	15.34
0.09	0.00	1.06	0.00	12.21	0.00	140.58	30.36
0.11	0.00	1.24	0.00	14.22	0.00	163.77	27.00
0.13	0.00	1.44	0.00	16.57	0.00	190.80	13.94
0.15	0.00	1.68	0.00	19.31	0.00	222.28	5.43
0.17	0.00	1.95	0.00	22.49	0.00	258.95	0.00
0.20	0.00	2.28	0.00	26.20	0.00	301.68	0.00
0.23	0.00	2.65	0.00	30.53	0.00	351.46	0.00
0.27	0.00	3.09	0.00	35.56	0.00	409.45	0.00
0.31	0.00	3.60	0.00	41.43	0.01	477.01	0.00
0.36	0.00	4.19	0.00	48.27	0.04	555.71	0.00
0.42	0.00	4.88	0.00	56.23	0.09	647.41	0.00
0.49	0.00	5.69	0.00	65.51	0.20	754.23	0.00
0.58		6.63		76.32		878.67	

Result: Analysis Table

ID: Attrition | Run No: 16 | Measured: 5/4/2010 5:22PM
File: NOBERT | Rec. No: 22 | Analysed: 5/4/2010 5:22PM
Path: C:\SIZERS\DATA\ | Source: Analysed

Range: 300RF mm | Beam: 2.40 mm | Sampler: MS1 | Obs': 10.0 %
Presentation: 3OAD | Analysis: Polydisperse | Residual: 0.501 %
Modifications: None

Conc. = 0.2326 %Vol | Density = 8.910 g/cm^3 | S.S.A.= 0.0042 m^2/g
Distribution: Volume | D[4, 3] = 166.71 um | D[3, 2] = 159.50 um
D(v, 0.1) = 125.84 um | D(v, 0.5) = 164.80 um | D(v, 0.9) = 210.28 um
Span = 5.124E-01 | Uniformity = 1.649E-01

Size (um)	Volume In %	Size (um)	Volume In %	Size (um)	Volume In %	Size (um)	Volume In %
0.05	0.00	0.58	0.00	6.63	0.00	76.32	0.47
0.06	0.00	0.67	0.00	7.72	0.00	88.91	1.39
0.07	0.00	0.78	0.00	9.00	0.00	103.58	4.74
0.08	0.00	0.91	0.00	10.48	0.00	120.67	13.84
0.09	0.00	1.06	0.00	12.21	0.00	140.58	27.88
0.11	0.00	1.24	0.00	14.22	0.00	163.77	29.63
0.13	0.00	1.44	0.00	16.57	0.00	190.80	15.60
0.15	0.00	1.68	0.00	19.31	0.00	222.28	6.10
0.17	0.00	1.95	0.00	22.49	0.00	258.95	0.00
0.20	0.00	2.28	0.00	26.20	0.00	301.68	0.00
0.23	0.00	2.65	0.00	30.53	0.00	351.46	0.00
0.27	0.00	3.09	0.00	35.56	0.00	409.45	0.00
0.31	0.00	3.60	0.00	41.43	0.02	477.01	0.00
0.36	0.00	4.19	0.00	48.27	0.04	555.71	0.00
0.42	0.00	4.88	0.00	56.23	0.09	647.41	0.00
0.49	0.00	5.69	0.00	65.51	0.19	754.23	0.00
0.58		6.63		76.32		878.67	

Result: Analysis Table

ID: Attrition | Run No: 17 | Measured: 5/5/2010 9:25AM
File: NOBERT | Rec. No: 23 | Analysed: 5/5/2010 9:25AM
Path: C:\SIZERS\DATA\ | Source: Analysed

Range: 300RF mm | Beam: 2.40 mm | Sampler: MS1 | Obs': 12.6 %
Presentation: 3OAD | Analysis: Polydisperse | Residual: 0.712 %
Modifications: None

Conc. = 0.2981 %Vol | Density = 8.910 g/cm^3 | S.S.A.= 0.0042 m^2/g
Distribution: Volume | D[4, 3] = 167.61 um | D[3, 2] = 159.35 um
D(v, 0.1) = 124.33 um | D(v, 0.5) = 165.79 um | D(v, 0.9) = 215.15 um
Span = 5.478E-01 | Uniformity = 1.758E-01

Size (um)	Volume In %	Size (um)	Volume In %	Size (um)	Volume In %	Size (um)	Volume In %
0.05	0.00	0.58	0.00	6.63	0.00	76.32	0.63
0.06	0.00	0.67	0.00	7.72	0.00	88.91	1.78
0.07	0.00	0.78	0.00	9.00	0.00	103.58	5.45
0.08	0.00	0.91	0.00	10.48	0.00	120.67	13.92
0.09	0.00	1.06	0.00	12.21	0.00	140.58	25.45
0.11	0.00	1.24	0.00	14.22	0.00	163.77	28.02
0.13	0.00	1.44	0.00	16.57	0.00	190.80	16.73
0.15	0.00	1.68	0.00	19.31	0.00	222.28	7.45
0.17	0.00	1.95	0.00	22.49	0.00	258.95	0.15
0.20	0.00	2.28	0.00	26.20	0.00	301.68	0.00
0.23	0.00	2.65	0.00	30.53	0.00	351.46	0.00
0.27	0.00	3.09	0.00	35.56	0.00	409.45	0.00
0.31	0.00	3.60	0.00	41.43	0.02	477.01	0.00
0.36	0.00	4.19	0.00	48.27	0.05	555.71	0.00
0.42	0.00	4.88	0.00	56.23	0.11	647.41	0.00
0.49	0.00	5.69	0.00	65.51	0.25	754.23	0.00
0.58		6.63		76.32		878.67	

Result: Analysis Table

ID: Attrition | Run No: 18 | Measured: 5/5/2010 10:23AM
File: NOBERT | Rec. No: 24 | Analysed: 5/5/2010 10:23AM
Path: C:\SIZERS\DATA\ | Source: Analysed

Range: 300RF mm | Beam: 2.40 mm | Sampler: MS1 | Obs': 12.5 %
Presentation: 3OAD | Analysis: Polydisperse | Residual: 0.514 %
Modifications: None

Conc. = 0.2760 %Vol | Density = 8.910 g/cm^3 | S.S.A.= 0.0479 m^2/g
Distribution: Volume | D[4, 3] = 162.00 um | D[3, 2] = 14.05 um
D(v, 0.1) = 120.39 um | D(v, 0.5) = 160.38 um | D(v, 0.9) = 209.47 um
Span = 5.554E-01 | Uniformity = 1.823E-01

Size (um)	Volume In %	Size (um)	Volume In %	Size (um)	Volume In %	Size (um)	Volume In %
0.05	0.22	0.58	0.00	6.63	0.00	76.32	0.69
0.06	0.12	0.67	0.00	7.72	0.00	88.91	1.93
0.07	0.03	0.78	0.00	9.00	0.00	103.58	5.90
0.08	0.00	0.91	0.00	10.48	0.00	120.67	15.36
0.09	0.00	1.06	0.00	12.21	0.01	140.58	28.66
0.11	0.00	1.24	0.00	14.22	0.02	163.77	25.69
0.13	0.00	1.44	0.00	16.57	0.07	190.80	14.21
0.15	0.00	1.68	0.00	19.31	0.11	222.28	5.96
0.17	0.00	1.95	0.00	22.49	0.14	258.95	0.00
0.20	0.00	2.28	0.00	26.20	0.15	301.68	0.00
0.23	0.00	2.65	0.00	30.53	0.13	351.46	0.00
0.27	0.00	3.09	0.00	35.56	0.08	409.45	0.00
0.31	0.00	3.60	0.00	41.43	0.02	477.01	0.00
0.36	0.00	4.19	0.00	48.27	0.02	555.71	0.00
0.42	0.00	4.88	0.00	56.23	0.05	647.41	0.00
0.49	0.00	5.69	0.00	65.51	0.12	754.23	0.00
0.58		6.63		76.32	0.29	878.67	